EFFECTS OF PREHEAT TEMPERATURE AND VITIATION ON REACTION KINETICS OF HIGHER HYDROCARBON FUELS

A Dissertation
Presented to
The Academic Faculty

By

Sampath Adusumilli

In Partial Fulfillment
of the Requirements for the Degree
Doctor of Philosophy in the
School of Aerospace Engineering

Georgia Institute of Technology
August 2019

EFFECTS OF PREHEAT TEMPERATURE AND VITIATION ON REACTION KINETICS OF HIGHER HYDROCARBON FUELS

Approved by:

Dr. Jerry M. Seitzman, Advisor,
School of Aerospace Engineering
Georgia Institute of Technology

Dr. Timothy C. Lieuwen,
School of Aerospace Engineering
Georgia Institute of Technology

Dr. Jechiel I. Jagoda
School of Aerospace Engineering
Georgia Institute of Technology

Dr. Wenting Sun
School of Aerospace Engineering
Georgia Institute of Technology

Dr. Devesh Ranjan
School of Mechanical Engineering
Georgia Institute of Technology

Date Approved: May 1, 2019

To my loving Amma, Nanna and Chellai.

(Padma, Suryanarayana and Divya Sree Adusumilli)

For your unconditional love and support which is always cherished.

Acknowledgements

This thesis is culmination of almost a decade long endeavor to gain knowledge and contribute towards the advancement of combustion science. It would have not been possible to complete this journey without the help of multiple people in my life. I would like to thank each one of them individually for being patient with me and helping me progress this far. I will mention some of the important characters here but might not be able to highlight everyone. So, before I begin I would like to thank each and every individual who I have interacted with during my time at Georgia Tech, each one of you have helped me become a better person and for that reason I am in great debt to all of you.

First, I would like to thank Dr. Jerry Seitzman, without his help this effort would not have been possible. His energy, motivation and spirit to solve research problems in the right way is inspiring and has influenced me to be a better researcher. The patience he has shown in discussing research results and to draw accurate conclusions has been invaluable to me. Apart from his guidance in research, our discussions on teaching methods and implementation of new courses have been enjoyable and influential. I am really thankful to him for providing me the opportunity to work on multiple research projects and work on my teaching skills during my time at Georgia Tech. He has always encouraged me to ask the right questions, taught me how to approach research problems and encouraged me to come up with innovative solutions.

I would also like to thank the members of the thesis reading committee Dr. Tim Lieuwen, Dr. Jeff Jagoda, Dr. Wenting Sun and Dr. Devesh Ranjan. Their comments and suggestions were valuable and significantly improved the quality of this dissertation.

Special thanks to Dr. Jagoda for helping me with all the administrative work and the encouragement he provided throughout my stay at Georgia Tech. Since the day I have been at Georgia Tech, Dr. Lieuwen has shown a special interest in improving the combustion lab culture and making it a more conducive environment to conduct research. His efforts have certainly paid off and I am thankful for his exertions in this direction. Also, I would like to thank Dr. Sun for letting me borrow some of his equipment to conduct this research and for letting me teach some lectures in his propulsion class.

This effort would not have been possible without the help of multiple research engineers (Dr. David Scarborough, Bobby Noble, Dr. Olksandr Bibik, Dr. Ben Emerson, Dr. Vishal Acharya, Brad Ochs, Chris Ballance and David Wu) in the combustion lab over the years. Special thanks to Kris Manion, Dan Fries and Seth Hutchins for making the lab more organized in the last few years. Also, I would like to thank all the graduate research collaborators for this work, Dr. Yash Kochar, Dr. Xiang Gao and Lisa Meyer without whose help some parts of this research would have stagnated. Yash's encouragement and mentorship in the initial days of this work pushed me to dwell deeper into research on chemical kinetics.

Over the years several undergraduate researchers have helped me in redesigning the experiment and running the bulk of Chemkin calculations, they are Cavanaugh Welch, Matthew Chan, Alexander Boisvert, Phoebe Zhang, Alexander Markov, John Amin and Sajid Shaheer. I really enjoyed interacting with all of them, mentoring these students over the course of couple of semesters has been a very rewarding experience for me. I would like to thank the sponsors of my research during my time at Georgia Tech, Combustion Science and Engineering Inc. (CSE, Inc.), Air force and Navy research laboratories,

MetroLaser Inc. and Southwest Sciences Inc. Special acknowledgement to Dr. Thomas Jenkins from MetroLaser is warranted here as I really enjoyed our research collaboration on PDV. The way we were able take an idea and completely transform it into a real world product over the course of three and a half years was really gratifying.

I had the privilege to teach some of the smartest undergraduates in the nation, thanks to several teaching opportunities provided by the aerospace engineering department. I would like to thank all the professors under whose guidance I was TA (Dr. Jerry Seitzman, Dr. Tim Lieuwen, Dr. Mitchell Walker, Dr. Suresh Menon, Dr. Wenting Sun, Dr. Jeff Jagoda, Dr. David Scarborough, Dr. Graeme Kennedy, Dr. Claudio Di Leo and Dr. Amy Pritchett), for guiding me when needed while also providing the freedom needed to teach effectively. Also, all my fellow TA's who taught the undergraduate fluids lab with me, your efforts in accommodating late schedule changes and on-the-fly problem solving made life interesting and enjoyable.

Over the years, several people at the combustion lab made life pleasant both in the lab and outside the lab. These are people I could have a technical discussion with and also socialize. First I would like to thank members of Dr. Jerry Seitzman's research group (Yash Kochar, Karthik Periagaram, Arun Radhakrishnan, Ravi Kiran, Nishant Jain, Brandon Sforzo, Lisa Meyer, Sheng Wei, Edwin Goh, Alex Miller and Aimee Williams) for bearing with me and also discussing complex research problems. A special mention to Nishant Jain, our friendship started with collaborating on class projects, lasted through qualifier study sessions, multiple car repair projects and late – night data campaigns. It is a friendship that I will cherish and remember for the good times. Though it is not a comprehensive list I would like to thank the following for making the lab a fun place and for being awesome

in general: Sai Thumuluru, Prabhakar Venkateswaran, Andrew Marshall, Christopher Foley, Matthew Quinlan, Ben Wilde, Travis Smith, Julia Lundrigan, Ianko Chterev, Vedanth Nair, Debolina Dasgupta, Hanna Ek, Matthew Sirignano, Nick Rock, Subodh Adhikari, Sai Kaza, Tom Pritchard, Angie Zhang, Raghul Manosh, Aravind Chandh, Jeong-Won Kim, Miad Karimi, Sukruth Somappa, Henderson Johnson, Dan Fries, Alexander Damiao, Gina Magnotti, Boni Yraguen, Leslie Hsao, Askar Kazbekov and Samuel Grauer.

Outside the confines of the lab, several people have helped me get through my time at Georgia Tech. First, I would like to thank members of the SFA group (Sandeep Kakumanu, Sravani Rachakulla, Arjun Kakumanu, Ravi Kovvali, Shilpa Mahamulkar, Srinath Pendyala, Bhavya Gunjali, Bhanu Sama, Balachandra Suri, Uma Moravapalle, Bhuvana Krishnaswamy, Raghu Vadali, Gautami Newalkar, Chandan Prasad, Ranjini Vaidyanathan, Ravi Kant and Yoshitha Rathore) for all the great and fun times over the years. The members of the ATLCREW (Pratik Mittal, Aditi Sharma, Dhruv Hoysall, Sushruth Surappa, Ashley Alva, Jaianandh Velrajan and Kirti Prabhakar) for staying young at heart and living life by the minute. The “Francis St gang” aka the GangsofAtlanta-pur (Eohan George, Riya Peter, Deepak Jose, Shubha Mitra barman, Murali Gopal, Bijoy Sasidharan, Gopika, Gautam Krishna, Luxmi Saha, Abraham Varghese, Sri Raj Paul, Sibi, Vaishak Chandran, Medhavi Mital, Mathews George and Yedurag babu) for trying to teach me Malayalam, encouraging me to cook and keeping me up to date on Indian politics. Swetha Ratan, Anusha Garapaty, Gautham Voleti, Nivedita Ravi, Umesh Unnikrishnan, Mohit Gupta, Rajiv Damodaran, Harsha Kota, Karthik Nayani and Sri Charan Yarlagadda for their friendship at different times during the past decade.

The badminton club at Georgia Tech served as an essential distraction and kept me physically fit. Some of the members (Justeen Lee, Ramon Sua, Lily Li, Amelia Tan, Dan Shen, Jinhyun Kim, Debra Wu, Nunthadech Rodcheuy, Mario Huang, Qiqin Xie, Sophie Li, Claire Cheng, Courtney Wong, Prof. Peng Qiu, Jiri Schimer, Hugo Bassas, Girish Mururu, Jiajia Xue, Melanie Coissard, Kevin Yin, Chunlok Lo, Ishan Kudale, Ishaani Mittal, Romain Gerbe, Sujay Pandey, Shivan Mittal and Hari Pavan Suryadevara) in this group have become good friends, motivated me to do well and encouraged me to participate in competitions regularly. Special thanks to Jiri Schimer who introduced me to the addictive habit of lifting weights in the gym. I would like to thank my undergrad friends, especially wing mates Sai Dhiraj Amuru, Raviteja Vemulapalli and Sandeep Sambaraju for staying in touch and keeping me grounded. Special shout out to my childhood friends (Tarun Tej, Halley Tej, Spoorthy Koganti, Krishna Koganti, Nagendra Kakani and Anusha Kakani) who would rush to my rescue whenever in need.

Without music I would not have completed this thesis writing process, I would like to thank the composers Wolfgang Mozart (GOAT), Hans Zimmer, John Williams, A.R. Rahman, Ilaiyaraaja, Mani Sharma and M.M. Keeravani. For their compositions the world is a richer place. Finally, I owe my deepest gratitude to my parents (Padma and Suryanarayana Adusumilli) and sister (Divya Sree Adusumilli) for letting me choose this unconventional path, and providing me with unconditional support and patience. They have dealt with my frustrations and idiosyncrasies admirably, in return provided me with only true love and for this I am forever grateful.

TABLE OF CONTENTS

List of tables

List of figures

Symbols and Abbreviations

S_L	Laminar flame speed
r_f	Flame radius in a spherical flame
K	Stretch rate
LDV	Laser Doppler Velocimetry
PIV	Particle Image Velocimetry
U	Nozzle exit velocity
α	Half cone angle of a Bunsen flame
Le	Lewis number
PFR	Plug flow reactor
χ_i	Mole fraction of species 'i'
ϕ	Equivalence ratio
T_u	Unburned premixed mixture temperature
BFT	Bunsen flame technique
$S_{L,u}$	Unburned laminar flame speed
$S_{L,b}$	Burned laminar flame speed
S_{L,u_o}	Unstretched laminar flame speed
S_{L,b_o}	Unstretched burned laminar flame speed
$\dot{m}$	Mass flow rate
ρ_u	Unburned gas density
ρ_b	Burned gas density
$\dot{Q}$	Volumetric flow rate
A_u	Unburned flame surface area

A_b	Burned flame surface area
TC	Thermocouple
D	Diameter of the burner
ICCD	Intensified charge-couple device
$S_{L,\ other}$	Flame speed measured using other techniques
$S_{L,\ BFT}$	Flame speed measured using Bunsen flame technique
r	Radial coordinate
z	Axial coordinate
R_f	Radius of the flame at a given height
h	Local height of the flame
H	Total height of the flame
a	Strain rate
MW	Molecular weight
L_u	*Unburned* Markstein length
L_b	*Burned* Markstein length
CFD	Computational Fluid Dynamics
DNS	Direct Numerical Simulation
$\dot{m}_{inlet}$	Total inlet mass flow rate
S_{L,u,m_o}	Measured unstretched flame speed
PSE	Percentage systematic error
Ze	Zeldovich number
β^o	Change in density in a flame
γ^o	Flame curvature
δ_T^o	Preheat zone thickness

T_{ad}	Adiabatic flame temperature
δ_f	Flame thickness
$S_{L,\ average}$	Average measured flame speed
SFT	Spherical flame technique
STFT	Stagnation flame technique
LM	Linear extrapolation methods
NLM	Nonlinear extrapolation methods
$T_{u,o}$	Reference preheat temperature
$S_{L,o}$	Laminar flame speed at $T_{u,o}$
γ	Temperature exponent
α_o, α_1, α_2	Coefficients of curve-fit for γ
β_o, β_1	Coefficients of curve-fit for $S_{L,o}$
ϕ_{max}	Maximum flame speed equivalence ratio
Θ	O_2 fraction in oxidizer
C	CO_2 fraction in oxidizer
a_i	Absorption coefficient of species *i*
c_j	Polynomial curve-fit parameters for absorption coefficient
$\dot{Q}_{radiation}$	Radiative heat loss
T	Local radiating gas temperature
T_b	Background temperature
p_i	Partial pressure of species *i*
CTR	Chemical effect compared to thermal effect
$S_L^{C_0}$	Flame speed with no CO_2 dilution
$S_{L,\ FCO_2}^{C}$	Flame speed with FCO_2 dilution

$S_{L,\,CO_2}^{C}$	Flame speed with CO_2 dilution
s_i	Sensitivity of reaction i
A_i	Pre-exponential factor of i^{th} reaction
k	Rate coefficient
b	Temperature exponent
R	Universal gas constant
E_a	Activation energy
$[X_i]$	Concentration of species i within a flame
$[X_{i,max}]$	Maximum concentration of species i within a flame
ROP	Rate of production

Summary

Conducting full-scale experiments as part of the design process of jet engine combustors is a costly and time-consuming process. Therefore engine developers have been increasingly using numerical modeling approaches to assess new designs or design changes. The reaction chemistry, which is dependent on the flow conditions, the fuel composition, and the oxidizer composition, plays an important role in the accuracy of these simulations. The kinetic mechanisms that describe this chemistry need to be validated. Various global combustion characteristics are used to validate mechanisms against experimental data; one of these is laminar flame speed (S_L).

In this work, laminar flame speeds of various fuels relevant to jet engine combustion are measured using a previously developed, modified Bunsen Flame Technique (BFT). The accuracy of the BFT is examined here, both through a comparison to experimental results from other standard approaches for a range of fuels and through a detailed analysis of the impact of flame stretch. The measured flame speeds are also used to test leading chemical kinetic mechanisms, primarily the NUI and USC models.

Laminar flame speeds of n-decane, ethylene and propylene are measured at conditions relevant to jet engine main combustors and afterburners. The experimental conditions include high preheat temperatures (up to 650 K) and reduced O_2 levels (down to 15% mole fraction in the oxidizer); the latter is relevant to vitiation, where there is partial pre-burning of the oxidizing flow. Furthermore, vitiation introduces combustion products such as CO_2 into the reactant stream that can participate in the combustion chemistry.

Therefore, flame speeds are measured using dilution with both CO_2 and N_2 (considered non-reactive) to study these effects.

S_L measurements for alkenes using BFT are within 10% of measurements from literature and chemical kinetic mechanism predictions at 300 K and atmospheric pressure. At high preheat temperatures, the mechanisms accurately predict S_L for ethylene mixtures, while they over predict S_L of propylene mixtures at 650 K. Vitiation studies at 650 K preheat show that for N_2 dilution and ethylene, the reduction in flame speed is mostly due to thermal effects. Some chemical effects were observed when the O_2 level in the oxidizer was reduced to 15% (vol.). For propylene, reducing O_2 had a larger impact on flame speed than that predicted by the mechanisms. With CO_2 as a diluent, the mechanisms over predicted the flame speed, and the prediction error increased with higher levels of CO_2. Reactions involving the allyl (C_3H_5-A) radical were identified as a likely source of the propylene flame speed errors, increase in the pre-exponential rate factor of the allyl-H recombination reaction improved the predictive capability of the mechanism at high preheat temperatures. Similarly, analysis of different sources of errors with CO_2 dilution suggest the third-body efficiency of CO_2 is underestimated in a three-body association (such as $H + O_2 (+M) \Leftrightarrow HO_2 (+M)$) type of reactions.

CHAPTER 1. Introduction

This thesis examines the effect of high preheat temperatures and vititation on chemical kinetics of high hydrocarbon fuels. This is accomplished by using laminar flame speeds (S_L) measured experimentally at conditions relevant to jet engine operations. The motivation for current work and its scope with respect to previous work is presented in this chapter.

1.1 Motivation

Modern aircraft derive their power from jet engines; they are widely used for both commercial and military purposes. These engines need to operate over a wide spectrum of conditions which include changes in operating temperature, pressure and fuel-oxidizer composition. These differences can affect the performance of the engine as they can lead to differences in flame temperature, efficiency of fuel consumption and can have adverse effect on turbine components located downstream of the combustor.

Pollutants in jet-engines are mainly formed due to incomplete combustion, which leads to the production of CO, unburned hydrocarbons (UHC) and soot. In addition, poor mixing and local hot spots can lead to elevated NOx output. Emission restrictions are becoming more stringent for commercial aircraft engines [1, 2]. In military aero-engines one of the main cause of pollutants is the presence of afterburners/augmenters [2, 3] which are used primarily to increase thrust. The combustion in these devices mostly occurs close to stoichiometric conditions and involves vitiated air combustion. Vitiated air consists of combustion products (CO_2, H_2O, CO, NO_x etc.) which leads to the oxygen content being

lower than in normal air and the presence of steam and carbon dioxide as additional diluents. This can alter the burning characteristics compared to combustion in standard air.

Table 1.1: Approximate typical inlet conditions for a turbine engine main combustors and afterburners [3].

Inlet conditions	Main Combustor	Augmenter
Temperature (°C)	350 – 650	650 - 1050
Pressure (atm)	10 - 30	0.5 - 6
Oxygen (% vol.)	21	12 - 17

Table 1.1 shows the typical inlet conditions present in gas turbine aeroengine main combustors and afterburners. Testing a combustion device for all the operating conditions experimentally is both impractical and prohibitively expensive, especially in the design process. Varying composition of a jet fuel could lead to differences in engine performance and the advent of alternative fuels [4] further complicates the testing processes. Thus, computational evaluation is becoming more important in the combustor design process [5-7]. To carry this out, several chemical kinetic mechanisms have been developed to predict the performance of liquid jet fuels [8, 9]. These kinetic models/mechanisms need to be validated before they can be used in simulations; some of the useful combustion characteristics for validation of these mechanisms against experimental data are: 1) ignition, 2) extinction, 3) speciation and 4) flame propagation. Representative data for each of these phenomena are often measured through: 1) autoignition delay time, 2) laminar

flame extinction strain rate, 3) species profiles in flow reactors and laminar flames, and 4) laminar flame speed.

This study focuses on the measurement of laminar flame speeds of higher hydrocarbon fuels (alkenes) that form an important part of jet fuel reaction chemistry. Laminar flame speed (S_L) is defined as the speed at which a flame propagates into a premixed mixture of reactants in a laminar flow. The most commonly used version of this propagation speed is defined for a flame that is adiabatic and free from stretch effects. The measurements in this work are made at conditions relevant to aeroturbine main combustors and afterburners. The following section briefly describes the different approaches used for the measurement of laminar flame speed. Relevant work already in literature about laminar flame speed measurements of alkenes is also discussed.

1.2 Literature Review

1.2.1 Flame Speed Measurement Techniques

Numerous techniques have been developed to measure unstretched laminar flame speeds of premixed mixtures. The major techniques used are based on a variety of flame configurations: the Bunsen flame, spherical flame, flat flame and counter-flow (opposed jet) or bluff-body stabilized stagnation flame [10-12]. The flame speed measured from each of these techniques often needs to be corrected for the effects of stretch or heat losses to the surroundings. Each of these techniques have advantages as well as limitations in terms of ease of measurement and accuracy. This section provides a brief discussion of these techniques, while the Bunsen flame technique is discussed in detail as it is the configuration used in this thesis.

1.2.1.1 Flat flame technique

The flat flame technique employs a burner to generate a thin flat flame over either a porous metal disk or a parallel series of small tubes forming a larger burner. Figure 1.1 shows the schematics of flat flame configuration to measure flame speed. The flame is stabilized by gradually reducing the flow rate through the burner [13] or by adjusting the heat flux to the burner [14, 15]. The flame speed is calculated by dividing the volumetric flow rate through the burner by the area of the flame.

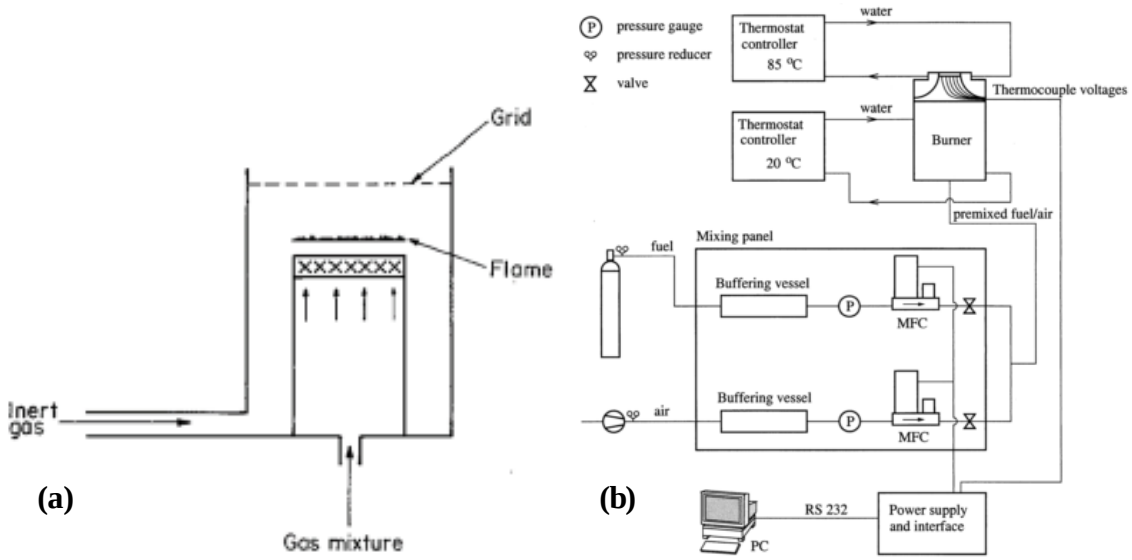

Figure 1.1: Schematics of a typical flat flame burner apparatus (a) without heat flux (adapted from [12]) (b) with heat flux adjustment (adapted from [15])

When used without the heat flux adjustment, the technique is limited to flame speed measurements of the order of 15 cm/s [12] as the flame would no longer be one-dimensional (it is either lifted and stabilized at only a few locations on the burner, or it is composed of multiple small flames). The adjustment of heat flux is achieved by cooling the burner using water and thus providing the ability to stabilize flat flames at higher flow

rates. For a given mixture, flame speed is calculated with varying cooling rates and S_L is calculated by extrapolating the cooling rate to zero.

Flat flames are in general hard to stabilize for mixtures with high laminar flame speed (> ~80 cm/s) [16] thus limiting the ability to measure flame speeds at high preheat temperatures. The highest preheat temperature at which flame speeds have been measured using this technique is 353 K. There are also limitations with respect to higher pressure measurements as it becomes harder to stabilize flames due to higher rates of heat transfer to the burner.

1.2.1.2 Spherical flame technique

The spherical flame technique uses a radially propagating flame in a quiescent gas to measure S_L. A premixed mixture of known properties is placed in a closed vessel and ignited at the center allowing a spherical flame to propagate into the mixture. Since the flame is highly curved, the flame speed is affected by the flame curvature which changes as the flame expands. To determine the unstretched flame speed value, either linear or non-linear methods are used to extrapolate the measured flame speeds to zero stretch. There are two variants for the spherical flame technique: (a) the constant pressure method, and (b) the constant volume method.

In the constant pressure approach, the flame is imaged using Schlieren or shadowgraph techniques with a high frequency response. The flame speed along the flame front is calculated as $S_L = dr_f(t)/dt$, where r_f is the flame radius. Since the flame front is highly curved, the flame stretch (K) is tracked with the flame speed and is given by $K = 2S_L/r_f$. To estimate the unstretched laminar flame speed value, several models have been

developed for linear and non-linear extrapolation. The uncertainties involved in both these methods is discussed in detail by Wu et al. [17]. More details about the experimental method, drawbacks and uncertainties are described in [18]. The main challenges for this method are related to the ability to achieve constant pressure combustion and the inability to reach high preheat temperatures due to experimental limitations.

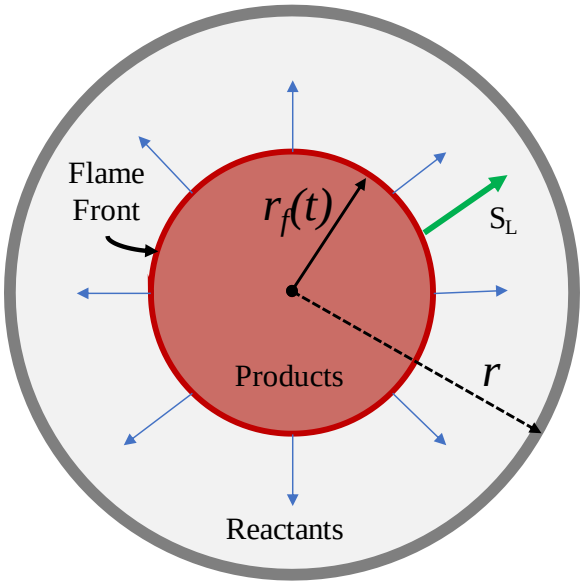

Figure 1.2: A sketch depicting propagation of a center ignited spherical flame into premixed reactants with flame propagation speed of S_L. The radius of the chamber is *r* and the instantaneous flame front is denoted by $r_f(t)$ (adapted from [16]).

The constant volume method uses an opaque spherical chamber and the flame speed is estimated by measuring the pressure-time history during flame propagation. Using the pressure-time history, an analytical expression can be derived for S_L, the details are given in [19]. Theoretically this approach can be used to measure flame speeds at high preheat temperatures, but since this approach does not consider flame stretch effects it is considered

less accurate. There is a large discrepancy between measurements from different groups for given premixed mixture making this technique unreliable as of now [19].

1.2.1.3 Opposed-jet/ stagnation flame technique

Similar to the spherical flame method, a strained stagnation flame can be used to estimate laminar flame speed of a given premixed mixture. By measuring the strain rate and strained flame speed of a stationary stagnation flame and extrapolating to zero strain the unstretched flame speed can be estimated [11, 12].

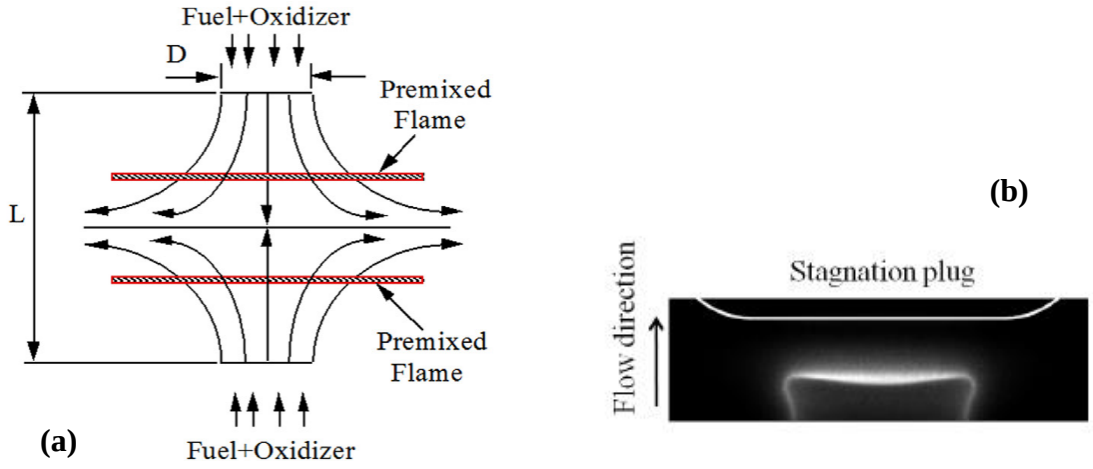

Figure 1.3: (a) Illustration of a stagnation flame using the opposed-flow twin flame configuration (adapted from [18]); (b) chemiluminescence image of a stagnation flame using a stagnation plug [20].

There are two approaches to generate a flat stagnation flame: the opposed-jet, twin flame configuration (Figure 1.3 (a)), and the stagnation plug configuration (Figure 1.3 (b)). The stagnation plug method is susceptible to heat losses to the plug, but these can be overcome by maintaining sufficient distance between the flame and the plug surface [20]. The opposed jet flames are subject to radiative heat losses but these are found to be

negligible [18]. The highly strained velocity flow field is captured using a non-intrusive technique such as Laser Doppler Velocimetry (LDV) [21] or Particle Image Velocimetry (PIV) [20]. Inlet velocity is varied to change the strain rate and the location of flame stabilization. For a particular inlet velocity, the flame speed and strain rate are determined as the minimum velocity before the flame and the maximum gradient in velocity respectively. The unstretched flame speed is achieved by extrapolating flame speed to zero stretch. Both linear [22] and non-linear extrapolation methods [23] can be used to achieve the final unstretched flame speed value.

1.2.1.4 Bunsen flame technique

Broadly speaking there are two basic approaches to measuring flame speed using Bunsen-type flames as shown in Figure 1.4.

Flame angle measurement approach

The flame angle measurement technique determines flame speed along the wings of the Bunsen flame using the following relation, $S_L = U \sin(\alpha)$, where α is the half cone angle of the flame and U is either the nozzle exit velocity [11] or a local flow velocity [24]. This approach assumes a singular (sharp) tip location for a Bunsen flame; while this is not generally true, depending on the mixture conditions this can be an acceptable assumption.

Area measurement approach

An average flame speed value can also be determined by measuring the flame area. Because a Bunsen burner flame is conical, aerodynamic strain and flame curvature affect these flames. Their total influence on the local flame speed along the flame surface is dependent on the type of the mixture. For example, a given fuel-air mixture at known

conditions has a specific Lewis number (Le) which influences the dependence of the flame speed on stretch [25].

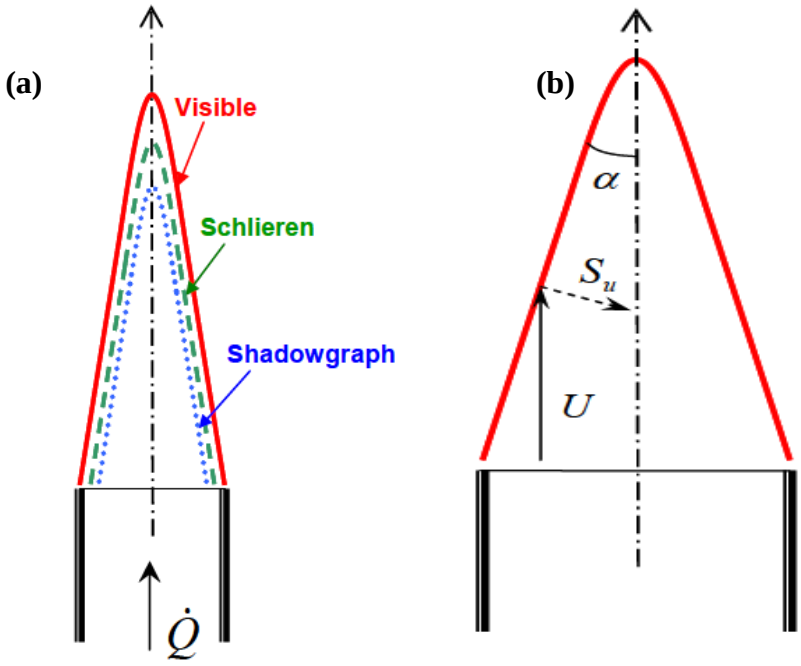

Figure 1.4: (a) Illustration shows the relative positions of the different optically accessible edges, adapted from [12, 20, 21]. (b) Illustration of laminar flame speed based on angle measurement method, adapted from[21].

As noted above, this method for measuring flame speeds relies on calculating the flame area, which is found from flame imaging. The spatially averaged flame speed is calculated by dividing the volumetric flow rate of the mixture by the measured flame area.

Review articles on laminar flame speed measurement approaches by Linnet [26], Andrews et al. [27] and Rallis et al. [28] discuss some of the earlier methods used to image Bunsen flames, primarily limited to Schlieren and shadowgraph approaches. The flame area measured with these imaging techniques led to systematic errors in the derived laminar flame speeds; essentially these approaches focused on determining the inner (unburned)

edge of the Bunsen flame (see Figure 1.4 (a)). These measurements were highly sensitive to flame curvature and stretch effects. Using chemiluminescence imaging of the reaction zone, improved Bunsen flame measurements were made by Natarajan et al. [21, 29-31] for syngas fuels. A similar approach was later employed by Kochar et al. [20, 32, 33] to measure laminar flame speeds of C1-C3 alkanes (methane through propane) and their mixtures at high pre-heat temperatures and pressures. Other researchers also used this approach to measure flames speeds of syngas and natural gas mixtures [34-36].

1.2.2 Flame speed measurements of n-decane

As discussed previously, understanding jet fuel chemistry is imperative to conduct full scale engine simulations. For these simulations, jet fuel chemistry is manifested through a chemical kinetic mechanism, composed of a number of reactions involving various species and with models for the reaction rate constant for each reaction. To validate chemical kinetic models, accurate composition of the jet fuel needs to be estimated. As the composition of a jet fuel varies depending on where it is sourced from, use of surrogate fuels is encouraged while measuring global chemical properties. This is done to accurately characterize a fuel and validate kinetic mechanisms based on this fuel.

Table 1.2 shows typical compositions of various standard distillate aviation fuels used in commercial and military jet-engines; of these, Jet-A is the most common. Jet-A is often replaced in controlled experiments by surrogate (non-distillate) fuels, which meet the overall specification requirements of Jet-A. On average, paraffins, i.e., n-alkanes, form the major component of jet fuel, and during oxidation n-alkanes are generally the most reactive component and act as the main driver for the combustion characteristics of jet fuels [2].

Table 1.2: Typical composition of some aviation fuels [37]

Property	Avgas	JP-4	JP-5	JP-7	Jet-A (JP-8)
Approximate Formula	C_7H_{15}	$C_{8.5}H_{17}$	$C_{12}H_{22}$	$C_{12}H_{25}$	$C_{11}H_{21}$
H/C Ratio	2.09	2.00	1.92	2.07	1.91
Average Composition					
Aromatics, vol%	25	10	19	3	18
Paraffins		59	45	65	45
Naphthenes		29	34	32	35
Olefins	10	2	2		2
Sulfur, ppm		370	470	2	490

Various studies have been performed to define surrogate fuels of Jet-A/kerosene; Edwards et al. [38] summarized surrogates for different aviation fuels and concluded that surrogate fuels with paraffins as major components chemically resembled their parent fuels. For example, the Aachen surrogate [39] is a binary fuel with a composition of 80% n-decane and 20 % 1,2,4-trimethylbenzene by weight, which was shown to have identical properties to Jet-A. n-decane is also used as one of the surrogate components to model synthetic paraffinic fuels such as HRJ and S-8 [40, 41]. Thus n-decane can be used as a model fuel to understand the chemical kinetic pathways of jet fuels that are important to laminar flame speed

Laminar flame speed measurements of n-decane have been made by several research groups using different techniques. Rasmussen et al. [42] measured laminar flame speed of n-decane at atmospheric pressure up to a pre-heat temperature of 473 K using a Bunsen flame technique. Kumar et al. [43] measured laminar flame speed using a twin

flame, opposed-jet configuration at atmospheric pressure and a range of preheat temperatures up to 470 K. Zhao et al. [44] determined laminar burning velocities of n-decane mixtures using a stagnation jet configuration. In that study, preheat temperature was increased to 500 K, and nitrogen dilution levels were varied. Ji et al. [45] measured laminar flame speeds of premixed n-alkane (C_5-C_{12}) flames at atmospheric pressure and preheat temperature of 403 K. These measurements were performed using a twin flame, opposed-jet configuration. Nishiie et al. [46] measured laminar burning velocity and Markstein lengths of n-decane, jet-A and S-8 fuels at 1 atm and 400 K preheat temperature using a spherical flame technique.

To help validate chemical kinetic mechanisms of jet fuels, flame speed measurements at engine relevant conditions are required. The previous measurements are limited to a maximum reactant preheat temperature of 500 K,[1] and few vitiation studies have been considered.

1.2.3 Laminar flame speed measurements of alkenes

The authors of references [39, 47, 48] stated that one fuel property that strongly influences performance in jet engines, such as soot formation and heat release, is overall H/C ratio. Table 1.2 indicates that for jet fuels the average H/C ratio is approximately two. The general formula for alkenes is C_nH_{2n} and thus they also have an H/C ratio of two. Alkenes also are key intermediates in the oxidation of higher hydrocarbons [49, 50] and have also been identified as one of the important precursors for soot formation in combustion systems [51]. Moreover, alkenes form the major products during thermal

[1] There are certain limitations to measure laminar flame speeds of jet fuels at these conditions and these are discussed in Chapter 2 of this thesis

cracking of hydrocarbons. For example, when liquid fuels are used as thermal heat sinks in hypersonic vehicles, the increase in temperature promotes thermal cracking and the formation of alkenes - specifically ethylene [52]. Also, modern approaches to develop chemical kinetic models divide reaction chemistry of jet fuels in to two stages (see Hychem model [53-56]). The first stage involves break down of large fuel species to smaller species (such as alkenes) via pyrolysis and the second stage is the oxidation of these smaller species to final products. The above mentioned reasons imply that alkene reaction chemistry not only forms an important part of jet fuel chemistry but also as a standalone fuel may have important chemical characteristics that are similar to jet fuels, thus making it valuable to study alkene kinetics at realistic jet engine operating conditions.[2]

Laminar flame speed measurements of alkenes have been reported by several research groups using different techniques. Raezer et al. [57] measured flame speeds of ethylene and air mixtures at atmospheric pressure and room temperature using double-kernel method (where two expanding spherical flame fronts approach one another). Egolfopoulos et al. [58] measured laminar flame speeds of C_2 hydrocarbons, including ethylene-air and acetylene-air mixtures, using a counter flow flame technique. The data was taken over a range of equivalence ratios and pressure from 0.25 to 3 atm. Hirasawa et al. [23] investigated the effect of binary fuel blends on laminar flame speeds with ethylene, n-butane and toluene. In that work, a counter flow flame technique was used with the reactants at atmospheric pressure and temperature and the equivalence ratio was varied between 0.7 and 1.4. Jomaas et al. [59] measured laminar flame speeds of C_2–C_3

[2] A detailed explanation of using alkenes (specifically ethylene and propylene) as important intermediates to understand reaction chemistry of liquid fuels at high preheat temperatures is provided in Chapter 2.

hydrocarbons using a spherical bomb technique while varying the pressure between 1-5 atm for a preheat temperature of 300 K. Hassan et al. [60] measured laminar flame speeds of several hydrocarbons including ethylene at high pressure (4 atm) and room temperature (300 K) using a spherical bomb technique. Kumar et al. [51] varied the preheat temperature up to 470 K at atmospheric pressure for ethylene-air mixture; nitrogen dilution studies were also performed. An opposed-jet twin flame configuration was used for these measurements, which were also compared to several leading chemical kinetic mechanisms of the time. It was observed that different techniques produced different results and the kinetic models did not match the measurements. The models were later modified to match the experimental data at room temperature while the high preheat temperature effects are largely unexplored. Burke et al. [61, 62] measured laminar flame speeds of propylene-air mixtures at room temperatures using several different techniques and found a spread in the experimental data. To increase the accuracy of flame speed prediction (by chemical mechanisms) at room temperature they modified the rate coefficient of C_3H_5-A + H reaction by a factor two.

To understand the combustion chemistry of jet fuels at operating conditions, it is also important to study the vitiation effects, i.e., the effects of additional diluents like CO_2 and H_2O and with reduced oxygen levels compared to fuel-air combustion. For example, the oxygen percentage in afterburners can be as low as 12% [3]; thus understanding the reaction chemistry at these conditions is essential for an effective design of afterburners. Natarajan et al. [31] studied the effect of CO_2 dilution on several syngas (H_2/CO) mixtures for preheat temperatures between 300 and 600 K and a pressure range of 1-5 atm. Zhao et al. [63] examined the effect of N_2 dilution on laminar flame speeds of propane-air mixtures

at atmospheric pressure over a preheat temperature range 300–550 K. Gokulakrishnan et al. [33] investigated the effect of CO_2 dilution on propane air mixtures at 650 K and atmospheric pressure.

1.2.4 Summary

Little work has been done to measure flame speeds of fuels relevant to aircraft jet engines at elevated preheat temperatures and to characterize the effects of vitiation on flame speed for these fuels. Most of the flame speed measurements conducted for n-decane are limited to 500 K preheat temperature, while for ethylene and propylene flames these are mostly limited to room temperature measurements. Furthermore there is also a lack of measurements for vitiated flow conditions where the oxygen content in the oxidizer is lower than that of air.

Based on the flame speed measurements at room temperature, changes to chemical kinetic mechanisms were made so as to match the predictions from these mechanisms with the experimental measurements. There is a need to validate these mechanisms at engine operating conditions for alkenes as it was shown previously for syngas [30, 31] and alkane [32, 33] measurements that elevated preheat temperature and vitiation effects are not accurately captured by chemical kinetic models.

The reaction zone area based Bunsen flame technique is one of the few approaches that has been employed to make flame speed measurements at high preheat temperatures. Thus it is a good candidate for measuring laminar flame speeds of liquid fuels and alkenes at similar conditions. However, there are questions about the accuracy of the approach due to stretch effects that remain to be addressed.

1.3 Thesis objectives

One objective of this thesis is to create a database of laminar flame speed measurements of alkenes (ethylene and propylene) at high preheat temperatures and low O_2 conditions relevant to jet engine operation. These measurements can be used to understand the effects of preheat temperature and vitiation on laminar flame speeds. Moreover, they can be used to assess the performance of leading chemical kinetic mechanisms. To this end, a second objective of the thesis is to provide a better understanding of preheat temperature and dilution effects on laminar flame speeds of ethylene and propylene, and to identify possible improvements in leading reaction mechanisms based on the flame speed measurements. A third objective of this work is to understand the limitations and accuracy of the Bunsen flame technique based on reaction zone area, with a special focus on sensitivity to flame stretch.

1.3.1 Thesis organization

This general outline of the thesis is as follows. Chapter 2 discusses the limitations on measuring flame speeds of liquid fuels at high preheat temperatures. Also, usage of alkenes as a key intermediate to understand the reaction chemistry of liquid fuels at engine operating conditions is discussed in that chapter. Chapter 3 provides the experimental approach used in this study, followed by a description of the modelling approaches used to answer questions pertinent to this thesis. Chapter 4 provides a validation of the Bunsen flame technique by comparing to measurements from standard stretch-corrected methods. Stretch and flame height effects on Bunsen flames are also examined in this chapter. Measurements of laminar flame speeds of ethylene-air and propylene-air mixtures at

various preheat temperature are presented in Chapter 5. The chapter includes discussion of data trends and comparisons to flame speeds predicted using leading chemical mechanisms. Chapter 6 covers the influence of reduced oxygen content associated with vitiation (using CO_2 and N_2 as diluents) on laminar flame speed. Again both measurements and results of 1-d flame simulations are compared and analyzed. Chapter 7 identifies several key reactions that may be responsible for the differences observed between the measured and predicted alkene flame speeds, including both preheat temperature and dilution effects. Finally, Chapter 8 provides a summary of accomplishments in this thesis along with recommendations for future work.

CHAPTER 2. Jet-fuel flame speed measurement limitations

The aim of this chapter is to discuss the limitations of laminar flame speed measurements of liquid jet-fuels at high preheat temperatures. Initially, experimental flame speeds at high preheat temperatures for liquid fuels are discussed. Limitations on flame speed measurements for liquid fuels at high preheat temperatures with current experimental capabilities are provided. Arguments regarding the usage of ethylene and propylene as important intermediates to understand reaction chemistry of liquid fuels at high preheat temperatures are then examined in detail. Flame speed and plug flow reactor modeling are performed using Chemkin-Pro [64] and are discussed in detail in the next chapter, as is the experimental facilities used to determine flame speed.

2.1 N-decane S_L measurements at high preheat temperatures

The effect of increase in preheat temperature on the simulated and measured laminar flame speeds of n-decane, a major constituent of jet fuels, is revealed in Figure 2.1. In general, increased preheating would be expected to lead to higher laminar flame speeds, as this produces higher flame temperatures, which in turn lead to higher flame speeds. This trend is captured by both mechanisms investigated (JetSurf [65] and CSE [66]); the measurements at 550 K, however, defy expectations: the flame speeds do not increase and in some cases decrease compared to the 450 K results. While not shown here, the measured flame speeds at an even higher temperature (650 K) were lower than those measured at 550 K.

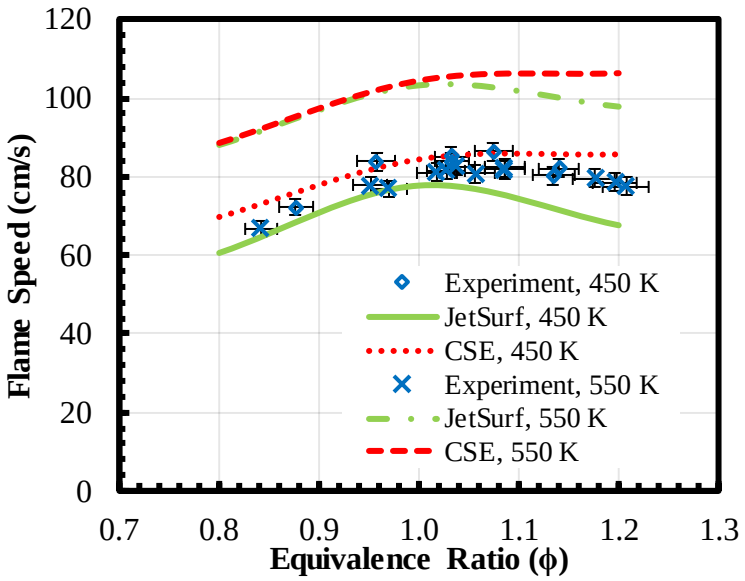

Figure 2.1: Laminar flame speed variation for n-decane/air mixtures for different preheat temperatures at atmospheric pressure.

Repeated measurements and calibrations verified that this behavior was not due to errors associated with flow rate or flame area measurements. To investigate possible chemical changes that could be occurring due to preheating, a plug flow reactor model was used with an estimated residence time based on the conditions in the heating zone of the plenum just upstream of the burner, where the temperature is increased from under 400 K to the final preheat temperature. Based on the preheater volume, the residence time of the gas in the heating zone is between 10-20 seconds, depending on the flow conditions. The computational approach used to perform these studies is discussed in the following chapter. The results from the CRECK mechanism [67] are presented here, as it is the most comprehensive mechanisms considered that includes both high and low temperature chemistry for n-decane.

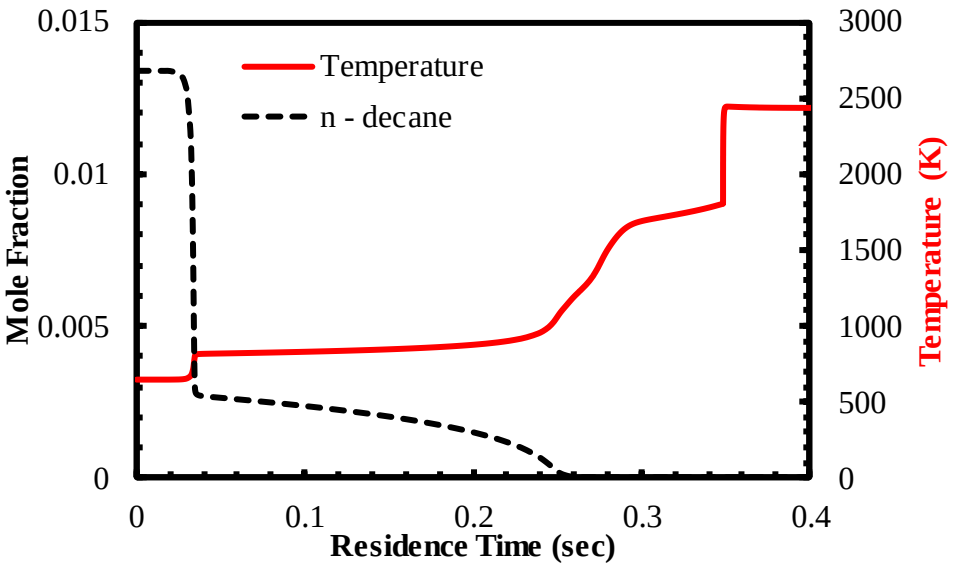

Figure 2.2: Two stage autoignition of n-decane air mixture using CRECK mechanism, at $\phi = 1$, $T_u = 650$ K and atmospheric pressure.

For inlet conditions based on one of the high preheat cases (650 K, ϕ=1), Figure 2.2 reveals the occurrence of autoignition in the heating zone of an adiabatic plug flow reactor (PFR) after a time that is an order of magnitude lower than the estimated residence time in the heating section of the experimental facility. A two-stage reaction process is clearly observed, with the first set of reactions that convert the parent fuel occurring at ~0.04s, and the second set that involve the major heat release start at a residence time ~0.24s. This two-stage process for low temperature autoignition of high-order hydrocarbon fuels has been observed previously [40, 68, 69].

If the full autoignition process was to occur in the actual preheater, the temperature of the mixture would tend to increase toward the adiabatic flame temperature (~ 2500 K). There is no evidence of this, as the thermocouple located just upstream of the burner exit remained at the chosen preheat temperature (e.g., 550 or 650 K). This suggests that the

plenum is acting as a heat sink and, combined with the feedback circuit present in the heating system, prevents the complete autoignition process (e.g., the second-stage reactions) from occurring.

As the measured temperature at the preheater exit did not change in time, simulations were repeated for a constant temperature PFR; this allows us to examine pyrolysis and partial oxidation effects occurring at low temperatures**.** Figure 2.3 shows results from such a simulation for the same inlet conditions examined above (650 K, $\phi = 1$). As in the adiabatic PFR simulation, the n-decane ($NC_{10}H_{22}$) concentration decreases rapidly after a residence time of ~40-50 ms. Thus the reactant mixture exiting the preheater and entering the nozzle of the burner is unlikely to contain much of the parent fuel. Rather, the Bunsen flame reactants include low temperature partial oxidation products. The products with the highest mole fractions are CO and H_2O, designated as major products and indicated on the right axis of the figure. The minor products with the largest mole fractions after ~100 ms include, in decreasing order, acetaldehyde (CH_2O), ethylene (C_2H_4) and CO_2 (see left axis).

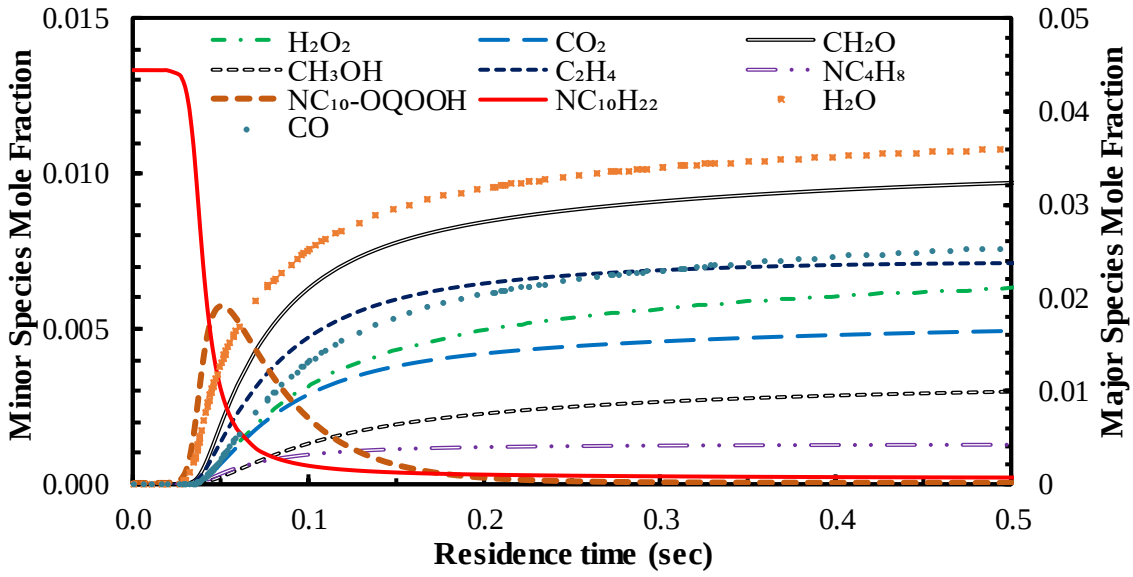

Figure 2.3: Constant temperature PFR simulation of products of low temperature, partial oxidation of n-decane and air (T_u = 650 K, ϕ = 1, and atmospheric pressure); right axis: mole fractions of major species (CO and H_2O), left axis: most prevalent minor species.

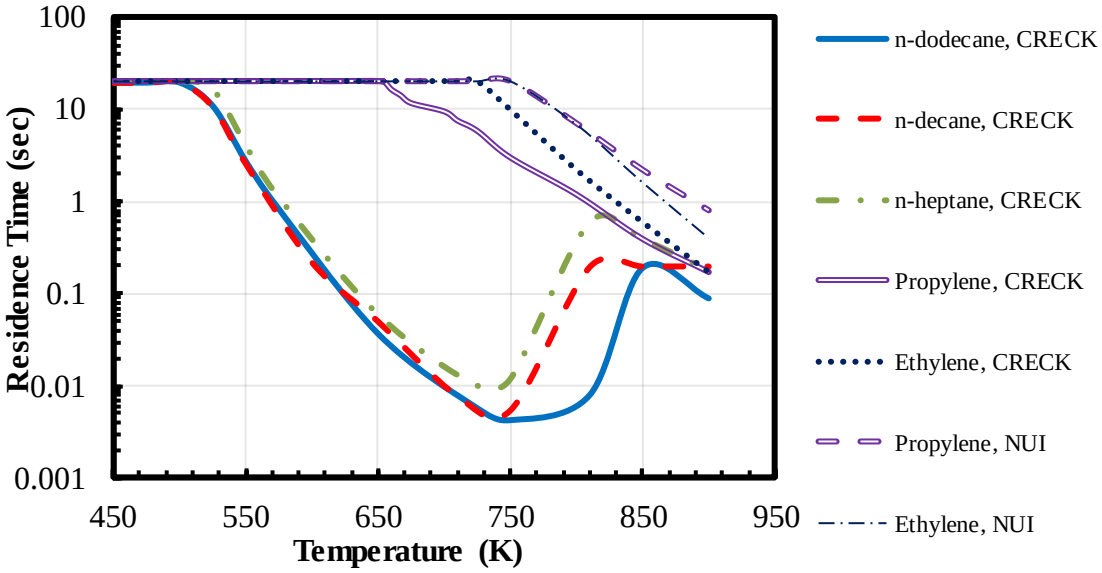

Figure 2.4: Residence time required for the mole fraction of fuel to decrease by ten percent of initial mole fraction simulated using CRECK [67] and NUI [61] (for ethylene and propylene), at ϕ = 1 and atmospheric pressure.

These effects are detrimental to the measurement of laminar flame speeds at high pre-heat temperatures for jet fuels. As seen in Figure 2.4, these constant temperature partial oxidation reactions also occur for other surrogate liquid fuels like n-dodecane and n-heptane at higher preheat temperatures. Taking a residence time of 10 seconds as a bench mark for the minimum time required to produce a uniformly preheated laminar flow, the constant temperature PFR model is run for these three liquid alkanes at various preheat temperatures. The figure shows the residence time required for the parent fuel mole fraction to decrease by 10 percent; this gives a nominal temperature up to which the laminar flame speed values can be measured experimentally for these potential jet fuel surrogates. For n-decane and n-dodecane this temperature is ~525 K, whereas for n-heptane it is ~540 K. Though the temperatures at which these fuels are partially oxidized are very close, the rate at which these reactions occur is significantly different.

2.1.1 HORIBA O_2 concentration measurements

The constant temperature model predicts that the fuel (n-decane) is partially oxidized at higher temperatures. To check this prediction, an experiment was devised to measure the mole fraction of O_2 in the stream using a HORIBA Gas analyser (PG-300); this gas analyser has the ability to measure the concentration of five species (O_2, CO_2, CO, SO_2, and NO_x) within a given mixture of gas. The concentration of O_2 is considered for this experiment, as it is present abundantly and the variation can be tracked. These measurements are generally a qualitative indication of reactions happening in the preheat chamber before the mixture reaches the burner edge. A probe is placed inside the preheat chamber where the fuel and air are already premixed, this probe collects a small sample of the mixture from the premixed and preheated chamber to measure the concentration of O_2.

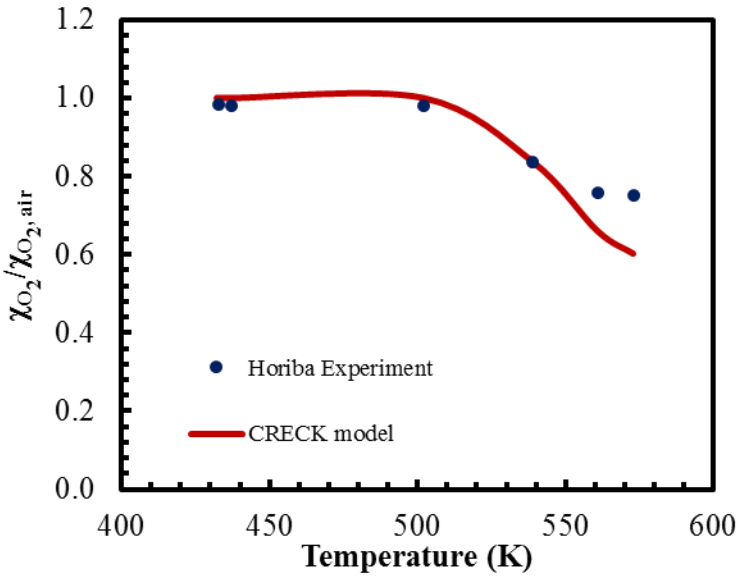

Figure 2.5: Measured O_2 mole fractions exiting preheater chamber for stoichiometric n-decane and air mixture at various preheater temperatures.

The results are displayed in Figure 2.5. The O_2 level drops beyond a preheater temperature of between 500 and 540 K. The figure also includes predictions from the constant temperature PFR model using the CRECK chemical kinetic model and a residence time of 10 s. The model predictions match the measured trend up to at least 550 K; furthermore, the model indicates the partial oxidation begins at a preheat value of ~500 K.

These measurements confirm the hypothesis put forward; specifically, measurement of flame speeds for liquid jet fuels and their surrogates at high preheat temperatures is not possible using the current measurement technique. Furthermore, other steady flow S_L measurement techniques (such as flat-flame, opposed-jet, and stagnation flame) would have similar preheat residence times, and quiescent approaches (spherical flames) require even longer preparation times to ensure uniform reactants. Thus the other established flame speed measurement approaches should suffer similar problems in

measuring flame speeds of liquid (jet) fuels at high preheat conditions. In fact, Won et al. [70] experimentally observed a similar influence of low-temperature chemistry for n-heptane in a constant temperature flow reactor while conducting turbulent flame speed measurements. Low-temperature chemistry was observed between 500 K and 600 K.

2.2 Alkenes as base fuels for jet fuel validation

The above analysis indicates that the measurement of laminar flame speeds at high preheat temperatures is not possible using current methodologies. The residence times need to be decreased from the order of seconds to the order of milliseconds, while keeping the flow laminar and generating a uniform gas mixture. Thus chemical mechanisms for jet fuels, alternate jet fuels, and other heavy, liquid-hydrocarbon fuels cannot be sufficiently evaluated with direct flame speed measurements.

One possibility is to consider the validity of using alkene flame speed measurements as an approach to (partially) validate jet fuel mechanisms at extreme conditions. Figure 2.6 depicts the variation of fuel species and the temperature inside an n-decane air flame at 650 K. As the temperature of the reactant mixture increases, reactions start occurring and the concentration of n-decane decreases rapidly, much like what occurred in the low temperature PFR simulations. During this process, there is a buildup of certain lower hydrocarbons: ethylene (C_2H_4), propylene (C_3H_6) and methane (CH_4). In addition, this zone contains high levels of H_2 and CO. Thus, these various fuels are the actual reactants in the heat release zone of the flame. While the chemical properties of syngas (CO and H_2) and methane have been extensively studied at higher temperatures, there is less data on alkene chemistry, especially at high preheat temperatures.

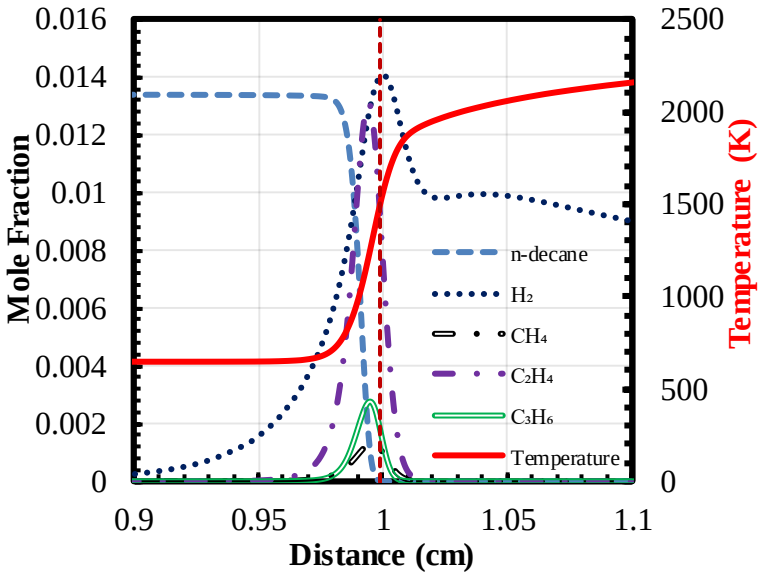

Figure 2.6: Simulated fuel species profile inside an n-decane/air laminar flame (using CSE mechanism) for ϕ = 1, T_u = 650 K and atmospheric pressure.

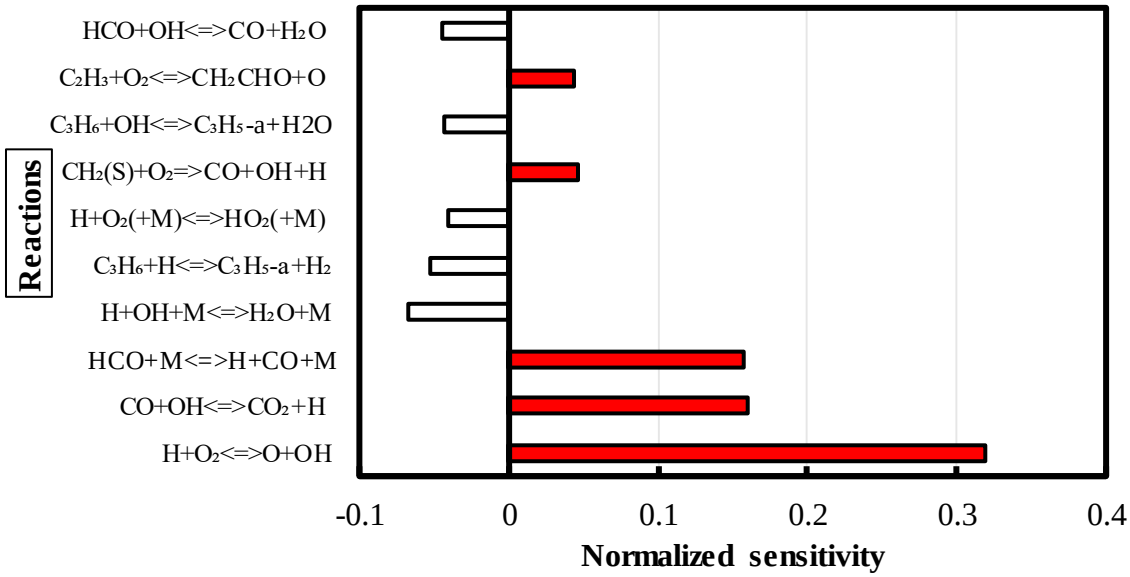

Figure 2.7: Normalized flame speed sensitivity to A-factor of rate coefficients of different reactions (using CSE mechanism) for n-decane/air mixture at ϕ = 1, T_u = 650 K and atmospheric pressure.

The importance of alkenes in jet fuel chemistry can be studied by performing a reaction sensitivity analysis on laminar flame speed and a reaction pathway analysis. Figure 2.7 shows the sensitivity of S_L to the A-factor of various rate coefficients for a stoichiometric n-decane/air mixture at a preheat temperature of 650 K, based on the CSE mechanism.[3] Normalized sensitivity provides an indication of how an S_L value would change with a change in the rate coefficient of a particular reaction, indicating which reactions have the most significant effect on flame speed value.

Considering the ten reactions that have the greatest sensitivity, the standard H_2/CO chemistry responsible for most of the heat release in a flame features prominently. The next set of reactions that influence flame speed involve alkenes (specifically C_3H_6) and these reactions negatively influence S_L, i.e., increasing the A-factor for these reactions leads to an S_L reduction. The reaction $C_3H_6+H \Leftrightarrow C_3H_5\text{-}a+H_2$ is the fifth most sensitive reaction and the most sensitive reaction involving a stable hydrocarbon.

Furthermore, the reaction pathway analysis performed for the same mixture (Figure 2.8) shows that the most important step in converting n-decane (the parent fuel) to CO_2 (a major product) is the formation of ethylene (C_2H_4). These results demonstrate that the formation of ethylene and its subsequent destruction is a major process in combustion of high order alkanes. Clearly, alkenes play a major role in affecting the laminar flame speed of n-decane/air mixtures.

[3] The details of how sensitivity analysis is performed are in Chapter 7 where chemical kinetics are discussed in extensive detail.

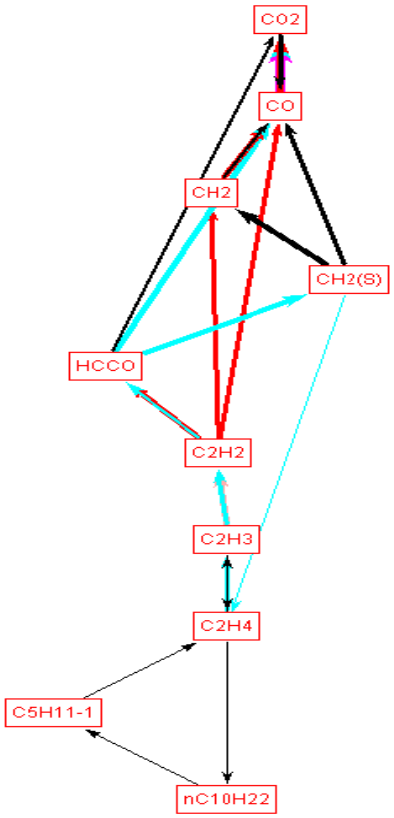

Figure 2.8: Reaction pathway analysis (CSE mechanism) of n-decane forming CO_2 for n-decane/air mixture of $\phi = 1$, $T_u = 650$ K and atmospheric pressure.

The importance of alkenes in jet fuel chemistry is further evidenced by a recent approach (HyChem) to chemical kinetic mechanism development that replaces the numerous and detailed pyrolysis and partial oxidation steps for complex (heavy hydrocarbon) jet fuels with a few "global" steps that produce smaller hydrocarbons considered to be important [53-56]. Essentially, the mechanism is based on the validated assumption that the conversion of the complex hydrocarbons to simple hydrocarbons occurs rapidly, much faster than the oxidation reactions that lead to the majority of the heat release. The smaller hydrocarbons identified in the HyChem mechanism are C_2H_4, H_2, CH_4, C_3H_6, 1-butene (1-C_4H_8), *iso*-butene (*i*-C_4H_8), benzene (C_6H_6), and toluene (C_7H_8).

The oxidation of these species is then modeled using smaller chemical mechanisms [61, 62, 71], which are tuned to study the oxidation of lighter hydrocarbon species. This approach indicates that accurate prediction of the chemistry of lower hydrocarbons, including ethylene and propylene, can lead to accurate predictions of the chemical behavior of heavier hydrocarbons.

Thus it may be possible to validate and improve chemical mechanisms being developed for jet fuels by measuring flame speed for alkenes (specifically C_2H_4 and C_3H_6) at high temperatures (and pressures), if they do not suffer from the same low temperature chemistry problems observed for the heavy alkanes. In addition to the previously discussed alkane results, Figure 2.4 includes results for the preheater residence times required to observe partial oxidation of C_2H_4 and C_3H_6. Much higher preheat temperatures (> 650 K) are required for these alkenes. Results are shown for two mechanisms, NUI which is tuned for alkene chemistry, predicts these reactions at an even higher preheat temperature compared to the CRECK mechanism. Thus it should be possible to obtain accurate flame speeds measurements of these alkenes up to at least 650 K preheat temperatures.

2.3 Summary

In this chapter, limitations on laminar flame speed measurements for liquid fuels are discussed. Due to low temperature pyrolysis and partial oxidation becoming relevant in the preheat chamber at high preheat temperatures it is not possible to measure S_L of liquid jet fuels and other complex, heavy hydrocarbons using contemporary techniques. On the other hand, the flame speeds of ethylene and propylene can be measured at high preheat temperatures (at least up to 650 K) without being affected by low temperature chemistry.

Since these alkenes also form important intermediates in jet fuel reaction chemistry, their oxidation chemistry is important to the understanding of jet fuel chemistry. Thus measuring flame speeds of alkenes at jet engine relevant conditions, and using these results to validate relevant chemical mechanisms will lead to better understanding of reaction chemistry of jet fuels and accurate prediction of their chemistry.

CHAPTER 3. Approach

There are several approaches to measure laminar flame speed as discussed in Chapter 1. These techniques can be broadly divided into stretch corrected measurements and measurements using weakly stretched flames. For the data measured in this thesis, the reaction-zone area Bunsen flame technique (BFT) is used. This chapter provides the details on how the BFT was implemented in this study, including the facility and all the measurement methods. This study also employs chemical reactor modeling to predict flame speeds and to simulate important aspects of preheat flow facilities. This chapter also details the different types of flow reactor models (from Chemkin-Pro [64]) employed; these include: a premixed flame reactor, a plug flow reactor and an opposed flow reactor. Finally, the detailed chemical mechanisms used in these models are presented, and the complexity of each is discussed.

3.1 Experimental Approach

The modified approach to measuring flame speed using Bunsen burner flames is described in detail in previous publications [20, 21, 29-33, 72-75]; a brief overview is provided here. Since a Bunsen flame is curved, it is prone to be affected by curvature and strain effects. Therefore it is prudent to examine these effects on flame speed measurements. Sun et al. [76] performed an integral analysis to describe the unsteady propagation of a curved flame in a strained field. Their analysis showed that the unburned side of the flame is generally affected by both curvature and strain effects, whereas the burned side of the flame is only affected by strain. Furthermore, by making sure the flame is steady, the strain effects can be minimized. Thus the burned flame speed ($S_{L,b}$) is affected

by strain, but a weak function of flame curvature. Choi et al. [77] demonstrated that for an axisymmetric Bunsen flame the effect of strain on $S_{L,b}$ is minimal on the linear portion of the flame (wings of the flame) when compared to the curved region at the tip of the flame. However, they also noticed that the curvature at the tip of the flame cannot be ignored. The effects of curvature on axisymmetric Bunsen flames for different mixtures is discussed in Chapter 4 of this thesis; it can be demonstrated that if sufficiently tall flames (large flame height (*H*) to burner diameter (*D*) ratio) are considered, the dominant contribution to total burned area is derived from the linear portion of the flame, and the contribution from the curved region is minimal.

The above discussion suggests that burned flame speed should be approximately equal to the unstretched one-dimensional burned flame speed i.e., $S_{L,b} = S_{L,b_o}$, if certain precautions are taken (for steady, tall axisymmetric flames). Natarajan et al. [31], based on these observations, first suggested that it is possible to measure laminar flame speed of a mixture using the burned area of Bunsen flame as opposed to the unburned area. The derivation is as follows. First from the continuity equation, the mass flowrate through the flame can be defines as $\dot{m} = \rho_i S_{L,i} A_i$, where $\dot{m}$ is the mass flow rate, ρ is the density, A is surface area, and the subscript i refers to a specific flame surface (e.g., u refers to the unburned surface ahead of the flame's preheat zone, and b represents the burned/product zone surface). Also for a one-dimensional flame, the continuity equation dictates that $\rho_u S_{L,u_o} = \rho_b S_{L,b_o}$. The unstretched laminar flame speed can then be calculated from the following equation (1),

$$S_{L,u_o} = \frac{\rho_b S_{L,b_o}}{\rho_u} \approx \frac{\rho_u S_{L,b}}{\rho_u} = \frac{\dot{m}}{\rho_u A_b} = \frac{\dot{Q}}{A_b} \quad (1)$$

where $\dot{Q}$ is the (measureable) volumetric flow rate of the reactants. Thus a reasonable approximation of the unburned, unstretched flame speed can be determined by measuring the *burned* surface area. In fact, measurement of the reaction zone area (~A_b) of a Bunsen flame, as opposed to the inner edge of the preheat zone, has been shown to provide a better estimate of the unstretched flame speed [31].

Previously this method has been used to measure the flame speeds[4] of syngas (H_2/CO) and alkane fuels with high accuracy. In the current work, alkene flame speeds are measured at different mixture conditions. The following subsections describe the experimental facility used to measure flame speeds, the flow metering techniques used to capture the volumetric flow rate of the reactant mixtures, and the chemiluminescence method used to image the flame and to calculate the burned flame area.

3.1.1 Experimental Facility

A schematic of the experimental facility is shown in Figure 3.1. This facility uses either a contoured nozzle or tube burner to generate the Bunsen flame. The fuel-air mixture of interest is created using a bank of calibrated rotameters. After creating the desired mixture, it is thoroughly mixed along the supply lines to the burner. The mixture is then passed through a plenum that is wrapped with heating tape to achieve the desired preheat temperature.

[4]For the purpose of this thesis, the unstretched flame speed (S_{L,u_o}) will be interchangeably used with flame speed (S_L) depending on context. For example, unstretched laminar flame speed experimental measurements are generally referred to as flame speed measurements.

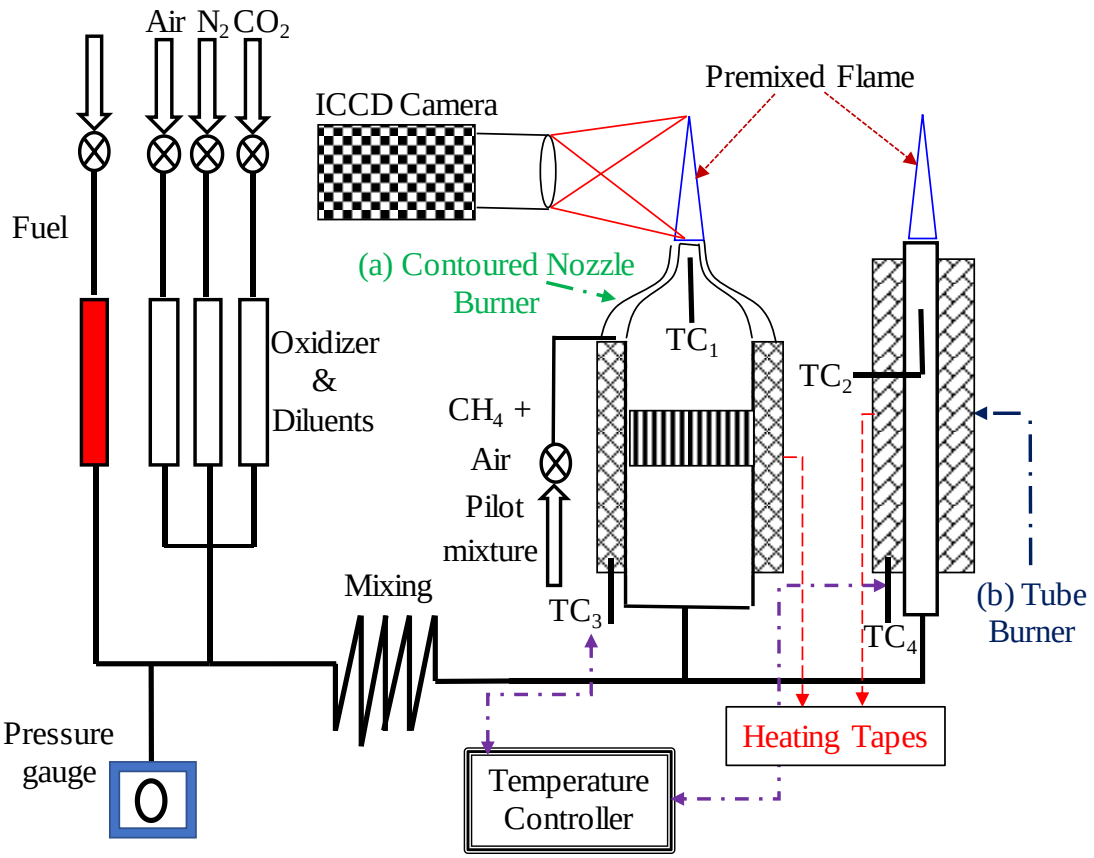

Figure 3.1: Schematic of the experimental facility to measure laminar flame speed using BFT at high preheat temperatures using either a contoured, axisymmetric nozzle burner or a straight, cylindrical tube burner.

The reactants are preheated in the mixing section and the burner plenum by electrical resistance heating tapes. The heating tapes are connected to a temperature controller that operates on a feedback loop while monitoring the temperature of the heating tapes using K-type thermocouples TC_3 and TC_4. The TC_1 and TC_2 thermocouples (also K-type) are used to measure the premixed (reactant) gas temperature. These thermocouples are placed at the center of the burner, ~25mm below the exit. Once the operating temperature is reached, the heating tape temperature is kept constant, thus maintaining the reactant temperature within ± 3 K from the temperature of interest.

The contoured nozzle and the tube burner aim to produce a uniform top-hat and parabolic velocity profiles respectively for the exiting gases, thus providing a smooth laminar flow. Depending on the flame speed of the mixture, different types of diameters (*D*) are used for the burners. The contoured nozzle burner used either a 9 or 6 mm diameter with contraction ratios of 72 and 161; this ensures a steady laminar flow even at high Reynolds numbers. The tube burner employed tubes of diameters ranging from 4.5-18 mm while maintaining the tube length to be at least 50*D* to ensure the flow is fully laminar and the exit velocity profile is fully developed to a parabolic profile. The flame is stabilized at the burner, which sits on the top of the plenum after the preheating zone. The burner is pilot stabilized in the case of the contoured nozzle or is not in case of a tube burner this pilot flame is produced with a sintered plate surrounding the nozzle; it is a near-stoichiometric, flat, annular, methane-air flame.

The complete burner assembly is placed in a nitrogen ventilated pressure chamber with optical access for flame imaging. A N_2 co-flow provides an inert environment and keeps the pressure chamber cool and windows clear of water vapor condensation. Optical access is provided by three quartz windows, these windows are 1 inch in thickness and 2 inches in diameter; these windows are rated for an operating pressure of 10 atm. The operating pressure for the current experiments varied between 29.94 and 30.35 in Hg (1.014-1.028 bar). This is a small variation with respect to its impact on flame speed, and the operating condition is denoted as atmospheric pressure throughout this thesis. For atmospheric pressure measurements the burner is placed in the pressure chamber but without the N_2 co-flow, the optical windows are left in place to sufficiently isolate the flame from drafts in the room which could disturb the flame and lead to unsteady flames.

The facility is also capable of measuring laminar flame speeds of pre-vaporized liquid fuel mixtures. This was achieved using both a commercially available vaporizer and a custom vaporizer, fabricated in-house to vaporize liquid fuel (n-decane). Complete details of the pre-vaporizing systems are discussed in Appendix A.

3.1.2 Flow metering and flow rate determination

The gases used in this work are procured from Airgas; their purity levels are shown in Table 3.1. The reactant gas flows are metered individually with a bank of rotameters and are introduced sufficiently far upstream to mix thoroughly before passing through the nozzle. Several rotameters are employed based on the required flow rate for each gas. Each rotameter is calibrated at an operating pressure of 80 psig; this ensures the flow leaving the rotameter is always choked. The gas rotameters are calibrated at the operating supply pressure with a bubble flow meter for low flow rates. The bubble meter is a Sensidyne Gilibrator2 standard flow calibrator, and three bubble cells were used. The bubble cells are interchangeable and are valid for three flow ranges: low flow cell with range 1 to 250 cc/min, standard flow cell with range 20 cc/min to 6 lpm, and high flow cell with range 2 to 30 lpm. The combined uncertainty in total mass flow rate is better than 2.7%; this uncertainty stems from the room pressure and temperature measurements as well as the uncertainty in the rotameter calibration. A detailed uncertainty analysis is discussed in Appendix B.

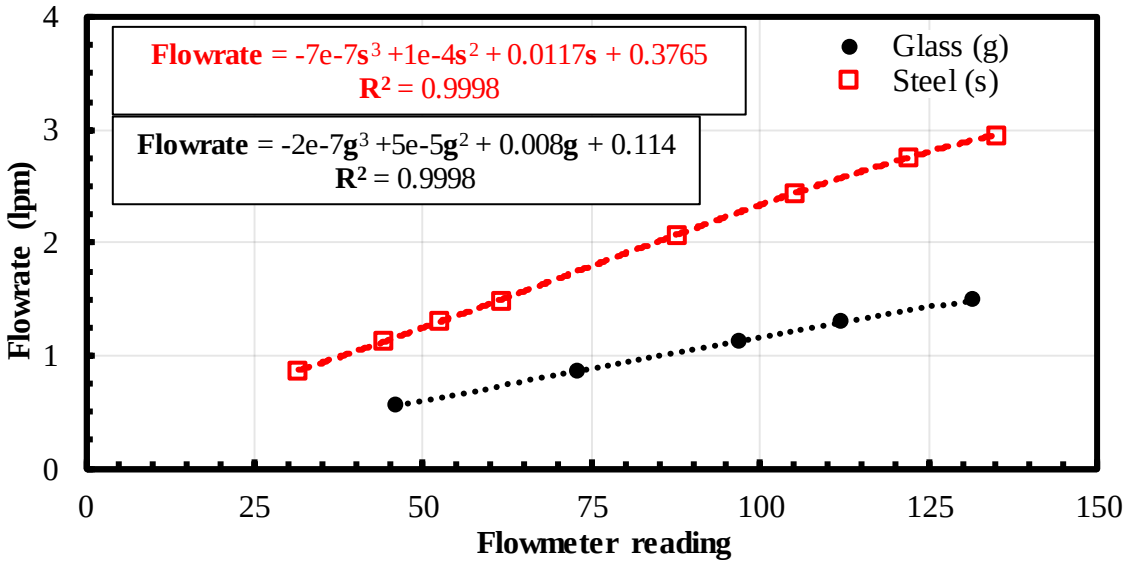

Figure 3.2: Example calibration plot for Matheson E602 (A) flowmeter calibrated using a Gilibrator bubble meter; the gas calibrated is ethylene at 80 psig.

Table 3.1: Purity levels of different gases used for the reactant mixture[5]

Gas	Grade	Minimum Purity	Impurities[6] (ppm)
CH_4	Chemically Pure	99.5%	$C_2H_6 \leq 1000$ $N_2 \leq 4000$
C_2H_4	Chemically Pure	99.5%	OHC[7] ≤ 1000
C_3H_6	Polymer	99.5%	OHC ≤ 4500
Air	Dry	O_2: 20-22%	<1000
N_2	Zero	99.998%	
CO_2	Instrument	99.998%	$N_2 \leq 70$ $O_2 \leq 20$

[5] http://airgassgcatalog.com/catalog/
[6] Only impurities greater than 10 ppm are reported
[7] OHC – Other hydrocarbons

The rotameters used in this study are Matheson high accuracy flow meters (Model FM-1050 series) with glass metering tubes (range of 150 mm), and both glass and stainless-steel floats. To calibrate a given rotameter for a particular gas, the gas pressure in the rotameter is maintained at 80 psig, and the glass and steel floats are maintained at a chosen position in the metering tube. Then the gas is directed into the bubble meter, and several readings (~6-10) are taken from which the average flow rate is calculated. This is repeated at several flow meter locations; in general, it is advised to avoid the first 30 mm and the last 20 mm of the metering tube due to high uncertainties caused by unsteadiness in the floats.

Then the results are fit to a third-order polynomial, separately for both the glass and steel floats. This polynomial can provide the flow rate at a given float location for a given flow meter, similarly a reverse curve fit is generated to get the float location for a given flow rate. An example calibration plot for the ethylene, along with the polynomial curves for both types of floats is shown in Figure 3.2. The high R^2 values shown here are typical of the calibration results. Each gas used has its own rotameter depending on the flow rate required; the gases exiting the rotameters are then mixed before they enter the preheater.

The flow rate required is based on an estimated flame speed from the computation modeling; in general, the velocity at the burner exit is assumed to be ~2-3 times the calculated flame speed. From this assumption, the required flow rate can be calculated based on the burner exit area. Once the total flow rate required is estimated, the composition of the gas is calculated using the equivalence ratio of the mixture and the composition of the oxidizer. The composition of the oxidizer changes for vitiated flow

conditions depending on the type of diluent used; in this thesis, N_2 and CO_2 are used as diluents of air to produce the oxidizer flow.

3.1.3 Flame area calculation

Using the optical access provided by the quartz windows, broadband chemiluminescence images of the Bunsen flame are collected by an f/4.5, 105 mm UV-Nikkor lens and recorded on a 16-bit ICCD camera. The pixel resolution of the imaging system is typically in the range 30–50 μm/pixel. The camera is sensitive in the visible and ultraviolet range and capable of capturing CH*, OH* and CO_2* chemiluminescence from the flame's reaction zone. In this thesis, broadband chemiluminescence is used to measure the burned flame area, as it was observed that the heat production zone (represented by the broadband CO_2* chemiluminescence) coincides with the reaction zone (represented by CH* and OH* chemiluminescence).

Figure 3.3 (a) shows the broadband chemiluminescence image of a stoichiometric ethylene-air flame at a preheat temperature of 650 K and atmospheric pressure. The thin heat-release/reaction zone can be clearly observed as the region with high intensity. To calculate the flame area of this region, the flame is first split into two halves based on the location of the tip. For each half, an edge detection algorithm based on the intensity gradient is employed to find the inner edge of the reaction zone (corresponding to the maximum gradient in the chemiluminescence signal). This location is chosen based on the analysis performed by Kochar [20] which demonstrated that there are no significant differences (<5%) between flame speeds measured using different locations (inner edge, outer edge or the center) of the reaction zone.

Figure 3.3 (b) shows the result of this edge-detection algorithm applied to the example of Figure 3.3 (a); the magenta colored dots are the location of the flame along the vertical axis. A polynomial curve-fit of fifth order through these edge pixels provides a smooth, analytic function. The area is then calculated assuming axisymmetry, e.g., by revolving the edge about the centerline. Each image thus provides two area measurements, one for each half image. The 100 reaction zone areas from 50 instantaneous images are averaged to determine the flame area, A_b, at each operating condition.

Any individual flame images that are: asymmetric, have open tips, or are lifted from the base are discarded from the average. The determination of whether a particular set of frames are symmetric and steady is done by calculating the difference in area generated by left and right half of the flame and the fluctuation in the mean area across all the frames under consideration respectively. In general, a first order determination is performed while performing the experiment, as the image exposure times are a few milliseconds highly unstable and asymmetric flames can be noticed by eye. Figure 3.4 (a) shows the representative symmetry of a flame, if the percentage difference between the areas measured using the left and right sides of a flame exceeds more than ±5%, the data set is discarded and the experiment is rerun at the appropriate conditions. To check the steadiness of a flame, the fluctuation in mean area is calculated across the 50 frames; if any of the frames have a fluctuation beyond ±5% they are discarded. If more than ten flames have these fluctuations, the whole data set is rejected, and the flame speed is measured again at the relevant operating condition. This method provides a certain way to check whether flames are axisymmetric as well as steady, this is crucial as the modified Bunsen approach described above assumes the flames to be so.

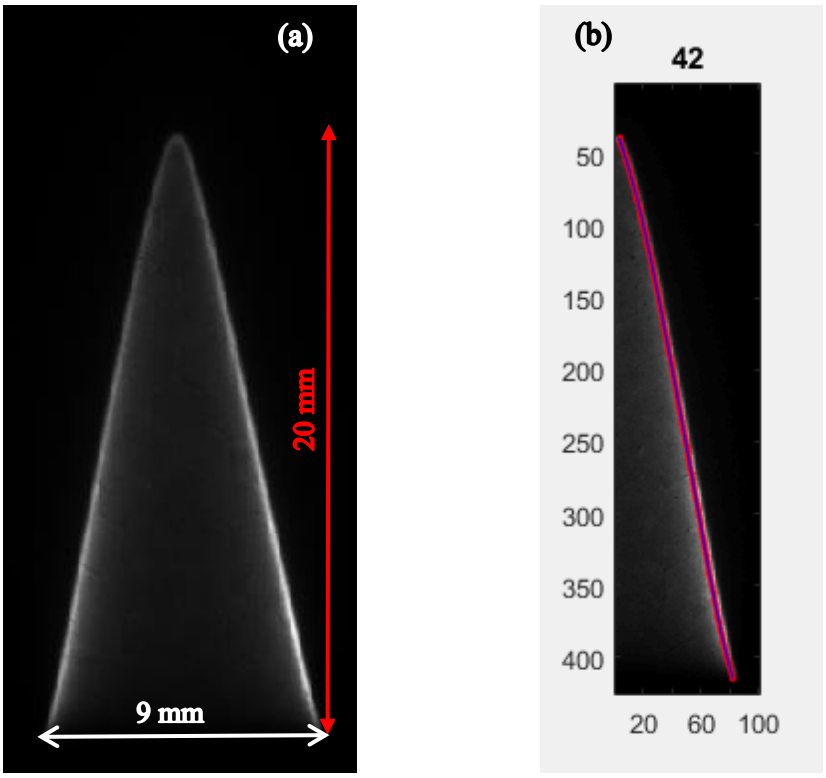

Figure 3.3: (a) Broadband chemiluminescence image of an ethylene-air flame captured at ϕ = 1, T_u =650 K and atmospheric pressure. (b) Corresponding flame edge-detection using a gradient based algorithm for a single frame (Frame number: 42, only edge detection for left half of the flame is shown here).

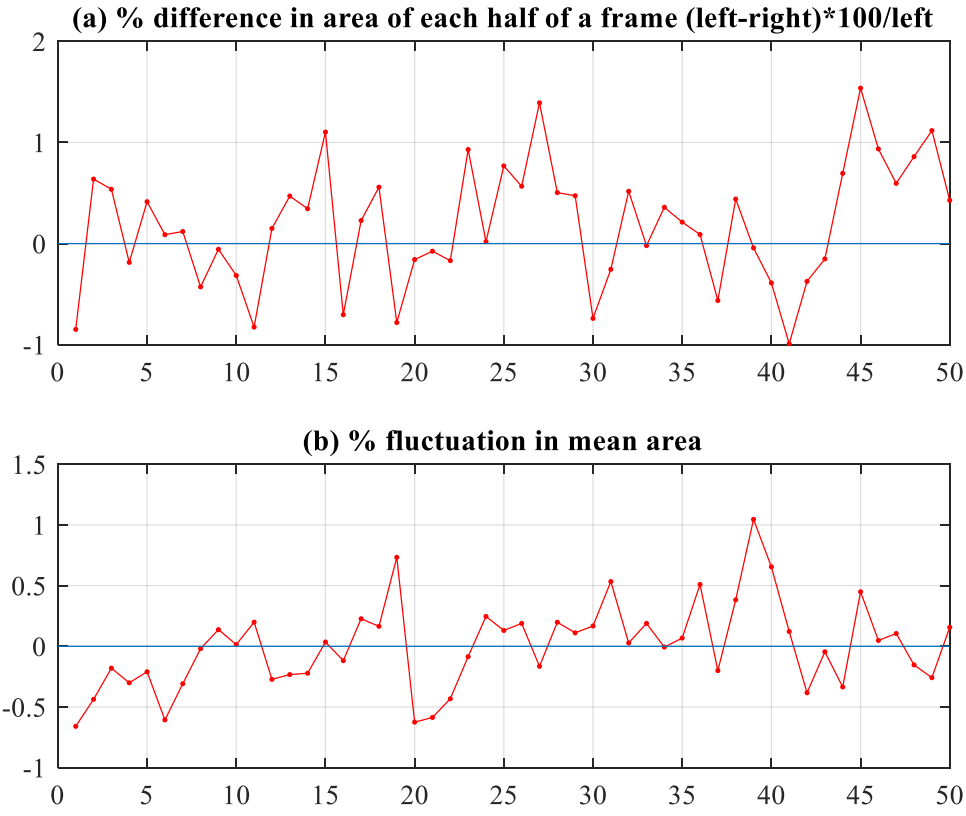

Figure 3.4: (a) Representation of flame symmetry by measuring percentage difference between areas calculated from two halves of the flame (b) Percentage fluctuation in the overall mean area across fifty frames, this represents steadiness of the flame.

3.2 Modelling Approach

The Chemkin-Pro[64] software is employed to model different kinds of flames and reactors to understand physical and chemical properties of heavy hydrocarbons. Mainly, flame speed predictions are used here to assess the performance of chemical kinetic models, while plug and opposed flow reactors are employed to examine potential systematic errors in the Bunsen approach for measuring flame speed.

3.2.1 Flame speed calculations

To predict the performance of chemical kinetic models, laminar flame speeds are computed using standard one-dimensional flame models. The accuracy of the kinetic models is tested by comparing measurements with unstrained laminar flame speeds calculated using the Chemkin PREMIX algorithm [78]. The simulations account for multi-component species diffusion and thermal diffusion (Soret) effects. The convergence of the solution is ensured by using a fine grid with a sufficiently large number of grid points. The final solution is obtained by using multiple continuations and progressively refining the grid using GRAD and CURV parameters to be 0.1. A finer grid is not used as refining the grid further increase the computation time by more than ten times while the flame speed value did not change by more than 1% as demonstrated by Kochar et al. [20, 32].

Apart from providing a flame speed value, these simulations also provide the species, temperature, and reaction rate profiles through the flame, which together are used to examine potential sources of error in the simulation predictions when compared to the experimental results. Also, a sensitivity analysis is carried out to identify reactions that are vital for flame propagation. This analysis provides a quantifiable dependence of the flame speed to changes in the pre-exponential factor of rate coefficients. Details about the sensitivity analysis are provided in Chapter 7.

3.2.2 Pyrolysis/partial-oxidation and auto-ignition calculations

To study the effects of reactions occurring in the mixing/preheat section of the flow facility, upstream of the burner nozzle, a plug flow reactor (PFR) is modeled in Chemkin [79]. Both the gas energy equation problem (auto-ignition) and the fixed temperature

problem (pyrolysis/partial-oxidation) can be solved. The PFR simulation is performed for a given residence time for the mixture in the preheat region. The residence time is calculated based on the volumetric flow rate and the volume of the preheating system. The effects of pyrolysis/ partial-oxidation at high preheat temperatures for heavy hydrocarbons were discussed in detail in Chapter 2.

3.2.3 Opposed-jet flame simulation

Premixed 1-d strained stagnation flames are simulated using the Chemkin-Pro OPPDIFF algorithm [80]. The distance between the jets is kept constant (20 mm), and the velocity is varied to change the strain rate and the flame stabilization location. Then the stretched flame speed and strain rate are determined as the minimum velocity before the flame and the maximum gradient of axial velocity before the flame, respectively; the latter occurs just before the minimum velocity location. The converged solutions in these simulations were obtained for a large number of grid points with implementation of continuations to gradually achieve a solution gradient and curvature of 0.1. OPPDIFF calculations are performed for three different fuel-air mixtures (CH_4, C_2H_4 and C_3H_8) representing fuels lighter, equal to and heavier than air. Three different equivalence ratios representing lean ($\phi = 0.6$), stoichiometric ($\phi = 1$) and rich conditions ($\phi = 1.4$) are studied at two different preheat conditions (300 K and 650 K) and atmospheric pressure.

3.2.4 Chemical Kinetic Mechanisms

A few well established chemical kinetic models are considered for the flame speed simulations. The CSE mechanism [66] can be used for n-decane and other higher order alkanes; it is a reduced order mechanism optimized for n-alkane fuel chemistry (435

species, 1714 reactions). The JetSurf reaction mechanism [65], which includes a higher number of chemical reactions but a lower number of species (348 species, 2163 reactions) was developed for a wider range of hydrocarbons including some aromatic compounds.

Table 3.2: Chemical kinetic mechanism considered for flame speed (PREMIX) predictions, PFR modeling (PLUG) and opposed jet flame modeling (OPPDIFF).

Mechanism	Fuels	Reactor	Species	Reactions
USC II	CH_4, C_2H_4, C_3H_6, C_3H_8	PREMIX, OPPDIFF	111	784
NUI	C_2H_4, C_3H_6	PREMIX, PLUG	315	1832
CSE	n-decane	PREMIX	435	1714
JetSurf	n-decane	PREMIX	348	2163
CRECK	n-heptane, n-decane, n-dodecane	PLUG	435	13,352

Alkene chemistry can be simulated using two well-known mechanisms tuned for gaseous fuel chemistry: USC [71] and NUI [61, 62]. These mechanisms were developed to understand the reaction chemistry of gaseous higher hydrocarbons (up to C_3-C_5) which will be of most relevance to this thesis. The USC mechanism is a reduced order mechanism with 111 species and 784 reactions, while the NUI mechanism is more comprehensive and is generated in a hierarchical way using mechanisms developed for lower order species and by adding the complex reactions of higher order hydrocarbons. It has 315 species and 1832 reactions. Both mechanisms are well validated with different kinds of fundamental

parameters using several experimental methodologies and are employed frequently in the literature.

The plug flow reactor study is performed with a more comprehensive mechanism that includes low temperature chemistry, which is unimportant for laminar flame speed modeling but plays a significant role in pyrolysis/partial oxidation reactions. This mechanism from CRECK [67] includes 435 species and 13,532 reactions, which is significantly more than the mechanisms used for flame speed measurements. In this thesis, the opposed jet model is used to understand Bunsen flame physics, so qualitative trends are of interest as opposed to the exact value. As these simulations are computationally intensive the reduced order USC mechanism will be employed so as to decrease the overall computation times.

CHAPTER 4. Validation results for Bunsen flame technique

This chapter examines the accuracy of the modern form of the Bunsen flame technique (BFT) for measuring laminar flame speed. This is accomplished by first validating current measurements of flame speed for alkene/air mixtures at standard conditions ($T_u \approx 300$ K and atmospheric pressure) with experimental data from the literature and kinetic model predictions. Possible sources of errors in measuring flame speed using the BFT are examined, including effects of stretch, strain and flame height. Then we determine the accuracy of the BFT technique with a comparison to standard stretch-corrected methods (spherical and stagnation flames) using data from the literature for a range of fuels: H_2/CO, alkane and alkene fuels, again at standard conditions.

4.1 Alkene Validation Results

4.1.1 Ethylene

Figure 4.1 compares the current BFT measurements of ethylene flame speed at several equivalence ratios with previous literature measurements for reactants at room temperature and pressure. The measurements are also compared with S_L predictions from two chemical kinetic models: the USC [71] and NUI [61, 62] mechanisms. Jomaas et al. [59] and Hassan et al [60] measured the flame speed of an aerodynamically stretched flame using the spherical flame technique. While Egolfopoulos et al. [58], Hirasawa et. al [23] and Kumar et. al [51] measured flame speed using the stagnation flame approach. The two mechanisms used to compare the experimental data, USC and NUI match very well with each other up to $\phi = 0.8$ (lean conditions) and differ at near-stoichiometric and

rich conditions. The experimental measurements follow a similar trend of agreement at lean conditions and small disagreements in the other two regimes. To quantitatively compare these measurements, the percentage difference between the literature and current measurements can be calculated.

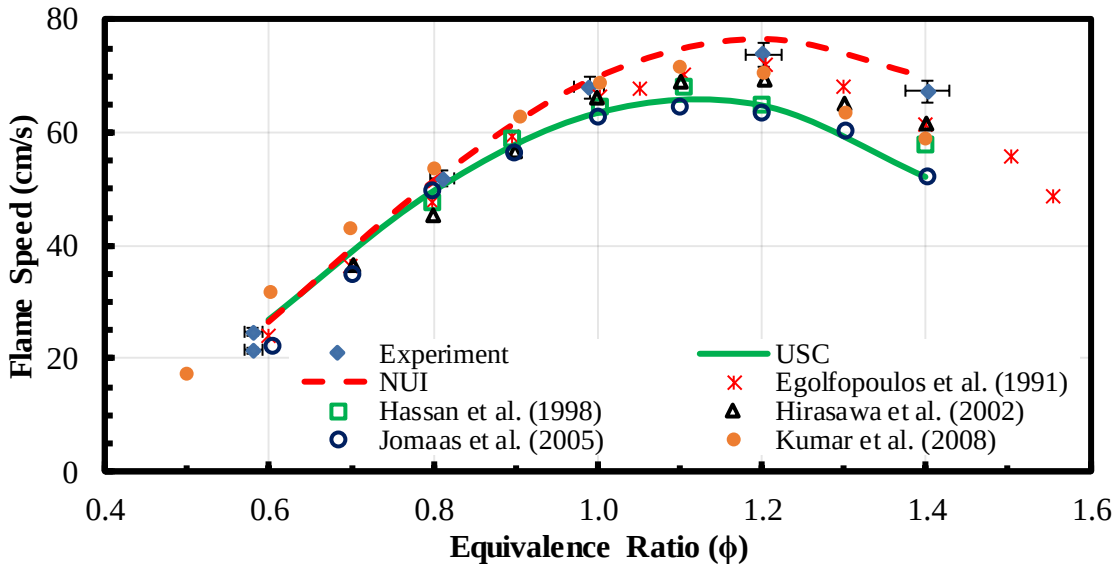

Figure 4.1: Validation of laminar flame speed measurements of ethylene/air mixtures at T_u = 300 K and atmospheric pressure; the error bars shown for the current measurements represent the random uncertainty in measured flame speed and equivalence ratio (with 95% confidence).

Figure 4.2 shows the percentage difference between the current measurements and the other results (both literature and model predictions). The percentage difference is calculated as shown in equation (2):

$$Percentage\ Difference = \frac{(S_{L,\ other} - S_{L,\ BFT})}{S_{L,\ BFT}} * 100 \qquad (2)$$

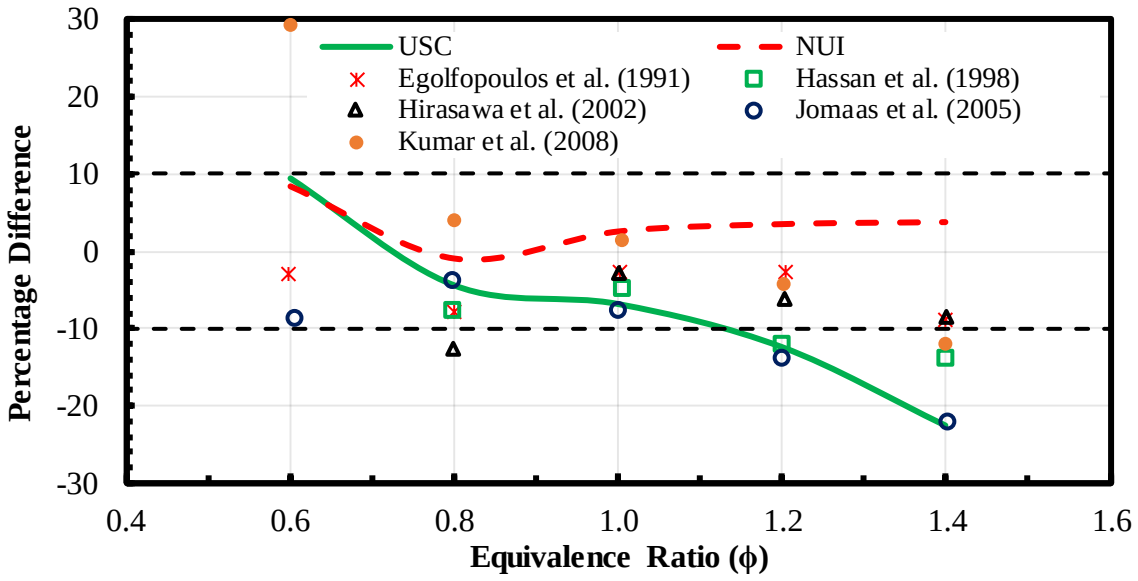

Figure 4.2: Percentage difference of measurements and kinetic model predictions from literature when compared with current BFT measurements of ethylene/air mixtures at T_u = 300 K and atmospheric pressure.

Several observations can be drawn from this graph. For example, the current data is within 10%[8] of the NUI kinetic model at all equivalence ratios. For the USC mechanism, the variation was within 10% for lean and stoichiometric cases, but the BFT result exceeds the USC prediction for rich conditions, by as much as 22% at ϕ = 1.4. Compared to the previous measurements, the current results are within 10% for most equivalence ratios. At only one condition, the richest (ϕ=1.4), do more than half of the previous data exceed this 10% range.

Examining each previous data set separately, the measurements from Egolfopoulos et al. are within 10% for all the equivalence ratios measured. The Jomaas et al. data matches

[8]In this thesis a percentage difference less than 10% will be considered as good agreement when comparing flame speeds. This is a standard widely used in literature when comparing flame speeds.

the USC model except at ϕ = 0.6, though the agreement with the BFT is still within 10% for the lean and stoichiometric mixtures. Conversely, the Kumar et al. data shows reasonable agreement at all conditions except at the leanest point (ϕ=0.6). The Hassan et al. and Hirasawa et al. measurements are lower than the current results at all equivalence ratios, but the differences are only more than 10% at ϕ = 0.8 for the Hirasawa data, and at rich conditions (ϕ = 1.2, 1.4) for the Hassan data. Still, the differences at these conditions are only slightly above the 10% range (12-14%). Thus we can conclude that measurements made using the BFT for ethylene at room conditions agree reasonably well with both previous measurements made using several different techniques and with the USC and NUI mechanism predictions.

4.1.2 Propylene

Similarly, Figure 4.3 compares the current experimental data for propylene/air mixtures at room conditions with previous experimental data and the chemical kinetic model predictions. The previous measurements utilize multiple techniques while the kinetic models remain the same from the ethylene/air comparison. The Princeton and TAMU results [62] and the Jomaas et al. [59] data were all obtained with spherically propagating flames, though using different extrapolation methods. Davis et al. [22] used the stagnation flame configuration, while the measurements acquired at VUB, Lund and LPRG [62] employed the heat-flux extrapolated, flat-flame approach. The largest spread amongst the previous measurements is observed on the rich side, where as the current BFT measurements differ the most from the previous measurements and chemical kinetic models on the lean side, especially below ϕ~0.7.

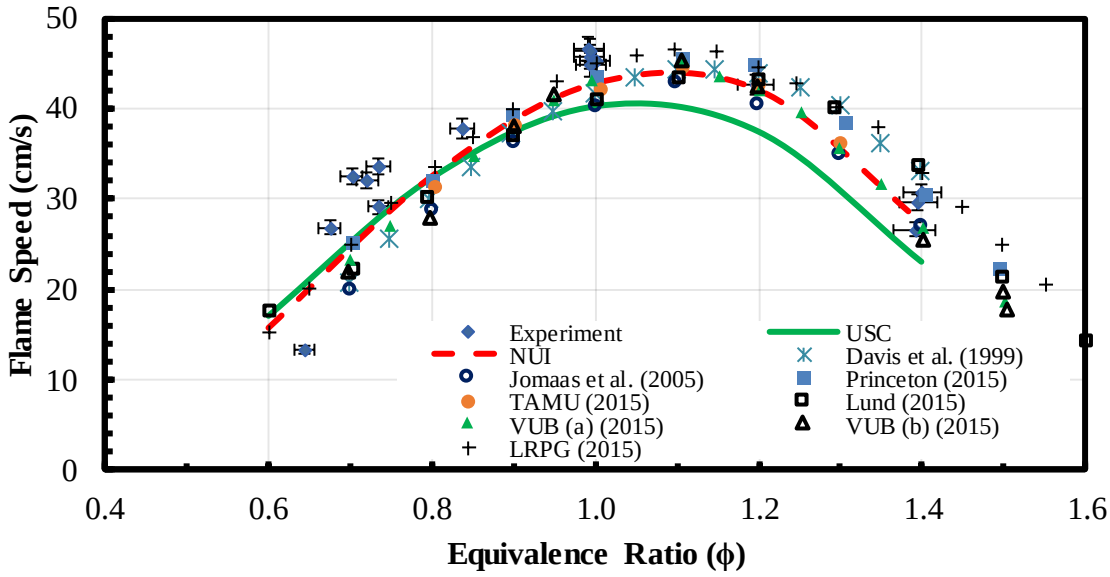

Figure 4.3: Validation of laminar flame speed measurements of propylene/air mixtures at T_u = 300 K and atmospheric pressure.

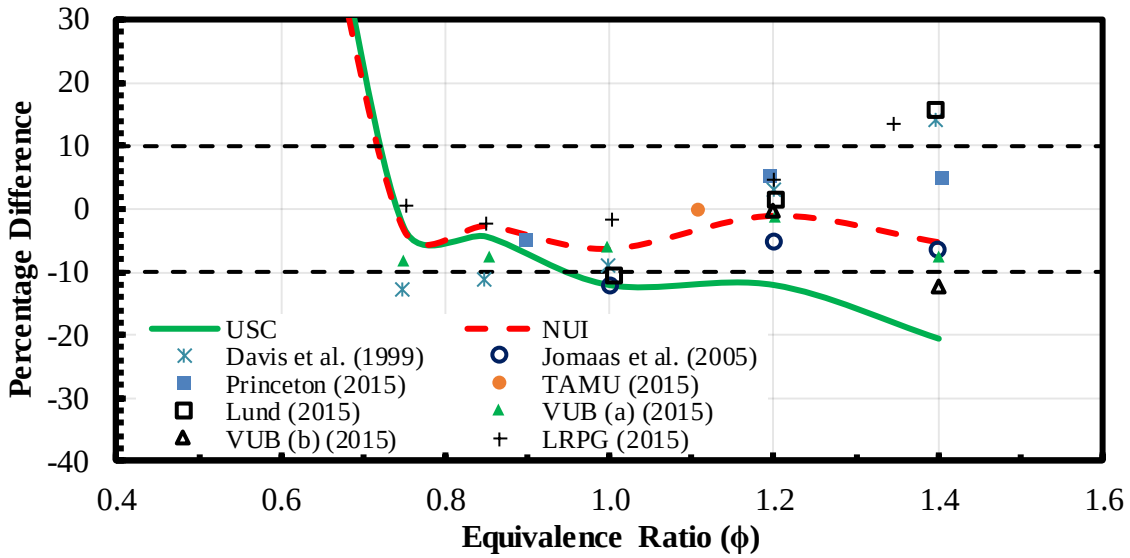

Figure 4.4: Percentage difference of measurements and kinetic model predictions from literature when compared with current BFT measurements of propylene/air mixtures at T_u = 300 K and atmospheric pressure.

Figure 4.4 provides a better picture by showing the percentage difference between the current BFT measurements and the other values, again using the definition from equation (2). As in the ethylene comparisons, the NUI predictions are closer to the current data, and most of the differences with the previous measurements are within ~10%, except for the richest condition tested (ϕ=1.4). For example, the current results are close to the literature data at ϕ=1; the percentage difference varies from -2% (LRPG) to -12% (Jomaas et al.). The differences from the simulation results also fall within this range. On the lean side, the BFT measurements also tend to be systematically higher than the other results, but again not by more than 12%. The exception is the leanest conditions tested, ϕ~0.65; there the BFT result is well below the other results. On the rich side, where there is a wider spread amongst the previous results, the BFT results tend to be in the middle of the spread. Also, as noted above, the rich BFT results lie closer to the NUI predictions.

This spread in the previous measurements for rich cases can be attributed to uncertainties in the experimental techniques. For spherical and counter flow flames, the uncertainties due to extrapolation are larger for mixtures with Lewis Number (Le) < 1 [17, 81, 82]; this corresponds to fuel rich mixtures in the case of propylene/air. For the heat flux method, the uncertainties are higher at higher equivalence ratio due to the uncertainties in the flow meter [15].

From these validation results, it can be concluded that systematic uncertainties in the current BFT, room temperature measurements are generally within ±10% for ethylene and propylene; though the propylene measurements exhibit higher inaccuracy for extremely lean conditions. This problem for very lean conditions could result from the proximity to propylene's lean flammability limit. This effect is discussed in further detail

in following chapters, though the uncertainty is hard to estimate and eliminate as flame behavior close to lean flammability limits is not well understood.

4.2 High Temperature Validation

The above comparisons were for room temperature reactants, where most previous data was acquired. The highest preheat temperature for which alkene data is available is T_u = 470 K, with ethylene/air mixtures. Figure 4.5 demonstrates the variation of laminar flame speed with equivalence ratio at this temperature and atmospheric pressure, and a comparison with measurements from Kumar et al. [51]. Laminar flame speed calculations made using the USC [71] and NUI [61, 62] mechanisms are also compared. The data trends are similar to the ones observed at room temperature measurements in Figure 4.1. The current measurements follow closely with the NUI calculations for all equivalence ratios except at ϕ = 0.6, where the current measurements are lower than all kinetic model calculations and the data from Kumar et al. For ϕ = 0.8 to 1.4 the USC calculations are always lower than the measurements. The Kumar et al. measurements are higher up to stoichiometric equivalence ratios and are either lower or matching at rich equivalence ratios.

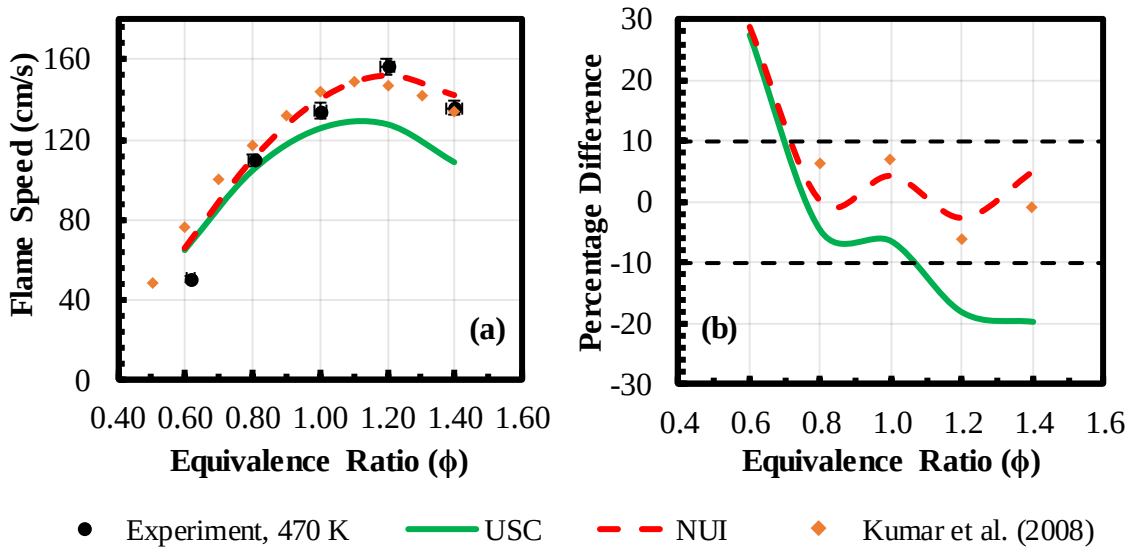

Figure 4.5: Validation of laminar flame speed measurements of ethylene/air mixtures at T_u = 470 K and atmospheric pressure.

For equivalence ratio between 0.8 and 1.4, the difference between the current data and the NUI mechanism is within ±5%, and when compared to the Kumar et al., the current results are within ±10%. At ϕ = 0.6, the current measurements are well below the other results, with 30-50 % differences. This may be attributed to a systematic error in the BFT, but the Kumar et al. data at this equivalence ratio is also higher than the model predictions, suggesting greater general uncertainty at very lean equivalence ratios. Still, these measurements indicate that unstretched laminar flame speeds can be measured with high accuracy using BFT at high preheat temperatures.

4.3 Stretch effects on Bunsen flames

While the accuracy of the BFT appears to be quite good, at least compared to other measurement approaches, for flame speed measurement of room temperature alkene/air mixtures, it is important to characterize the sources of the uncertainty to understand how

BFT accuracy might change at other operating conditions, e.g., higher preheat temperatures. Furthermore, this knowledge should be useful to other researchers who wish to employ this relatively simple approach for flame speed measurement.

The random and systematic uncertainties in the Bunsen flame technique can be attributed to the following sources. The flame speed is based on two inputs (measurements): the flow rates of the reactants and the resulting (reaction zone) flame area. In addition, there are measurements needed to characterize the flame conditions: flow rate measurements will also impact the flame's equivalence ratio, and the temperature of the reactants must be determined. The flow rate measurements are potential sources of both random and systematic uncertainty, and account for a combined uncertainty of 1-3% in the flame speed measurements (discussed in Appendix B). The total error in flame speed contributed by the random uncertainty in area measurements is ~1% (Appendix B). The total combined uncertainty in flame speed due to these errors is less than 5%, however, we have seen larger differences between BFT and stretch-corrected measurements for certain mixture conditions.

Finally, the current approach relies on the assumption that the flame speed in the burned gases is only weakly effected by stretch effects. This assumption can lead to systematic uncertainties in the measured (unburned) flame speed and there are no previous estimates of the accuracy of BFT flame speeds due to stretch. To provide an in-depth view of stretch effects in Bunsen flames, we consider an axisymmetric Bunsen flame in a cylindrical coordinate system. The flame stretch evaluated at the surface is given by the following equation (3),

$$K = -\frac{\sin\alpha}{r}\frac{\partial}{\partial r}(rw\cos\alpha) - \cos\alpha\ \frac{\partial}{\partial z}(w\cos\alpha) \tag{3}$$

where K is the stretch rate, w is the exit velocity at the burner tip, α is the half angle at the tip of the flame, r and z are the radial and axial coordinates in the cylindrical system respectively. The derivation of the above equation is provided in detail in Chapter 10.2 of Law [11]. In the above equation, w and α are functions of r and z. For first-order calculations, an assumption can be made that the flame surface is a circular cone with a sharp apex implying w and α are constants, then stretch is given by:

$$K = -\frac{U\sin 2\alpha}{2R_f} \tag{4}$$

where R_f is the radius of the flame at a given height and U is the (uniform) velocity at the exit of the burner. The Bunsen flame is negatively stretched in contrast to most other flame configurations used to measure flame speed, e.g., stagnation flames, which are positively stretched. As given in equation (4), the amount of stretch increases as R_f decreases, i.e. as the flow moves downstream.

The stretch rate variation along the flame based on the flame height (h) is calculated using equation (4), here, the total height of the flame is characterized by H/D. U is varied from 50 to 500 cm/s, covering a wide range of possible flow velocities, and thus flame speeds. Figure 4.6 shows the variation of stretch with distance above the flame base. In general, the stretch is small (e.g., $|K| < 50\text{-}300\ s^{-1}$) until the top of the flame (e.g., last 1-10% of the height). Furthermore at lower Burner velocities, the maximum stretch is lower than at higher velocities for both short and tall flames. But high burner exit velocities would

correspond to flames with high flame speeds, e.g., mixtures with high preheat temperatures, whose dependence on stretch is generally expected to be lower.

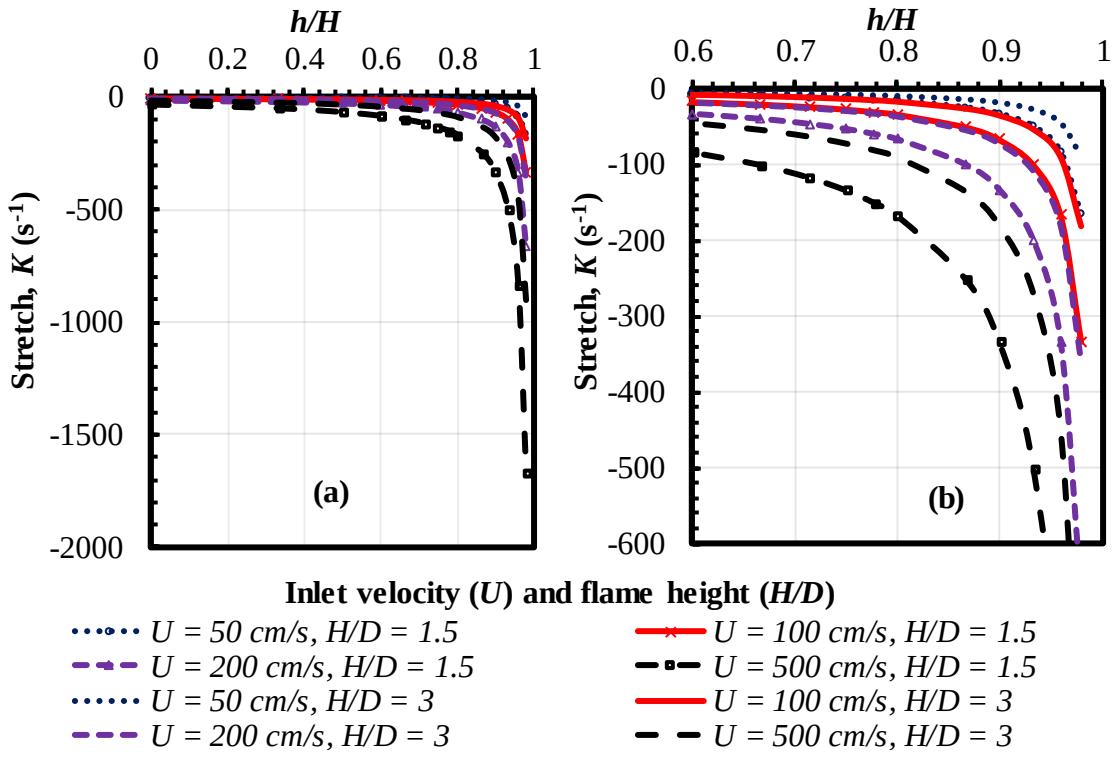

Figure 4.6: Stretch rate variation with normalized height of the flame for flames with different total *H/D* ratio, representing a short flame (*H/D* = 1.5) and a tall flame (*H/D* = 3), (a) for the complete flame and (b) only top half of the flames.

This indicates that the stretch effects are exceptionally higher at the tip of the flame. These effects can be reduced by making sure that the contribution of the tip area to the overall area of the flame is negligible; this can be achieved if sufficiently tall flames are employed. Also, the effect of stretch on flame speed could be dependent on the composition and conditions such as preheat temperature and pressure of the mixture. In the following subsections, first we present the effect of height of the flame on the measured flame speed by employing current experimental measurements. Later the dependence of flame speed

with stretch for several fuel/air mixtures is examined using computational modeling, and an effort to quantify the systematic error to a first-order is presented.

4.3.1 Flame height effects

Previous BFT studies indicated that sufficiently tall flames provide reasonably accurate measurements of the unstretched laminar flame speed [20, 21]. The authors in those studies reached this finding by comparing S_L measurements of flames with different heights; they found that flame speed became independent of flame height (H) when it exceeded the diameter of the burner (D) by two times, i.e., for $H/D > 2$.

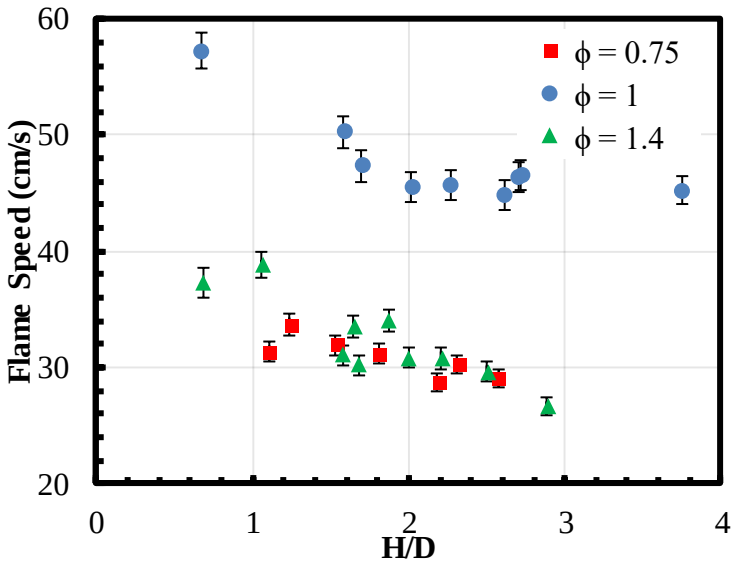

Figure 4.7: Variation of flame speed with height of the flame (H/D) for propylene-air flames at T_u = 300 K, P = 1 atm, (a) ϕ = 0.75 (b) ϕ = 1 (c) ϕ = 1.4.

To test this hypothesis in the current results, flame speeds were measured for propylene-air mixtures at three equivalence ratios using flames of different height (see Figure 4.7). Flame speed was measured using the same method described in the approach section for all cases, while the flame height was measured using the difference between

pixel positions of the flame base and the flame tip. This pixel count was then multiplied with the conversion from pixel to real word distance measured using the calibration image. For the three equivalence ratios shown here, using flames with *H/D* less than two produces flame speeds that are higher than the flame speeds measured with *H/D* greater than two. Above *H/D* of two, the flame speeds measurements tend to remain constant, at least within the error bars of each measurement. At ϕ =1.4 an anomaly is observed for the tallest flame (*H/D* = 2.9); the flame speed is lower than the other measurements compared to the random measurement uncertainty.

Short flames are more affected by stretch because the true tip of the Bunsen flame is not conical, but rounded. The negative stretch here reduces area of the flame, thus producing a higher flame speed value in the experiments. These results support the hypothesis proposed in previous work [20, 21], that using tall flames reduces the effects of stretch on Bunsen-based flame speeds. The current method of calculating flame speed from Bunsen flames provides a value closer to the unstretched flame speed if it is taken care that the flames are sufficiently tall, i.e., with *H/D* > 2.

4.3.2 Estimation of systematic error in S_L due to stretch

To further examine the impact of stretch on the current measurements, an estimate of the systematic error in the BFT approach needs to be calculated. This systematic error would be dependent on the composition and operating conditions of the mixtures under consideration. To examine the flame speed variation with stretch an opposed-jet flame modeling (OPPDIFF [80]) approach in Chemkin [64] is considered, as discussed in Chapter 3. This modeling approach provides the variation of flame speed with strain rate (a) in a

flat stagnation flame; but for a forward stagnation flame, as shown by Law [11], the stretch rate is equal to the strain rate, i.e.,

$$K=a \tag{5}$$

In the current approach, the burned surface area is used to calculate the (unburned) laminar flame speed, as detailed in Section 3.1. One of the key assumptions in this approach is that the burned flame speed is weakly or negligibly effected by stretch, i.e., $S_{L,b}= S_{L,b_O}$. To check the validity of this assumption and estimate the systematic error in measured flame speed, we first examine the impact of mixture conditions on both the unburned and burned flame speeds. Then using this quantified impact, an estimate of the systematic error is calculated for Bunsen-based flame speeds for the traditional approach using the unburned flame area and the current approach based on the burned area.

4.3.2.1 Unburned flame speed variation with stretch

Flame speed calculations at various stretch rates for three different fuels methane (CH_4), ethylene (C_2H_4) and propane (C_3H_8), all burning with air, are shown in Figure 4.8. The fuels chosen represent mixtures where molecular weight (MW) of the fuel is lighter (CH_4), equal to (C_2H_4) and heavier (C_3H_8) than air. Calculations are made at three different equivalence ratios representing very lean (ϕ = 0.6), stoichiometric (ϕ = 1) and moderately rich (ϕ = 1.4) flames. This spread of fuel and equivalence ratios provides mixtures with varying Lewis numbers (Le), which is desirable to investigate stretch effects since the stretch-dependence of flames is highly dependent on the Le of a mixture. The stretched flame speeds are shown normalized by their corresponding zero-stretch values.

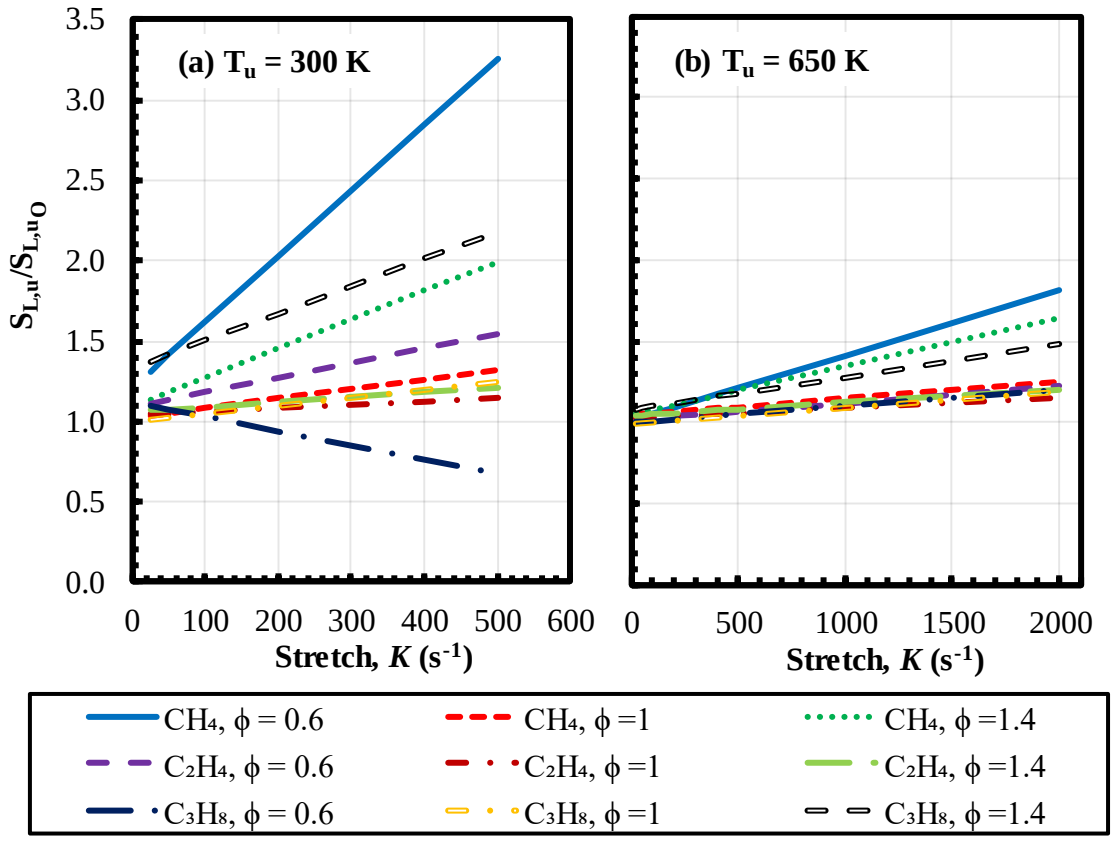

Figure 4.8: Normalized flame speed ($S_{L,u}/S_{L,u_o}$) variation with stretch rate (K) for several fuels at three different equivalence ratios, atmospheric pressure and two different preheat temperatures (a) T_u = 300 K (b) T_u = 650 K.

These results show that the normalized flame speed follows the following relation discussed extensively in literature [11, 25]

$$\frac{S_L}{S_{L,u_O}} = 1 + \left(\frac{L_u}{S_{L,u_O}}\right) K \tag{6}$$

where L_u is the *unburned* Markstein length. It is typically a mixture property and is largely an indication of the Lewis number effect on flame speed. The unstretched flame speed used to normalize the flame speed from OPPDIFF is calculated using the PREMIX model in Chemkin. The USC mechanism was used to perform OPPDIFF calculation as it is a

reduced order mechanism and qualitative trends shouldn't differ between mechanisms. Typically all the curves calculated here should converge at a normalized flame speed value of one for zero stretch conditions, but some discrepancies can be observed depending on the type of mixture under consideration. This can be attributed to non-linear effects for near zero-stretch flames as discussed extensively in the literature [17, 82].

Considering stretched flames at the low reactant temperature of 300 K (Figure 4.8 (a)), it is clear that the molecular weight of a fuel has an impact on flame behavior. For the lighter-than-air fuel (CH_4), the flame speed always increases with stretch at all the equivalence ratios considered. For the heavier-than-air fuel (C_3H_8), the same dependence on stretch is observed for the stoichiometric and rich condition, while the opposite trend is found for the lean mixture For C_2H_4, which has nearly the same molecular weight as air, the flame speed again increases with stretch, but the effect is small. Also, it is important to note that stretch effects are small for stoichiometric mixtures with all three fuels when compared to their lean and rich mixtures. This indicates that at room temperature conditions stretch effects could become prominent for heavier than or lighter than air fuels at sufficiently lean and rich conditions.

When the preheat temperature of the mixtures is increased to 650 K, the effect of stretch on flame speed is reduced as can be observed in Figure 4.8 (b). Irrespective of fuel and equivalence ratio, the dependence of flame speed on stretch is less than 20% until the flames become highly stretched ($K > 500\ s^{-1}$), and such large impacts are only observed for the light fuel (CH_4) away from stoichiometric conditions, and for the heavy fuel (C_3H_8) only under the rich condition. This reduced dependence on stretch is likely due to the fact that flame thickness decreases with an increase in preheat temperature, thus making it

harder for stretch to influence flame propagation. In conclusion, stretch effects on unburned flame speeds are not negligible for many flame conditions. How this variation in unburned flame speed with stretch will manifest as a systematic error are discussed in a later subsection of this chapter.

4.3.2.2 Burned flame speed variation

A similar modelling approach is used to calculate stretch effects on the burned surface. For steady flames, previous studies have shown the flame speed at the burned surface is independent of curvature and only a function of the stretch induced strain [17, 76, 77]. For the stagnation flame, it is common to define the burned flame speed ($S_{L,b}$) as the speed at the location of maximum heat release. The strain is used in the analysis is the previously defined value for the unburned side of the flame; this strain value is commonly chosen as it is easier to estimate and also close to the strain magnitude of the flow near the end of the burned surface.

The burned flame speed calculated is normalized by their corresponding zero-strain burned flame speed values (calculated using the PREMIX model in Chemkin). These results show that the normalized burned flame speed follows the following relation similar to the unburned flame speed relation (variation with stretch as opposed to strain) and discussed extensively in literature [17, 77].

$$\frac{S_{L,b}}{S_{L,b_O}} = 1 - \left(\frac{L_b}{S_{L,b_O}}\right) a \tag{7}$$

where L_b is the *burned* Markstein length. Burned flame speed calculations for the same fuel-air mixtures analyzed in the previous section are shown in Figure 4.9. The normalized flame speed variation with strain follows the typical linear relation for all mixtures under

consideration. As discussed before, the normalized flame speed does not converge to a value of one at zero-strain conditions for some mixtures; this is again attributed to non-linear effects for near zero-strain flames.

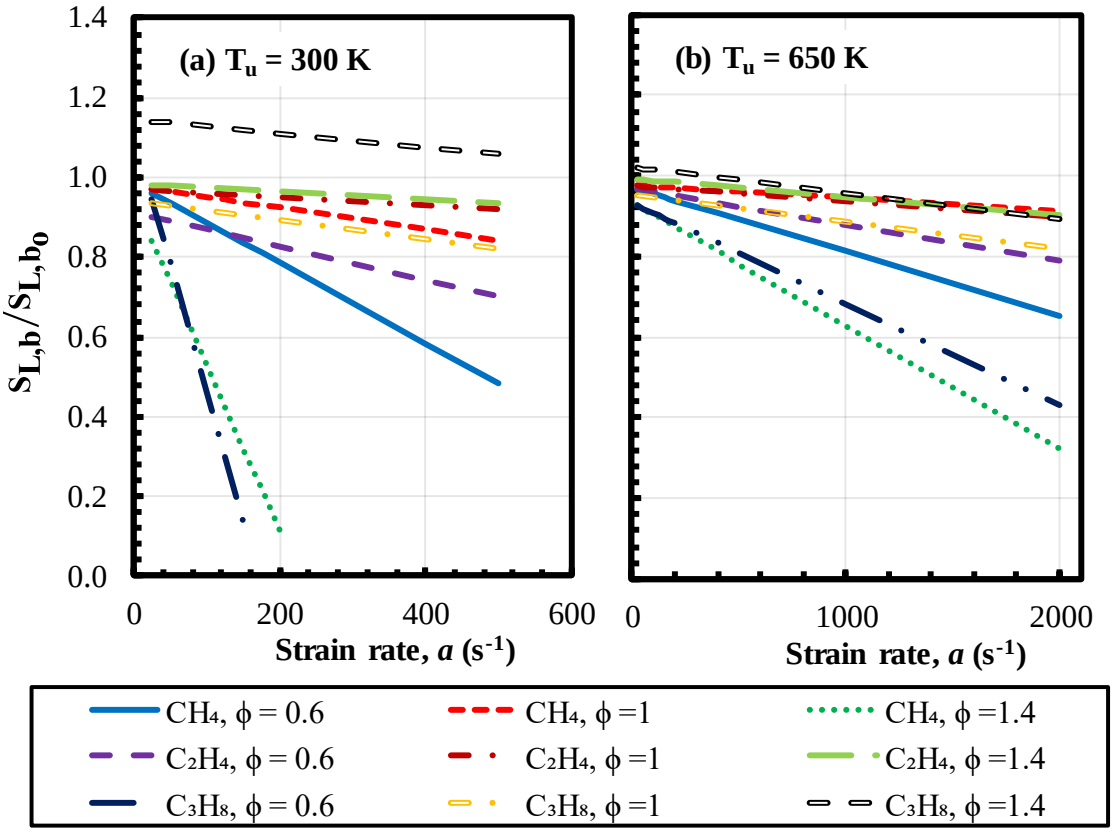

Figure 4.9: Normalized burned flame speed ($S_{L,b}/S_{L,b_o}$) variation with strain rate (a) for several fuels at three different equivalence ratios, atmospheric pressure and two different preheat temperatures (a) T_u = 300 K (b) T_u = 650 K.

For all the flames under consideration, Figure 4.9 shows the flame speed always decreases with an increase in the strain; this is quite different than the impact on the unburned flame speed seen previously. The amount by which the flame speed changes is largely dependent on the composition of the fuel-air mixture under consideration. For example, consider mixtures at the low preheat condition (Figure 4.9 (a)). The largest effects

of stretch-induced strain on flame speed are observed for the rich CH_4-air and lean C_3H_8-air mixtures. The lean CH_4-air mixture is also moderately affected by strain. Thus these results indicate that when mixture Lewis number deviates from the Le = 1 condition, the effect of strain on $S_{L,b}$ generally increases.

For mixtures with a preheat temperature of 650 K (Figure 4.9 (b)), the effect of strain is greatly reduced. For none of these mixtures does the strain dependence impact the flame speed by more than 25% until the flames become highly strained (a > 500 s^{-1}),and for most of the mixtures, this impact on the flame speed would require strain rates above 1000-2000 s^{-1}. Another key point to notice is the slope (or L_b) for these mixtures is nearly the same except when the mixture has a large deviation from unity Lewis number. This is again in contrast to the unburned flame speeds, which show a greater variation in L_u. Furthermore for a given mixture, $|L_b| \geq |L_u|$. This seems to be contrary to the assumption that the burned surface is less affected by stretch effects when compared to the unburned surface; this apparent inconsistency is examined below.

4.3.2.3 Error estimation

Now that the effect of stretch on the both the unburned and burned surfaces has been established, a methodology to quantify this effect on the final measured flame speed needs to be developed. The ideal way to estimate this error would be simulating a Bunsen flame using Computational Fluid Dynamics (CFD) methodologies such as Direct Numerical Simulation (DNS), but that work is beyond the scope of this study. A first-order estimate of the effect of stretch on the measured flame speed can be carried out by using a mass flow rate integration analysis that includes the stretch sensitivities (L_u and L_b)

identified from the stagnation flame analysis. First we examine the systematic error in the unburned flame speed, which occurs at the unburned flame surface.

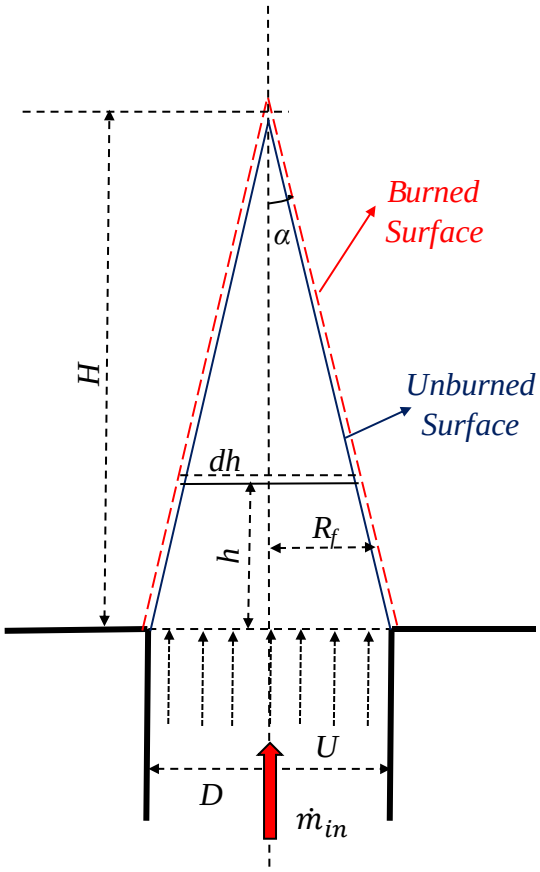

Figure 4.10: An illustration of a perfectly conical flame showing the unburned and burned surfaces of a premixed flame. The elemental flame surface and the dimensions of the flame under consideration are also indicated.

Considering a perfectly conical flame (Figure 4.10), a constant exit velocity profile through the burner diameter and assuming that the flame extends up to the burner lip (ensuring that the mass entering through the burner always burns through a flame), a mathematical formulation can be developed as follows. The mass flow rate through the elemental flame surface at height h and a radius of R_f is:

$$d\dot{m} = \rho_u S_{L,u} dA_u = \rho_u S_{L,u} \left(2\pi R_f \frac{dh}{\cos\alpha}\right) \tag{8}$$

$$\tan\alpha = \frac{D}{2H}$$

where α is the conical angle of the flame which is assumed to be a constant for the purpose of this analysis. The total mass flow rate through the flame can be calculated by integrating this elemental mass flow rate over the total height (H) of the flame. This mass flow rate must be equal to incoming mass through the burner based on mass conservation.

$$\dot{m}_{inlet} = \rho_u U \left(\frac{\pi D^2}{4}\right) = \int_0^H d\dot{m} \tag{9}$$

The inlet velocity and the measured laminar flame speed are related using the following equation for the traditional approach based on unburned flame area:

$$S_{L,u,m_o} = \frac{\dot{Q}}{A_u} = \left.\frac{\pi D^2 U}{4}\right/ \frac{\pi D H}{2\cos\alpha} \tag{10}$$

$$\Rightarrow \quad U = \frac{S_{L,u,m_o}}{\sin\alpha}$$

where S_{L,u,m_o} is the measured laminar flame speed. Substituting U in equation (9) and using the relationships for $S_{L,u}$ and K given by equations (6) and (4), the following can be obtained:

$$\frac{\rho_u S_{L,u,m_o} \pi D^2}{4\sin\alpha} = \frac{2\pi\rho_u}{\cos\alpha} \int_0^H \left[S_{L,u_o} - L_u \left(\frac{S_{L,u,m_o} \sin 2\alpha}{2R_f \sin\alpha}\right)\right] R_f dh \tag{11}$$

$$\frac{S_{L,u,m_o}}{S_{L,u_o}} = \frac{1}{1 + 4\left(\frac{L_u}{D}\right)\cos\alpha} \tag{12}$$

The systematic error in measured flame speed can be obtained from equation (12), and is only dependent on the unburned Markstein length (L_u), the diameter of the burner (D) and the height (H) of the flame (since $1/cos\alpha = \sqrt{1+(D/2H)^2}$). For tall flames, the effect of α is minimal (< 1%); this means that the systematic error in measured flame speed introduced due to stretch on the unburned surface is independent of the flame height *for perfectly conical flames*. (Note: real Bunsen flames have curved tips, which is why it was stated earlier that flames with $H/D > 2$ are desirable.) The major error is due to the stretch effects; for the systematic error to be small, L_u/D needs to be a small. This can be achieved by either using burners of large diameter or for mixtures with a low L_u.

The current measurement approach uses the Burned surface area to measure laminar flame speed. A similar integral approach to the one showed above can be used to estimate the systematic error in this approach. The following equation shows the dependence of S_{L,u,m_o} to strain in the flow field:

$$\frac{\rho_u S_{L,u,m_o} \pi D^2}{4 \sin\alpha} = \frac{2\pi\rho_b}{\cos\alpha} \int_0^H \left[S_{L,b_o} - L_b a\right] R_f dh \tag{13}$$

To estimate the systematic error an analytical expression for the strain rate (a) on the elemental burned surface is needed. There is no straightforward way to estimate this analytical expression, but the strain in a Bunsen flame is stretch induced due to the fact that the curved flame is not normal to the velocity flow field. A highly conservative estimate of the strain would be that it is equal to the stretch (K) in the flame, by substituting the stretch value from equation (4) the following estimate for the systematic error is obtained:

$$\frac{S_{L,u,m_o}}{S_{L,u_o}} = \frac{1}{1 - 4\left(\frac{\rho_b}{\rho_u}\right)\left(\frac{L_b}{D}\right)\cos\alpha} \tag{14}$$

The systematic error in the unburned flame speed calculated from *measuring the burned area* has a similar form to the unburned area result, except the ratio of *burned* Markstein length to burner diameter (L_b/D) is now multiplied by the flame density ratio (ρ_b/ρ_u). As discussed above, the systematic error should be essentially independent of α for sufficiently tall flames. The additional density ratio term tends to reduce the error in the modified approach as the burned gas is of much lower density in comparison to the unburned gas. Thus even though the magnitude of L_b is greater than L_u, based on the stagnation flame modeling, the overall error in measured flame speed can be lower. The next section compares the systematic error between the two approaches and explores the reasons behind the differences.

4.3.2.4 Traditional vs modified BFT approach

The percentage systematic error (PSE) in both traditional and modified BFT approaches is given by equation (15). Here PSE is the magnitude of the error in the measured flame speed relative to the "true" unstretched, 1-D laminar flame speed.

$$\text{PSE} = \left|\frac{S_{L,u,m_o} - S_{L,u_o}}{S_{L,u_o}}\right| * 100 \tag{15}$$

Figure 4.11 shows PSE for both the traditional and modified BFT approaches for fuel/air mixtures whose stretch dependency on flame speed were presented above. The systematic error in the traditional method is higher than in modified approach for most mixtures. This indicates that the flame density ratio parameter plays a significant role in reducing the systematic error. In general, the errors for the modified approach are less than 10%; the two cases where the PSE is significantly higher are for mixtures previously

identified to have a large burned Markstein length, i.e., rich methane-air and lean propane-air at 300 K.

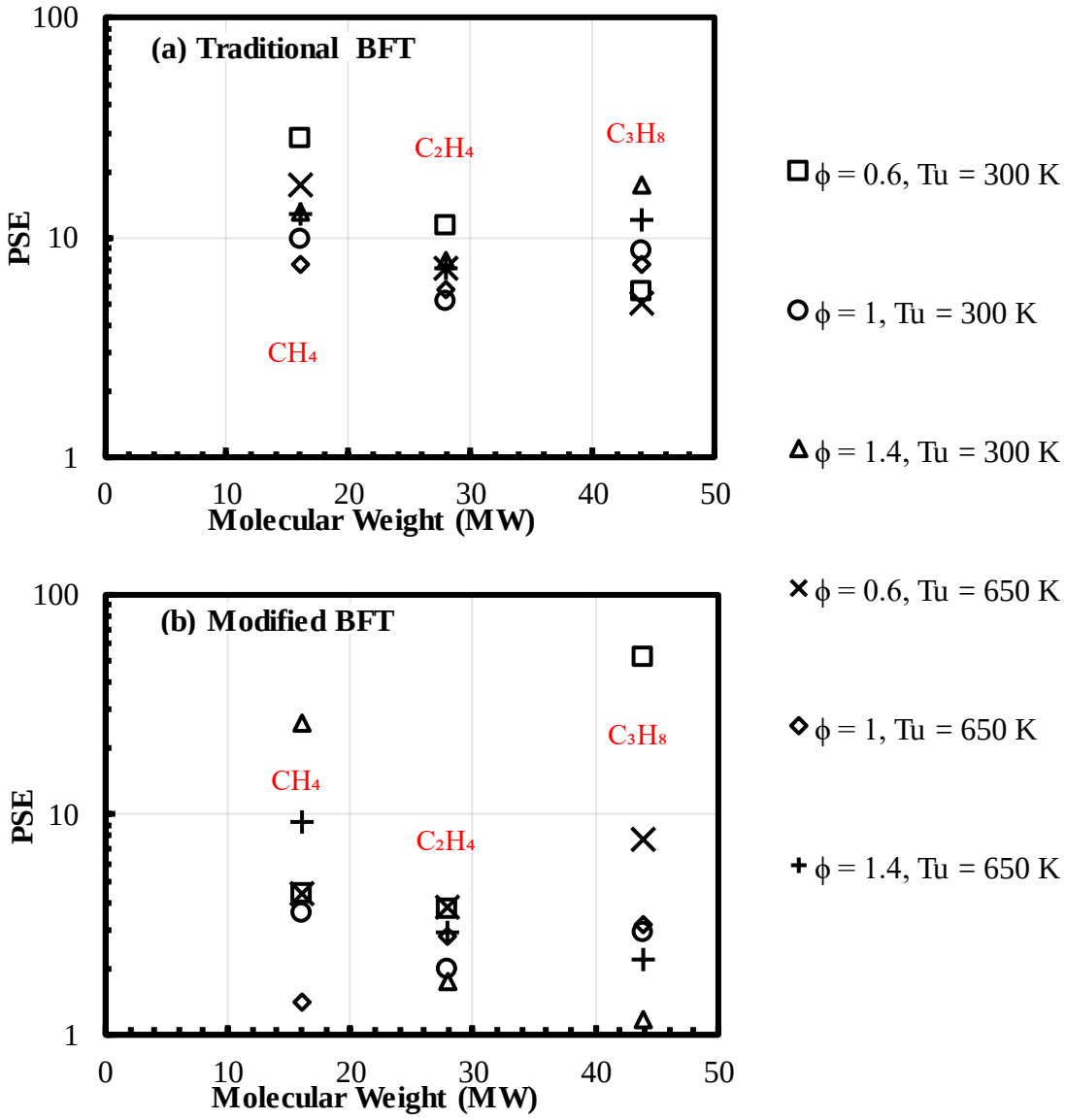

Figure 4.11: The percentage systematic error in the measured flame speed in both (a) traditional and (b) modified BFT approaches for several different fuel/air mixtures.

At the higher preheat temperature, the error falls below 10% for all the mixtures with the modified approach, whereas in the traditional approach, the error for these mixtures does not change by a significant margin. It is important to note that these two

mixtures have Lewis number values greater than one, suggesting that such mixtures might suffer from larger systematic errors. At this point, it is important to note that the systematic uncertainty obtained for the traditional approach may be an underestimate; the reasoning behind this statement is included in the following.

To have a better understanding of why mixtures with Le > 1 have high systematic errors in the modified BFT approach let us examine the asymptotic analysis performed by Sun et al. [76]. They estimated that for a weakly stretched steady flame the unburned flame speed and burned flame speed vary as follows:

$$\frac{S_L}{S_{L,u_O}} = 1 + \frac{Ze}{2}\left(\frac{1}{Le} - 1\right)\frac{\beta^o a \delta_T^o}{S_{L,u_o}} + \gamma^o \delta_T^o \tag{16}$$

$$\frac{S_{L,b}}{S_{L,b_O}} = 1 + \left[\frac{Ze}{2}\left(\frac{1}{Le} - 1\right) - \frac{1}{Le}\right]\frac{\beta^o a \delta_T^o}{S_{L,u_o}} \tag{17}$$

where Ze is the Zeldovich number, β^o is factor which accounts for the change in density due to the flame, a is the strain rate, γ^o is the flame curvature and δ_T is the preheat zone thickness of a premixed unstretched flame. From this asymptotic analysis it is evident that flame curvature does not directly affect the flame speed of the burned surface. The burned flame speed is a function of the mixture conditions (i.e., *Ze*, *Le*), flame thickness and strain (including stretch-induced strain). The unburned flame speed is dependent on these parameters and pure curvature.

Since the stagnation flame used to calculate L_u and L_b does not exhibit curvature, the estimated uncertainty in the flame speed based on the unburned Bunsen flame surface does not include this effect. This is the reasoning behind the earlier statement that the calculated errors for that approach may be underestimates. On the other hand, since L_b is

not expected to exhibit an influence of pure curvature, we can be more confident that the uncertainties predicted for the modified BFT are not underestimates.

As the burned flame speed is only dependent on the strain for certain mixture conditions, there could be scenarios where the systematic error can be reduced. The effect of strain vanishes for burned flame speed if the coefficient before strain in equation (17) equals to zero, this is only possible if the following condition is met:

$$Le = 1 - \frac{2}{Ze} \tag{18}$$

If the mixture under consideration is such that it deviates from this conditions by a large amount then the effect of strain on the burned flame speed could be large, leading to higher systematic errors. Since $Ze > 0$, this condition can only be met for mixtures with $Le < 1$. Previously, we saw that cases with Le > 1 at 300 K had the highest systematic errors, which is consistent with the implications of the asymptotic analysis (As an aside, Calvin [83] used an asymptotic analysis for a weakly wrinkled spherical flame to show $Le < 1-2/Ze$ would lead to the onset of thermos-diffusive cellular instabilities on the flame surface.). Moreover, the asymptotic expression suggests we should expect strain dependence of the burned flame speed even for unity *Le* mixtures, where the dependence is created by the $Ze/2$ term in equation (17). This is a possible reason for the similar L_b (slopes) in Figure 4.9 for many of the mixtures with *Le* close to one.

Since equation (17) also suggests the strain dependence is proportional to the unstretched flame thickness, we can compare it for the various mixtures, with $\delta_f = (T_{ad} - T_u)/ (dT/dx)_{max}$, where T_{ad} is the adiabatic flame temperature. Figure 4.12 shows the comparison of the flame thicknesses of the mixtures analyzed, along with both the

unburned and burned Markstein lengths. Recall that in measuring S_L using the burned surface approach, the effect of L_b is reduced by a factor of the density ratio. So the parameters compared are L_u and $\left(\frac{\rho_b}{\rho_u}\right) L_b$ (the *modified-burned Markstein* length),

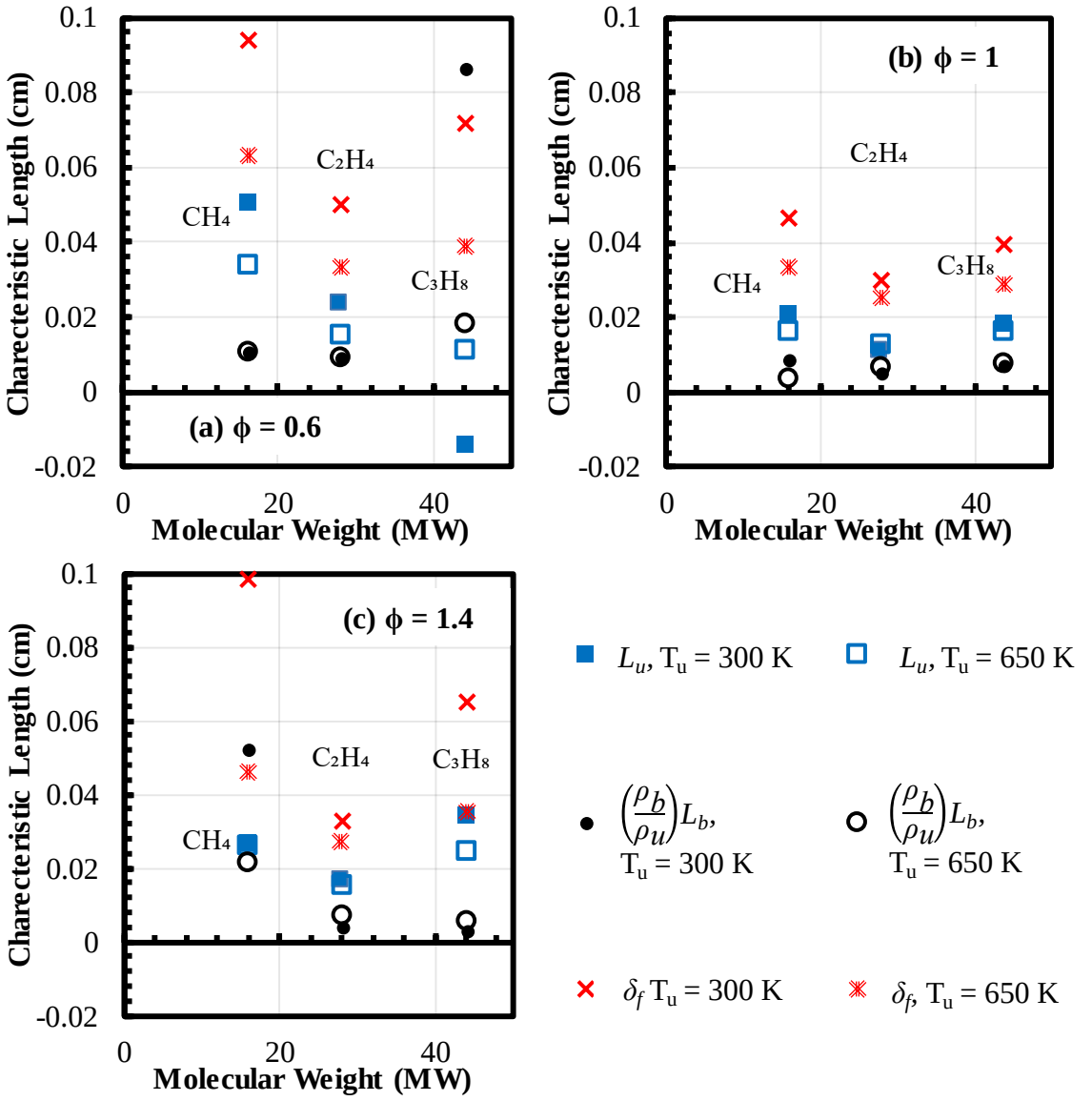

Figure 4.12: Unburned (L_u), modified-burned Markstein length (ρ_b/ρ_u)L_b and flame thickness (δ_f) variation for different fuels and equivalence ratios (a) ϕ =0.6, (b) ϕ = 1, and (c) ϕ = 1.4. Calculations for preheat temperatures of 300 K and 650 K are shown here.

It can be clearly observed that the flame thickness and stretch effects are directly correlated, i.e., the lower the flame thickness, the lower the stretch effects. This can be observed when the flame thickness is reduced either by increasing the preheat temperature or by moving closer to stoichiometric conditions. In both cases, the Markstein lengths move closer to zero. The only cases where this does not hold are for L_u at 300 K with lean propane and rich methane, i.e., where $Le > 1$.

In conclusion, stretch effects on the burned flame speed are in general lower than on the unburned speed. For certain mixtures, specifically for $Le \gg 1$, the effect of stretch could significantly affect the measured flame speed using the modified BFT. If the relation shown in equation (18) is close to being satisfied, then the effect of stretch on flame speed measurements using the modified BFT should be small. As the preheat temperature increases, the accuracy of the measured flame speeds tends to improve for the modified approach (unlike the traditional BFT approach). Also, it is prudent to keep in mind that these errors are first-order estimates, and we have used a conservative estimate to obtain the systematic uncertainty for the modified BFT method; in reality the strain value for the Bunsen flame is likely lower than the value used here, which would lead a reduced estimate of the systematic errors. In the next section, measurements made using the modified BFT at 300 K in this and previous studies are compared to stretch-corrected flame speed measurements based on other techniques to experimentally verify the accuracy of the Bunsen approach based on the burned surface area.

4.4 BFT Validation for Several Fuels

In the previous sections, it was established that the current Bunsen technique for measuring *unstretched* flame speeds provided reasonably accurate, room-temperature alkene-air results relative to stretch-free and stretch-corrected approaches. Moreover, an estimate of the systematic uncertainties indicated that the approach should often be capable of producing values within ±10% of the true unstretched flame speed. Therefore, it is interesting to ask a broader question; what is the relative accuracy of BFT measured S_L values compared to the most common stretch-corrected approaches, based on data available in the literature.

The available BFT data is compared to measurements made using the spherical flame technique (SFT) and the stagnation flame technique (STFT), with both linear extrapolation methods (LM) and nonlinear extrapolation methods (NLM). Different types of stagnation flames are included in the comparison, specifically twin flames generated using opposed-jet approaches and flames generated using a stagnation plate. Measurements are compared at three different equivalence ratios representing lean (ϕ = 0.7), stoichiometric (ϕ = 1) and rich (ϕ = 1.3) mixtures. These comparisons are made at standard conditions (T_u ~ 300 K, atmospheric pressure and air as the oxidizer) where the largest set of data is available for multiple fuels. Results from each source at a given condition (fuel and ϕ) are compared to the average flame speed ($S_{L,average}$) for the same condition based on all sources, and the percentage difference is reported:

$$Percentage\ Difference = \frac{(S_L - S_{L,\ average})}{S_{L,\ average}} * 100 \tag{19}$$

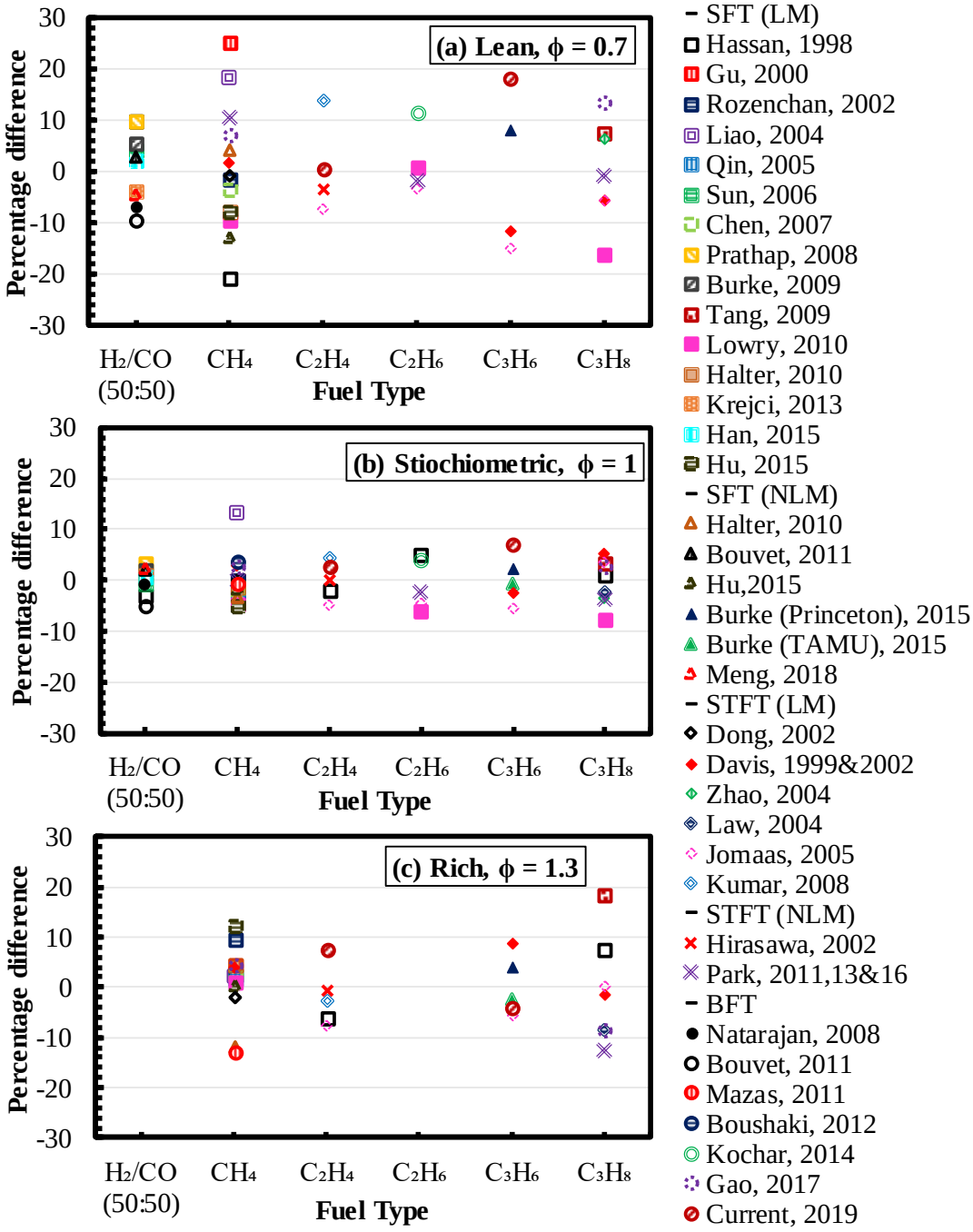

Figure 4.13: Percentage difference between various measurements and average flame speed value for several fuels at three different equivalence ratios and room conditions. (SFT – Spherical flame technique, STFT – Stagnation flame technique, LM – Linear extrapolation model, NLM – Nonlinear extrapolation model and BFT – Bunsen flame technique).

Figure 4.13 shows the results of this comparison; no results are shown for syngas (H_2/CO) and ethane mixtures at the rich condition as there are no BFT data available for these conditions. Here BFT measurements from Bouvet et al. [34], Mazas et al. [35], Boushaki et al. [36], Kochar [20], Gao [75] and the current work for alkenes are shown; all of these studies adopted the technique first used by Natarajan et al [31]. SFT measurements using LM method are shown from Hassan et al. [60], Gu et al. [84], Rozenchan et al. [85], Liao et al. [86], Qin et al. [87], Sun et al. [88], Chen et al. [89], Prathap et al. [90], Burke et al. [62], Tang et al. [91], Lowry et al. [92], Halter et al. [93], Krejci et al. [94], Han et al. [95], and Hu et al. [96]. SFT measurements adopting NLM method are shown from Halter et al. [93], Bouvet et al. [97], Hu et al. [96], Burke et al. [62] and Meng et al. [98]. For stagnation flames, STFT measurements using LM are shown from Dong et al. [99], Davis et al. [22, 100], Zhao et al. [63], Law et al. [101], Jomaas et al. [59], and Kumar et al. [51]. While STFT measurements with NLM approach are shown from Hirasawa et al. [23] and Park et al. [102-104].

At stoichiometric conditions, the results in Figure 4.13 show that measurements from all the techniques, including the BFT, lie within ±10% from the average; also there are no clear systematic differences between the techniques. For lean conditions, some differences between techniques are evident. BFT measurements fall within ±10% range for most fuels except C_2H_6, C_3H_6 and C_3H_8, some issues when measuring flame speed using BFT for lean flames close to flammability limit were discussed previously and manifest as higher flame speeds than expected here. Also, there is a wider spread amongst measurements in the literature for methane air flames indicating the presence of uncertainties in the other techniques as well. There is some spread for measurements of

C_3H_6 and C_3H_8 but due to lack of appreciable number of data points this cannot be classified as technique uncertainties.

Similarly, for rich mixtures while most measurements lie within ±10% of the group average, a large spread is observed for measurements of C_3H_8. Again, due to lack of sufficient number of data points this cannot be attributed to a systematic error in a measurement technique. Also, measurements from Georgia Tech (Natarajan, Kochar, Gao and the current work) compare well with measurements from other groups who have employed the BFT technique as proposed by Natarajan et al.

Each technique has its own uncertainty and they are well documented, these uncertainties stem from the type of mixture whose flame speed is being measured. For example, the wider spread in measurements at lean equivalence ratio for lighter than air fuels and at rich equivalence ratios for heavier than air fuels can be attributed to Lewis number effects. Mixtures with large deviation from Le = 1 have higher uncertainties in flame speed measurements as the flame thickness increases and preferential diffusion of fuel and air could lead to unstable flames and pose difficulties in measuring flame speeds.

Overall, by comparing S_L measurements for different fuels it can be ascertained that BFT flame speeds can have an accuracy comparable to other established techniques. While stretch effects can significantly impact the flame speed measurement, using tall flames can still provide measurements that are generally within ±10% of measurements from other techniques. At high preheat temperatures stretch effects should be even smaller, making the BFT a good candidate for measuring flame speeds at these conditions.

4.5 Summary

In this chapter, the validity of the Bunsen flame technique to measure unstretched laminar flame speed for a number of fuel-air mixtures was considered. From comparisons to experimental results from other standard approaches for ethylene and propylene (the focus of the current study) at low preheat, results for stoichiometric and rich conditions showed excellent agreement, within ±10%. For lean mixtures, the ethylene data again matched well with measurements from the literature and from the chemical kinetic model calculations. The lean propylene measurements differed slightly from previous work, possibly due to proximity to the flammability limit.

To investigate the systematic uncertainty (or accuracy) of the current measurement approach due to stretch, the effects of stretch on Bunsen flame speeds was analyzed. One significant finding was that using tall flames ($H/D > 2$) makes the result independent of flame height, which was attributed to the reduction in the impact of the highly curved flame tip. A first-order estimate of the systematic error in the current Bunsen flame technique was obtained, using stretch sensitivities from a stagnation flame calculation combined with a mass flow rate integral analysis. It was observed that laminar flame speed based on the burned surface measurement is affected by stretch, but the uncertainty decreases at higher preheat conditions. Furthermore, the current approach is a significant improvement over the traditional unburned area measurement approach for most mixture conditions, except perhaps Lewis number is much greater than unity, which was verified by examination of an asymptotic analysis. In many cases, the analysis revealed that the modified BFT approach is capable of producing values within ±10% of the true unstretched flame speed.

Flame speed measurements using the modified BFT were also compared to stretch corrected spherical and stagnation flames. These comparisons were made for several fuels at room temperature and pressure for lean, stoichiometric and rich conditions. Some uncertainties were observed for mixtures with Le ≠ 1, these uncertainties are not limited to BFT measurements but also arise for stretch corrected techniques as well. The comparisons also showed that the BFT results were often within 10% of the mean flame speeds based on all the approaches.

Overall the results of this chapter show that if proper experimental practices are employed, the modified BFT approach can be used in many cases to measure unstretched flame speeds with an accuracy comparable to other approaches. In the next few chapters, preheat temperature and vitiation effects on laminar flame speeds of ethylene and propylene are examined. A large database of alkene S_L measurements generated by employing BFT is used to understand these effects.

CHAPTER 5. Preheat temperature effects

This chapter discusses the effect of preheat temperature on laminar flame speed measurements. As previously described in Chapter 1, S_L is dependent on several factors; this chapter describes the results of measurements taken at different preheat temperatures over a wide range of equivalence ratios for both ethylene and propylene, along with a limited data set for n-decane. The measurements are compared to simulations using standard chemical kinetic mechanisms in order to ascertain their predictive accuracy for elevated preheat temperatures (possible improvements in the chemical mechanism are examined in a later chapter). Furthermore, the preheat temperature dependence of the flame speeds is analyzed, and the large experimental data base is used to develop an empirical formula to estimate laminar flame speed as a function of preheat temperature and equivalence ratio.

5.1 Experimental measurements and chemical kinetic model predictions

5.1.1 N-decane

Figure 5.1 shows the variation of laminar flame speed of n-decane-air mixtures with equivalence ratio at T_u =450 K and atmospheric pressure. Laminar flame speeds were measured between equivalence ratios of 0.8-1.2 and are compared with the CSE and JetSurf chemical mechanisms described in Chapter 3.

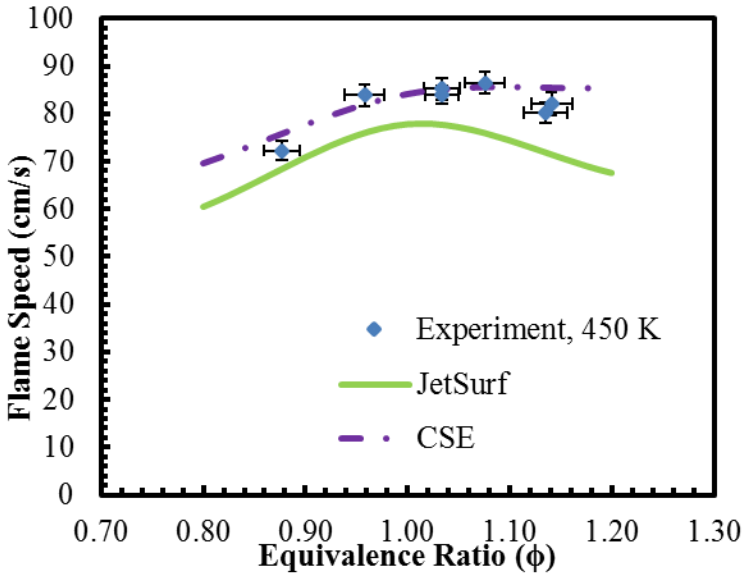

Figure 5.1: Laminar flame speed measurements of n-decane-air mixtures compared to chemical kinetic models at T_u =450 K and atmospheric pressure.

The CSE chemical kinetic model follows the measurements closely while the predictions from JetSurf are always lower than the experiments. The peak laminar flame speed for these measurements occurs at equivalence ratio of 1.05; this equivalence ratio is closer to one than for lower order alkanes, where the peak occurs at an equivalence ratio closer to 1.1 [20, 32, 75], and for syngas [29-31] with the peak at even richer mixtures. The measurements shown here are limited to the above equivalence ratios as the initial focus was to understand the reaction chemistry in afterburners where the equivalence ratio is close to being stoichiometric and in-flow temperatures range as low as 650 °C [3].

Measurements at higher preheat temperatures are affected by fuel breakdown due to reaction chemistry. As discussed in Chapter 2, low temperature oxidation and pyrolysis reactions have large effects on n-decane-air mixtures at high preheat temperatures. These effects are prevalent due to low temperature chemistry becoming important for long

residence time. Long residence times are unavoidable in any flow reactor type setup to measure laminar flame speeds, thus limiting the ability to measure laminar flame speeds of liquid fuels at high preheat temperatures. For n-decane at even moderate preheat residence times, measurements are limited to ~500 K before partial oxidation reactions prevent accurate measurements, as shown in Figure 2.4.

To understand the effect of preheat temperature on laminar flame speeds of liquid fuels, alkenes were chosen as representative fuels as discussed in Section 2.22.2. In the following subsections, two fuels are chosen, i.e., ethylene (C_2H_4) and propylene (C_3H_6) to understand high temperature effects on laminar flame speed. Each fuel's measurements are discussed separately and are compared to the leading chemical kinetic mechanisms identified in Section 3.2.4.

5.1.2 Ethylene (C_2H_4) and propylene (C_3H_6)

Laminar flame speeds of ethylene-air and propylene-air mixtures at atmospheric pressure were measured at a number of preheat temperatures: 300 K, 450 K, 470 K (ethylene only) and 650 K; and for several equivalence ratios ranging from 0.6-1.4. This covers a wide range of equivalence ratios and provides the ability to understand preheat effects on S_L at fuel-lean, stoichiometric, and fuel-rich conditions. The data for these measurements are shown in Figure 4.5 and Figure 5.2.

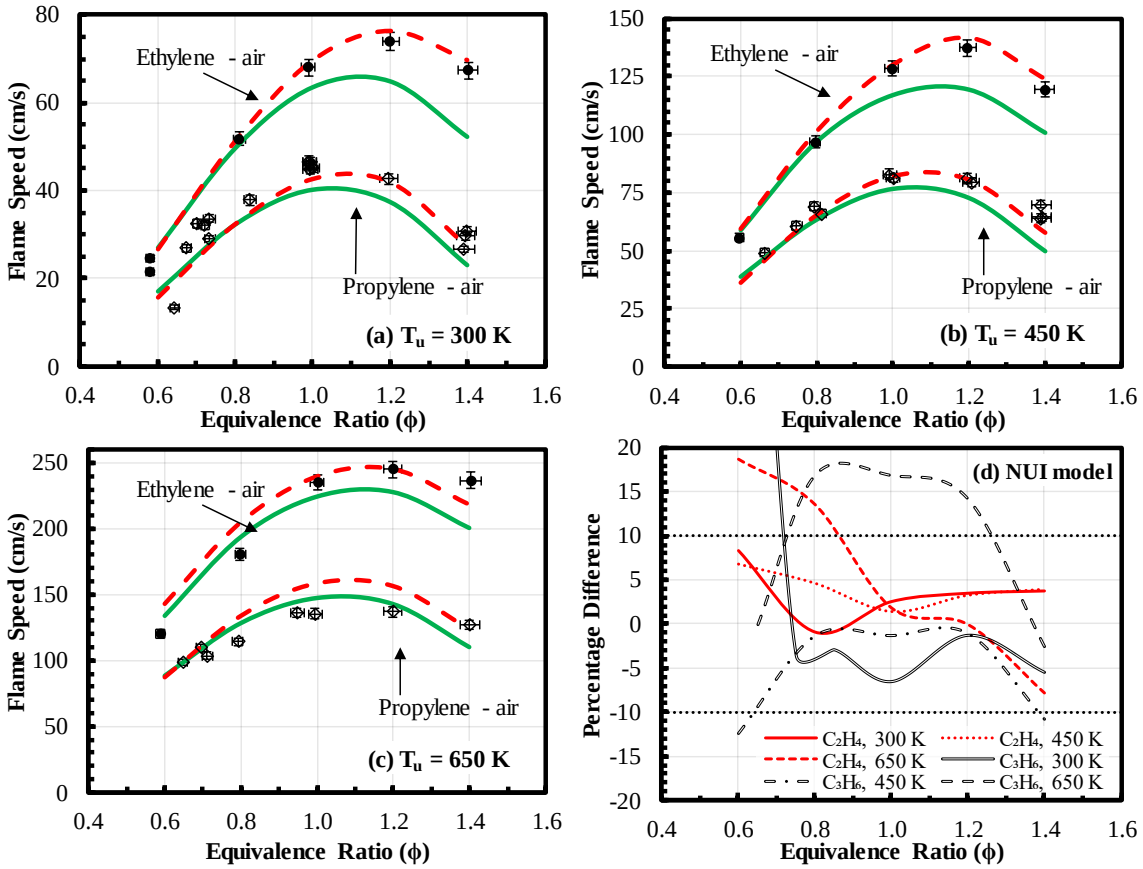

Figure 5.2: Laminar flame speed variation with equivalence ratio at various preheat temperatures and atmospheric pressure for ethylene-air and propylene-air mixtures (a) T_u = 300 K, (b) T_u = 450 K, (c) T_u = 650 K (d) percentage difference between model predictions and measurements. (● - Ethylene-air experimental measurements, ◊ – Propylene-air experimental measurements, —— USC kinetic model and — — — NUI kinetic model)

At 300 K as seen in Figure 5.2 (a), the experimental values closely match the NUI mechanism predictions, at least within ±10%. The USC mechanism matches well at lean equivalence ratios but differs significantly from the measured flame speed values at rich equivalence ratios. The percentage difference is as high as 25% at ϕ = 1.4.

At 450 K (Figure 5.2 (b)), the trends are similar to those at 300 K. The measured flame speed values match closely with the NUI predictions, within a difference of ±10%. The USC mechanism shows similar trends to those observed at 300 K. At the highest preheat temperature (650 K, see Figure 5.2 (c)), the measured laminar flame speed trends differ when compared to 300 K and 450 K. The NUI mechanism over predicts flame speed at all equivalence ratios; while the USC mechanism is within ±10% at lean and stoichiometric conditions, but at rich equivalence ratios under predicts the flame speed by a large margin. The peak laminar flame speed occurs at $\phi = 1.2$ in the measurements, as well as in the NUI predictions; while for the USC mechanism, the peak occurs at $\phi = 1.1$ at all three preheat temperatures. The drop-off in flame speed for rich conditions is similar for the measurements and the NUI mechanism, while the USC mechanism produces a much steeper drop in flame speed.

For propylene-air mixtures, the experimental results at 300 K (Figure 5.2 (a)) are within ±10% for both kinetic models at stoichiometric conditions. For rich mixtures, they agree with the NUI model results, whereas the USC mechanism under predicts the measured values. For lean equivalence ratios, the measurements are higher than the simulation results, and both kinetic models predict nearly the same flame speeds. Overall, the propylene measurements are within ±10% of the NUI model for ϕ above ~0.7, whereas the USC mechanism under predicts the measurements by more than 10% for rich mixtures. The factors which could influence the measurements at leaner equivalence ratios were discussed in Section 4.3.

At 450 K (Figure 5.2 (b)), the experimental flame speeds again agree well with the NUI predictions; across the complete equivalence ratio range tested, the difference ranges

from 0 to −10%. Conversely, the USC mechanism predicts lower flame speeds, especially at near-stoichiometric and rich conditions. Overall, the 450 K measurements are closer to the model results when compared to the 300 K case, where the models tended to under predict the measurements. This trend with preheat temperature continues at 650 K; the mechanisms now tend to over predict the measured propylene-air flame speeds. This can be clearly seen in Figure 5.2 (c); now, the USC mechanism, with lower flame speeds than the NUI results, is the closest to the measurements except at the rich end (ϕ=1.4).

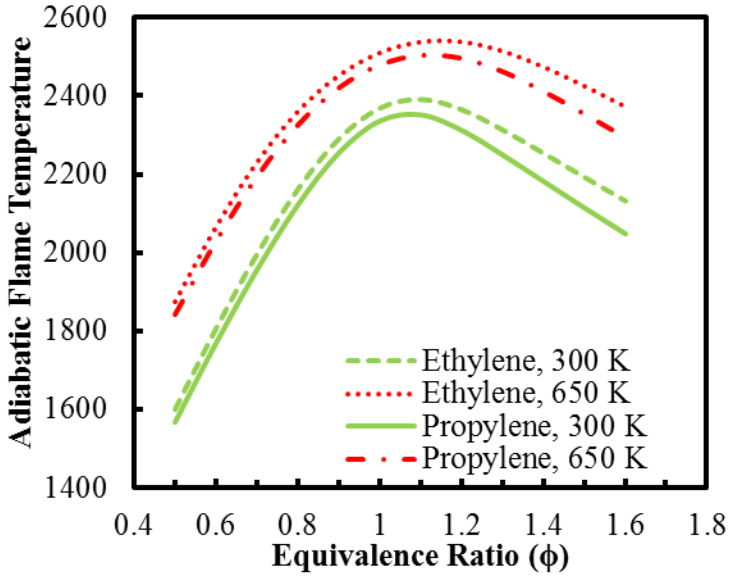

Figure 5.3: Adiabatic flame temperature variation with equivalence ratio for propylene-air and ethylene-air mixtures at different preheat temperatures.

In addition, the peak laminar flame speed occurs between ϕ = 1 and 1.2 for the experiments, which is in good agreement with the models, which predict the peak at ϕ = 1.1. This is a lower equivalence ratio when compared to the ethylene-air mixtures. This effect can be attributed to the lower adiabatic flame temperatures (T_{ad}) of propylene-air

flames when compared to ethylene-air mixtures (Figure 5.3). T_{ad} peaks closer to $\phi = 1.2$ for ethylene-air mixtures while for propylene-air mixtures the peak occurs at $\phi = 1.1$.

The measured and predicted flame speeds are much lower for propylene than for ethylene. Flame speed is highly dependent on adiabatic flame temperature, and propylene-air mixtures do have lower temperatures than ethylene-air mixtures, by ~5% (Figure 5.3). However, this is not sufficient to explain the 50% difference in flame speeds for the two fuels. The model predictions follow the same trend at all preheat temperatures, i.e., USC and NUI peak at $\phi = 1.1$, while the trend at rich conditions is different for measurements and models. At every preheat temperature, the USC and NUI mechanisms produce a steep drop-off in flame speed at rich conditions; the experimental measurements follow the predicted trends at 300 and 450 K. Since the adiabatic flame temperature drop-off is the same regardless of the preheat conditions, it is notable that the flame speed behaviour for measurements for propylene-air mixtures at rich equivalence ratios mirrors that of ethylene measurements at 650 K.

In conclusion, the NUI chemical mechanism predicts laminar flame speed values closest to the measurements for ethylene at all preheat temperatures and propylene at temperatures of 300 K and 450 K. The USC mechanism is closer to the experiments at the highest preheat temperatures for both ethylene and propylene. The sensitivities of the mechanisms to preheat temperature are different from each other and from the experimental measurements. Also, the preheat temperature dependence for ethylene flame speeds is different than for propylene. This indicates that the reaction chemistry of the fuels as modelled is different even though they belong to the same class of hydrocarbons. The difference between the flame speed predictions between the two models is small at lean

conditions, but grows larger at near stoichiometric conditions and is the greatest at rich conditions for both the fuels. To understand these differences, the temperature dependence is investigated at three equivalence ratios representing lean, stoichiometric and rich cases. In a later chapter, the differences between the chemical kinetic models and the differences in reaction chemistry between these two alkenes are explored using sensitivity analysis.

5.2 Temperature dependence

In this section, the temperature dependence of flame speed for ethylene-air and propylene-air mixtures at different equivalence ratios is investigated. To compare the temperature dependence, the ratio of flame speeds ($S_L/S_{L,o}$) is considered as a function of the temperature ratio ($T_u/T_{u,o}$), where S_L is the flame speed measured at T_u and $S_{L,o}$ is the flame speed measured at a (reference) preheat temperature $T_{u,o}$ = 300 K.

Figure 5.4 (a) shows the dependence of the normalized flame speed on preheat temperature for ethylene-air mixtures. The flame speeds predicted with the USC and NUI reaction mechanisms have similar dependence on preheat temperature, and that dependence matches the experimental results reasonably well. There are certain features of note.

To start, the preheat temperature dependence for lean mixtures (ϕ = 0.6) is significantly higher than for near-stoichiometric (ϕ = 1) and rich (ϕ = 1.4) conditions. The relative increase in flame speed from 300 to 650 K is roughly 40% more at lean conditions. Also, the USC mechanism faithfully reproduces the experimental sensitivity for lean conditions at the highest preheat, while the NUI result suggest a slightly higher sensitivity. For near stoichiometric conditions, both mechanisms indicate the same sensitivity, which

also matches the measured results. The only condition for which the models differ significantly from each other is the rich case; the NUI mechanism predicts a lower temperature dependence than the USC outcome, resulting in a 20% difference in normalized flame speed at 650 K. As the experimental measurements lie nearly half way between the two models, neither model can be judged superior for the rich condition.

In the previous section, the dependence of flame speed on temperature for propylene-air seemed to be different than for ethylene-air mixtures. Figure 5.4 (b) confirms this. Both the experimental and simulation results indicate the temperature dependence for lean mixtures is the again the highest, however rich mixtures now show more temperature sensitivity than near-stoichiometric flames. In fact, the simulations predict that the propylene temperature sensitivity is nearly the same as for ethylene at the lean and near-stoichiometric conditions. This suggest the main difference between the fuels with respect to preheating could correspond to rich propylene chemistry.

In comparing the experiments and simulations for propylene, there are two notable differences. First, both mechanisms over predict the temperature sensitivity for near-stoichiometric conditions. The difference between the model predictions and experiments for the normalized flame speed is close to 20% at 650 K. Second, the measured temperature dependence is significantly different than the model predictions at the lean (ϕ=0.65) condition. The measurements have a much higher dependence on preheat temperature; this could either indicate a significant deficiency in the chemical mechanism, or it could be a result of some systematic error in the measurement of flame speed at this equivalence ratio.

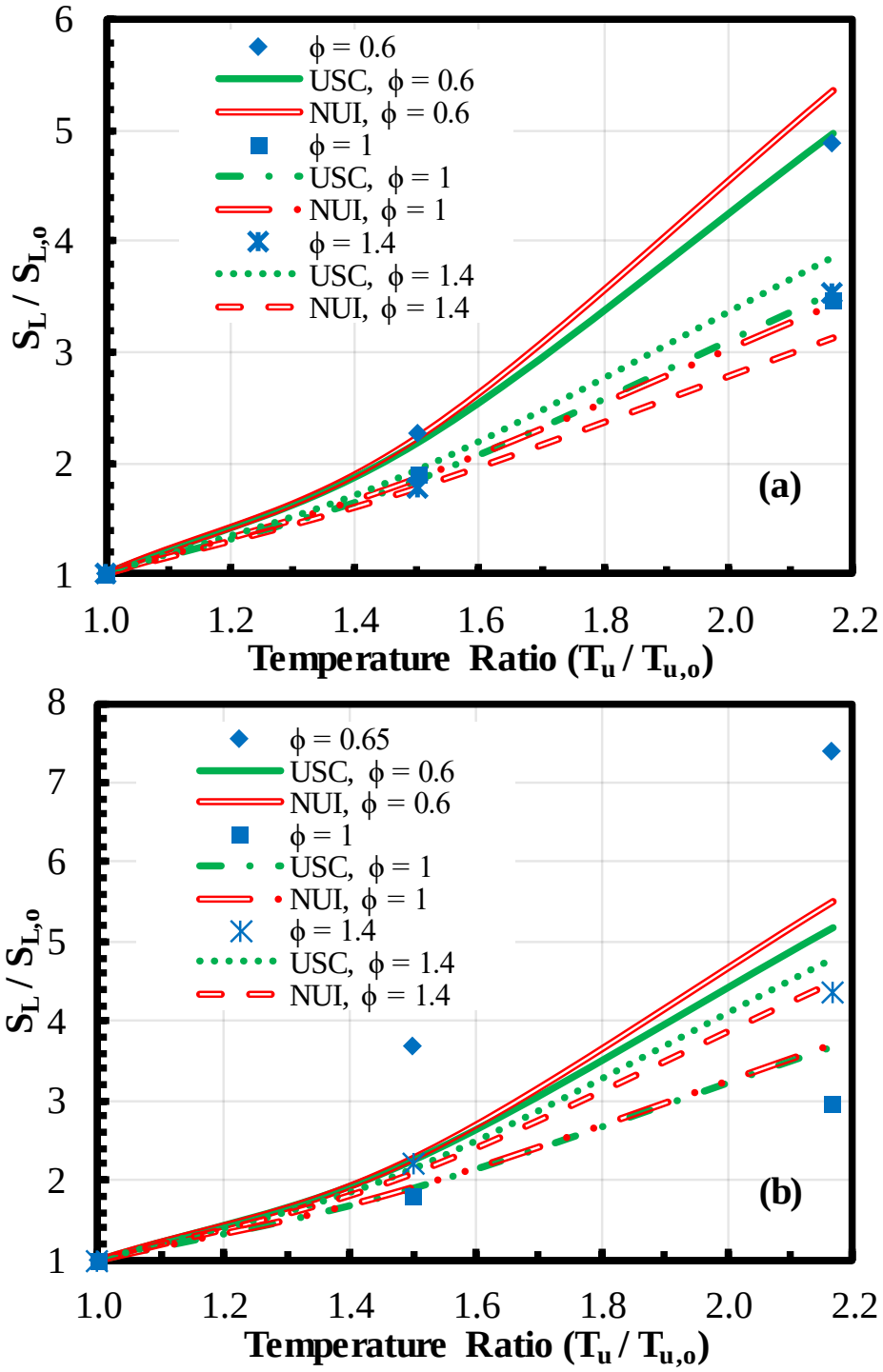

Figure 5.4: Flame speed ratio variation with temperature ratio (with reference $S_{L,o}$ measured at $T_{u,o}$ = 300 K) for both experiments and simulations: (a) ethylene-air mixtures and (b) propylene-air mixtures.

Since the relative change in the lean flame speed from 450 to 650 K is similar for both experiments and predictions (~2-2.4 times), the error would most likely be in the flame speed measured at 300 K. This is quite probable, as it was previously shown (Section 4.1.3) that the propylene flames at extremely lean equivalence ratios (ϕ<0.7) are very weak and difficult to stabilize due to the proximity to the lean flammability limit (ϕ ~ 0.5 for propylene-air mixtures) [105]. This is not an issue for lean ethylene-air flames as the flammability limit (ϕ~0.4) is farther away from the leanest ethylene cases in the current measurements.

5.3 Empirical modelling for temperature effects

Predicting laminar flame speeds using chemical kinetic simulations is a computationally intensive task and access to software packages like Chemkin can be limited. Therefore, it may be useful in some circumstances to be able to calculate laminar flame speeds at a given preheat temperature and equivalence ratio using an analytic model. To this end, this section describes an empirical model for flame speeds of ethylene- and propylene-air mixtures derived from the current measurements. Based on the discussion in the previous section and the results from Figure 5.4, it can be inferred that the normalized flame speed would correlate with normalized preheat temperature as a power law.

Equation (22) provides such a power law, where γ is the temperature exponent. Previously, γ has been shown to be a function of equivalence ratio for several fuels [106-110], but these were limited to alkanes and alcohols. Metghalchi et al. [107] first suggested a linear relationship for γ with ϕ for several fuel-air mixtures based on measurements with preheat temperature up to 350 K. Later studies found that the variation of γ with ϕ is highly

dependent on the fuel-air mixture and the relationship is not linear [109-111]; for example, a quadratic dependence, e.g., equation (20), provides a better fit. Flame speed variation with equivalence ratio typically is parabolic and the $S_{L,o}$ relationship with ϕ shown in equation (21) is adapted from [107].[9] From the current measurements, values for these constant were determined using a least-squared fitting approach, and the results for ethylene-air and propylene-air mixtures are shown in Table 5.1 and Table 5.2.

$$\gamma = \alpha_0 + \alpha_1\phi + \alpha_2\phi^2 \tag{20}$$

$$S_{L,o} = \beta_0 + \beta_1\left(\phi - \phi_{max}\right)^2 \tag{21}$$

$$\frac{S_L}{S_{L,o}} = \left(\frac{T_u}{T_{u,o}}\right)^{\gamma} \tag{22}$$

Table 5.1: Quadratic coefficients for temperature exponent (γ) derived from curve fit between γ and ϕ as shown in Figure 5.5 (a) and to be used in equation (20).

Fuel	α_0	α_1	α_2
Ethylene	4.9112	-6.8443	3.3711
Propylene	3.1056	-2.486	0.9654

[9] Historically, this relationship has remained the same, but as the accuracy of measured flame speed has increased, the values of β_0, β_1 and ϕ_{max} for a given fuel have changed.

Table 5.2: Parabolic curve fit values for flame speed measurements ($S_{L,o}$) at $T_{u,o}$ = 300 K as shown in Figure 5.5 (b) and to be used in equation (21).

Fuel	β_0	β_1	ϕ_{max}
Ethylene	73.8603	-130.73	1.2
Propylene	45.343	-134.41	1.1

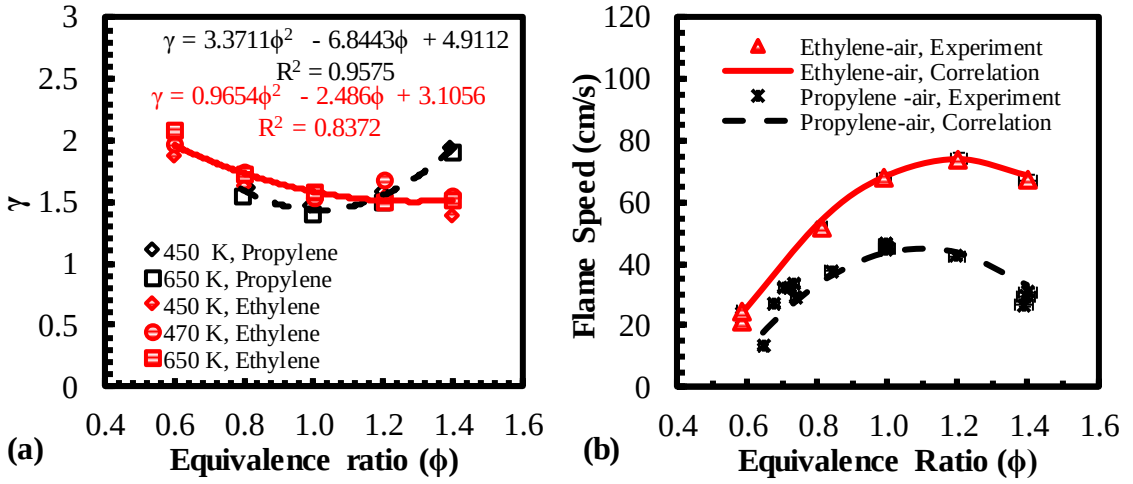

Figure 5.5: (a) Dependence of temperature exponent (γ) with equivalence ratio for both ethylene-air and propylene-air mixtures using experimental data at high preheat temperatures; (b) parabolic curve fit between flame speed ($S_{L,o}$) at $T_{u,o}$ = 300 K and equivalence ratio.

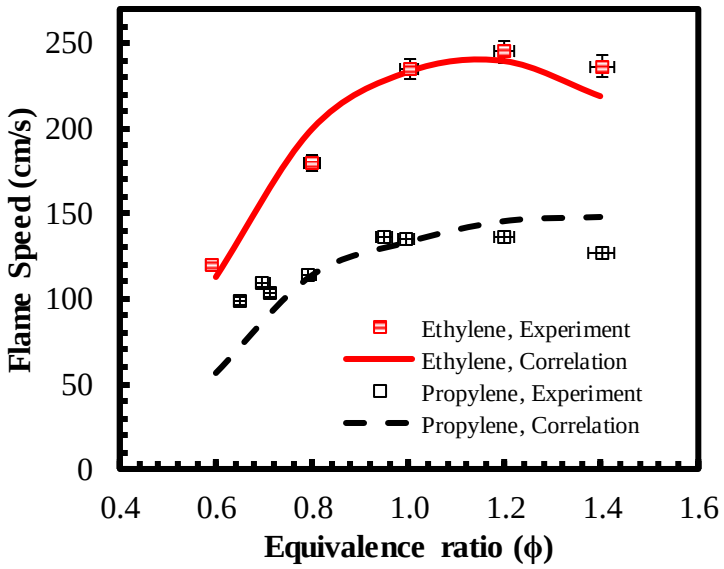

Figure 5.6: Comparison of flame speeds from derived correlations and experimental data for ethylene-air and propylene-air mixtures at T_u = 650 K and atmospheric pressure.

Figure 5.5 (a) shows the variation of temperature exponent γ with equivalence ratio (ϕ) for ethylene-air and propylene-air mixtures. It can be noted for the several preheat temperatures, the value for γ does not change much with ϕ. For propylene-air mixtures, only the results for equivalence ratios from 0.8-1.4 is used, as the confidence in flame measurements for ϕ<0.8 is low (see Section 4.1.3). But the curve fit is used to estimate the flame speed at these equivalence ratios as there is no obvious reason for γ to follow a different trend at these equivalence ratios. Also, some experimental data has been interpolated wherever experimental data is not available at an equivalence ratio. For example for propylene-air mixtures at T_u = 300 K, there is no experimental data at ϕ = 0.8. To calculate the flame speed value at this equivalence ratio interpolation is performed between measured flame speed values at equivalence ratios of 0.78 and 0.84.

The curve fit shows that for both fuel-air mixtures the coefficient of determination (R^2) value is close to one, indicating a high degree of confidence in the quadratic curve fit. These curve fits use data points based on the measurements taken for mixtures at different preheat temperatures: 15 points are used for ethylene-air; the propylene-air fit has only 8 points. These are sufficient number of points to attain a reasonable fit as the curve-fit is being used to generate a function between two variables (γ and ϕ). Figure 5.5 (b) shows the parabolic curve fit of $S_{L,o}$ at $T_{u,o}$ = 300 K for flame speed measurements. These curve fits follow equation (21) and the coefficients determined are shown in Table 5.2. These curve fits closely follow the experimental values at all equivalence ratios for both fuels; any differences between the fits and measurements are within the experimental uncertainty.

Figure 5.6 shows the performance of the empirical correlations when compared to the experimental data at a preheat temperature of 650 K for both ethylene-air and propylene-air mixtures. The correlation works well for ethylene-air mixtures at most equivalence ratios; while there are disagreements with the model at ϕ = 0.8 and 1.4, they lie within 5% of the experimental values. For propylene-air, the correlation model is close to the experimental flame speeds at near stoichiometric conditions, but under predicts at very lean conditions and over predicts at the richest condition. The lean disagreement may result from extrapolating the γ curve fit to these conditions, as noted above. The disagreement at the most rich condition could be due to the quadratic model not performing adequately at these equivalence ratios, perhaps a higher order model would be more appropriate for propylene-air mixtures.

Overall, the correlation model accurately predicts flame speed of ethylene-air mixtures whereas further work needs to be carried out to improve the model for propylene-

air mixtures. This could be accomplished by measuring flame speeds at more preheat conditions and reducing the uncertainties in flame speed measurements of weak flames close to flammability limits.

5.4 Summary

Flame speed data for ethylene- and propylene-air mixtures have been obtained over a wide range of equivalence ratios (~0.6-1.4) and for preheat temperatures from 300 to 650 K, which is a much higher reactant temperature than previous studies and thus significantly extends the existing flame speed data base for these fuels. Similarly, results for n-decane flames were obtained at 450 K preheat. Based on these measurements, empirical models were developed that provide flame speed as a function of preheat temperature and equivalence ratio for both alkene fuels.

The experimental measurements were also compared with simulations performed with a few leading chemical kinetic mechanisms. For ethylene-air, the NUI mechanism results agree well with the measurements, while the USC mechanism tends to under predict flame speeds for near stoichiometric and rich conditions. Both mechanisms, however, produce a similar sensitivity of flame speed to increases in preheat temperature, and it generally matches the experimental data.

For propylene-air mixtures, however, the ability of the models to reproduce the experimental results is degraded. In general, the NUI mechanism performed better at lower preheat conditions, while the USC model was closer to the experiments at the highest preheat temperature (650 K). Both models predict a higher dependence of flame speed on preheat temperature for near-stoichiometric mixtures when compared to the measurements.

Also, both the simulations and measurements show that the dependence of laminar flame speed on preheat temperature is different for ethylene and propylene; propylene exhibits an enhanced temperature sensitivity for rich mixtures. Though both fuels are alkenes, ethylene is more explosive and produces much higher flame speeds at comparable mixture conditions. The differences in reaction chemistry between the two alkenes is discussed in detail in 0, by employing tools such as sensitivity analysis.

CHAPTER 6. Vitiation effects

In this chapter, the effects of vitiation on laminar flame speeds of ethylene and propylene are examined. In vitiated systems, e.g., staged combustion and exhaust gas recirculation, the main diluents are nitrogen (N_2), water (H_2O) and carbon dioxide (CO_2); addition of these diluents tends to reduce the flame speed, with CO_2 having the largest impact and N_2 the smallest. The diluents can influence flame speed through their thermal (e.g., specific heat) and chemical properties. The diluents used here are representative of both non-reactive (N_2) and reactive (CO_2) diluents.

Considering the flow conditions in combustors and afterburners, as shown in Table 1.1, afterburners have significantly lower O_2 percentage when compared to the main combustor. Also, the average temperature of the reactants in afterburners is much higher due to the presence of hot products from the main combustor. Based on these reasons, dilution effects at a reactant preheat temperature of 650 K for ethylene and propylene mixtures are examined. The oxygen content, the diluent composition and the temperature of a mixture define the extent of vitiation, while the diluent could be either N_2 or CO_2. First N_2 dilution results are presented for both fuels, then CO_2 dilution effects are examined. Based on these measurements, the performance of selected, leading chemical kinetic models is also evaluated.

6.1 N_2 dilution effects

6.1.1 Experiment vs chemical kinetic models

Since O_2 content is one of the main factors that is different in vitiated combustors when compared to regular combustors, flame speed measurements at different O_2 levels are measured in this study. These levels are kept constant between the different diluents making it possible to compare them. The highest O_2 content corresponds to undiluted air, which is 21% of the oxidizer by mole. To keep a track of O_2 fraction in the mixture, a parameter Θ is defined as:

$$\Theta = \frac{[O_2]}{[\text{Total Oxidizer}]} \tag{23}$$

The value of Θ generally varies between 0.15 and 0.21 in this work, although some measurements at Θ=0.12 are presented. As noted above, the oxidizer is a mixture of O_2, N_2 and CO_2, with N_2 being the major component (as is typical in air-based systems).

Figure 6.1 shows the effect of reducing the O_2 concentration in the oxidizer, while adding a chemically non-reactive diluent (N_2). There are two distinct trends for ethylene and propylene when the S_L measurements are compared with predictions from chemical kinetic models. While the ethylene measurements are closer to the model predictions, the propylene measurements are significantly different. For ethylene mixtures, the USC mechanism most accurately predicts the flame speed at both the low O_2 conditions. This is consistent with the experimental data presented in the previous chapter for ethylene-air mixtures at 650 K. For propylene-air mixtures, the measurements presented in the previous chapter were lower than the mechanism predictions; this trend continues for the N_2 dilution

cases. However, the difference between the measurements and predictions is significantly higher (up to 110%) for dilution cases. This is notable as such a significant difference is not observed with ethylene as the fuel.

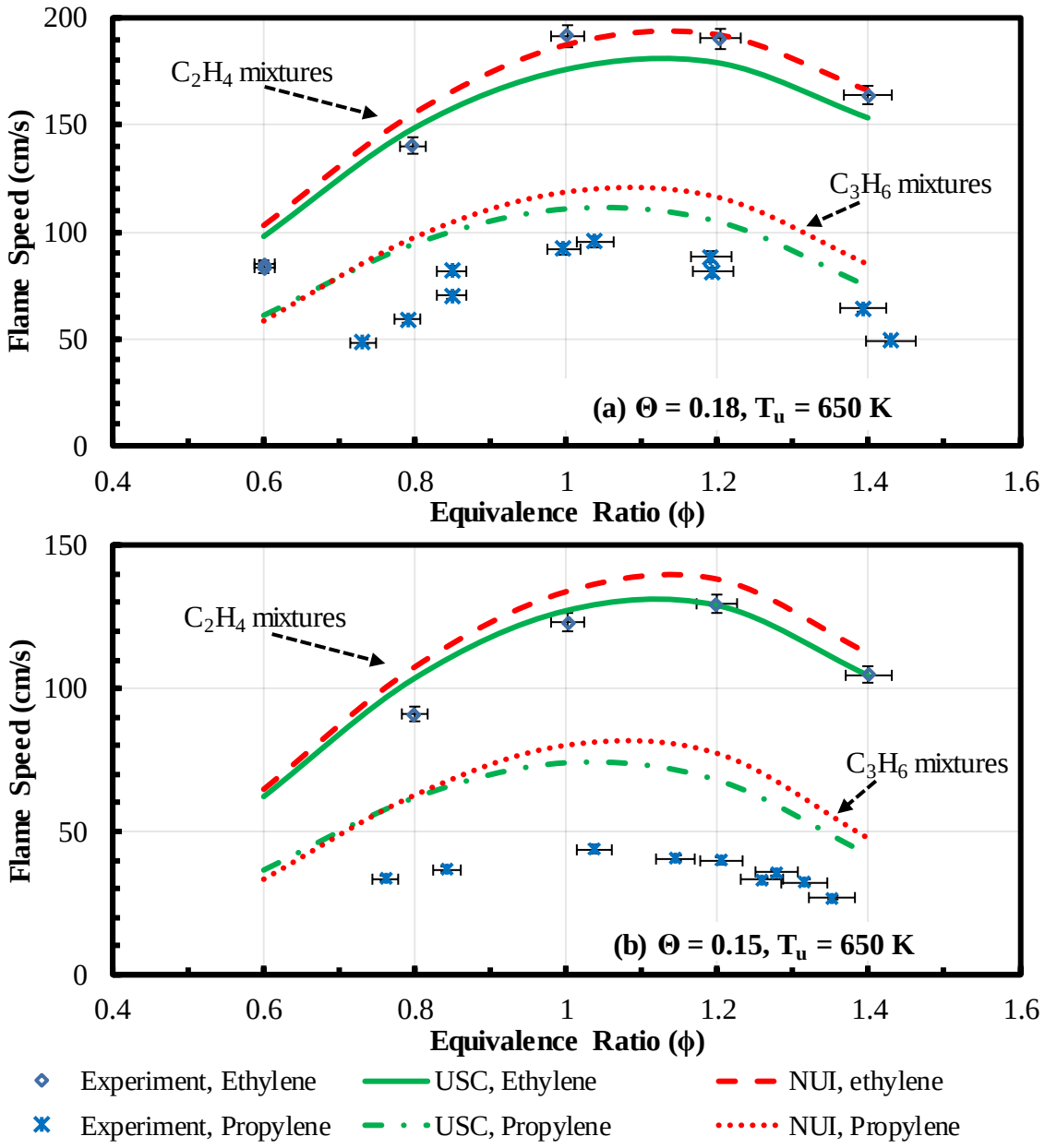

Figure 6.1: Comparison of laminar flame speed measurements with chemical kinetic models for ethylene and propylene with N_2 diluted air, at atmospheric pressure and (a) T_u = 650 K, Θ = 0.18 (b) T_u = 650 K, Θ = 0.15.

The difference between experimental and predicted flame speeds for propylene could be due to: 1) systematic errors in the measurements, or 2) deficiencies in the models that lead to larger flame speed errors at low O_2 content. After repeated experimental measurements with careful recalibration of the rotameters, and changes to the imaging optics and pilot flame, these were ruled out as sources of error. Furthermore, the lower than predicted flame speeds were visually observed through the presence of taller or open tip flames when the experimental flow conditions were chosen based on the predicted flame speeds. There is a possibility that these flames are stretch effected, but considering the flame speeds are higher than for those of mixtures at 300 K. The flame thickness should be comparable or even smaller for these high preheat flames reducing the effects of stretch. These observations increase confidence in current measurements and indicate that chemical kinetic models systematically overestimate flame speed for propylene mixtures with low O_2 content. The reasons behind these discrepancies between the fuels are explored in the next chapter.

The significant reduction in flame speed at low O_2 content for propylene made it impossible to measure flame speeds at lower preheat with dilution. Thus for propylene mixtures, the vitiation measurements are limited to 650 K. For ethylene, however, measurements were acquired with a preheat temperature of 450 K and $\Theta = 0.18$. Additionally, some ethylene measurements were made at $\Theta \cong 0.15$ and a preheat temperature of 450 K, but not at all equivalence ratios; due to low flow rates, the measurements at different equivalence ratios correspond to slightly different Θ. This is also the case for ethylene measurements that were made at 300 K for $\Theta \cong 0.18$ and 0.15. These

measurements at different preheat temperatures and dilution conditions are used to explore flame speed dependence on O_2 concentration.

6.1.2 %O_2 dependence

The dependence of flame speed on O_2 level is presented in this section. The measured flame speeds are normalized with the corresponding value for the same fuel, preheat temperature and equivalence ratio, but with undiluted air. Experimental and predicted (NUI mechanism[10]) results are normalized by their own corresponding undiluted values. Figure 6.2 shows the variation of the normalized flame speed with Θ for ethylene mixtures at three equivalence ratios: 0.8, 1 and 1.4.

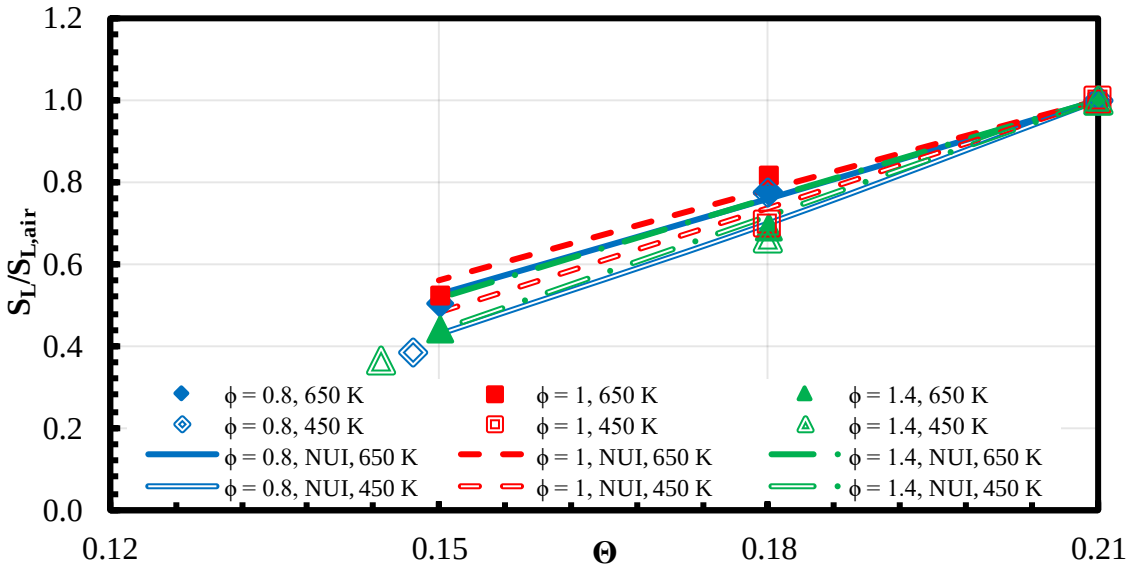

Figure 6.2: Normalized flame speed dependence on O_2 fraction in the oxidizer for C_2H_4-air-N_2 mixtures, at selected ϕ's and preheat temperatures of 450 and 650 K. Lines represent NUI kinetic model predictions; symbols are measurements.

[10] NUI mechanism is chosen here as it accurately predicts the flame speeds of alkene/air mixtures at most preheat conditions.

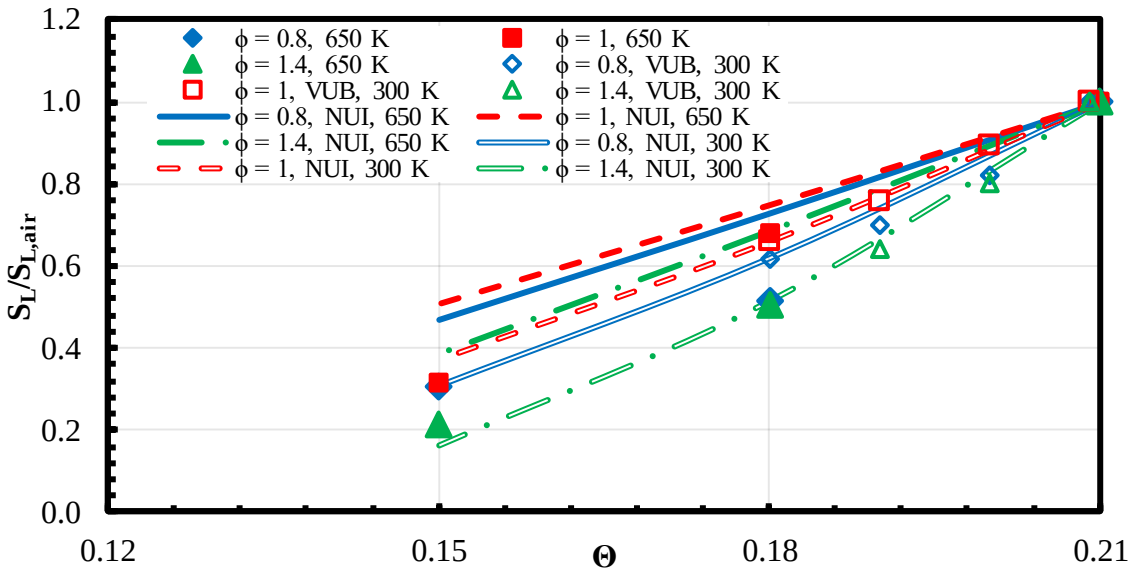

Figure 6.3: Normalized flame speed dependence on O_2 fraction in the oxidizer for C_3H_6-air-N_2 mixtures, at selected ϕ's and preheat temperatures of 300 and 650 K. Lines represent NUI predictions; symbols are measurements, this work and VUB[62].

Several observations can be made from this data. First, when normalized, the measurements and model predictions agree well at almost all the conditions; there are small differences between the model and experimental results but these generally lie within the experimental uncertainty[11]. Second, in most cases the normalized flame speed is a nearly linear function of Θ. Third, the sensitivity of the normalized flame speed to O_2 level varies between the lean, stoichiometric, and rich cases. For example, the stoichiometric condition shows the least sensitivity to Θ (lowest slope). The differences, however, are not substantial; in all cases the normalized flame speed drops by 52±4% from Θ=0.21 to Θ=0.15. Fourth, the trends are nearly the same at preheat temperatures of 450 and 650 K, although the higher preheat temperature generally produces a somewhat reduced sensitivity

[11] This is also true for the data at 300 K, which are not shown here.

to O_2 level in the oxidizer. Thus it can be concluded that for ethylene flames, the effects of vitiation are weakly dependent on preheat temperature compared to the impact of reduced O_2 fraction.

The impact of vitiation is markedly different for propylene compared to that for ethylene as discussed in the previous section. This is further evident in Figure 6.3, which shows the variation of normalized flame speed with Θ. The effect of vitiation on flame speed is higher for propylene mixtures when compared to ethylene mixtures. For example at $\Theta = 0.15$, the normalized flame speed value varied between 0.4 and 0.5 for ethylene mixtures at all different preheat temperatures. But for propylene mixtures this value varies between 0.2 and 0.5 suggesting that according to the chemical mechanism the effect of vitiation is more pronounced at 300 K when compared to 650 K.

The lower effect of vitiation at 650 K for propylene mixtures is not observed in the experimental data, which includes the current measurements at 650 K and literature data at 300 K[12] (Burke et al. [62] based on a flat-flame configuration). The 300 K experimental data matches the predictions up to $\Theta = 0.18$ at the three ϕ's shown here. At 650 K, the current measurements follow the 300 K trends, however the model does not predict as significant an effect on flame speed. Combined with the fact that for ethylene mixtures the effects of vitiation are weakly dependent on preheat temperature changes, we can conclude that the NUI mechanism over predicts flame speed at high preheat vitiated conditions. In Section 5.1, similar effects were observed for propylene-air mixtures indicating this could be an issue with simulations not able to accurately predict flame speeds at high preheat

[12] Literature values are used as the current experiments were unable to produce vitiated flames at low preheat temperatures.

temperatures for propylene mixtures, and this effect is more evident in vitiated cases. Further analysis of these inaccuracies in the simulations is discussed in Chapter 7.

6.1.3 Lean fuel % effects

It is generally observed in previous studies [12] that for lean premixed flames, the flammability limit defined in terms of the fuel concentration is nearly independent of the amount of O_2 in the oxidizer if the diluent is N_2. This is attributed to O_2 and N_2 having nearly the same molecular weight and heat capacity (c_p); as N_2 is nearly inert, its primary impacts on flame propagation are through diffusivity and heat absorption. Thus for lean mixtures, it is matters little whether the oxidizer contains excess O_2 or additional N_2. Thus for lean fuel-N_2-O_2 mixtures, we might expect flame speed would be a function only of fuel fraction (of course, for a fixed fuel, preheat temperature and pressure). This hypothesis is examined in Figure 6.4 and Figure 6.5, which show the variation of flame speed with fuel fraction for lean mixtures; both experimental measurements and the NUI model predictions are shown for comparison.

For ethylene (Figure 6.4), the model predictions agree reasonably well with the hypothesis at all preheat temperatures; the deviation from the best fit line is less than 10% except for the stoichiometric cases (where there is no "excess" O_2). The flame speed measurements also show a nearly linear dependence on fuel fraction for a fixed preheat temperature, though the measured speeds are lower than the predicted values, which is consistent with Figure 6.1 (a) for the lean data. The difference between the measurements and the NUI predictions is most notable at the highest preheat temperature, which is consistent with the earlier finding that the NUI mechanism over predicted the preheat

temperature dependence of the flame speed (Figure 5.4 (a)) for lean, undiluted C_2H_4-air mixtures. The differences between the NUI predictions and experiments are not greater than 20%, and compared to the USC mechanism predictions, the experimental flame speeds differ less than the established 10% accuracy of the measurement technique.

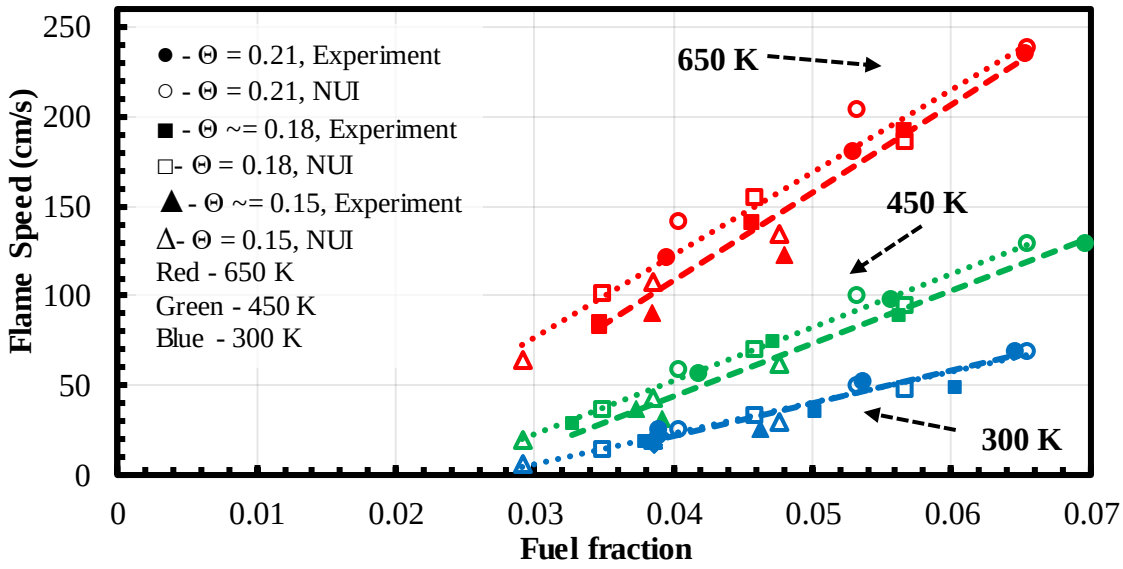

Figure 6.4: Flame speed variation with fuel fraction for lean C_2H_4-air-N_2 mixtures at three preheat temperatures. Dotted lines show linear best fit to the NUI predictions and the dashed lines show linear best fit to the experimental data.

For propylene (Figure 6.5) and considering first only the model predictions, we again see that the results nearly collapse to a line (for a fixed T_u). Thus the model predictions are consistent with the hypothesis that reducing the O_2 content of the oxidizer under lean conditions at fixed equivalence ratio primarily impacts the flame speed through reducing the fuel fraction and thus lowering the flame temperature. It is important to note, however, that the 650 K predictions show more deviations from the best-fit line compared to the ethylene results (Figure 6.4). This suggests that the chemical impact of lowering the

O_2 level is more significant for propylene compared to ethylene, especially at higher preheat temperatures.

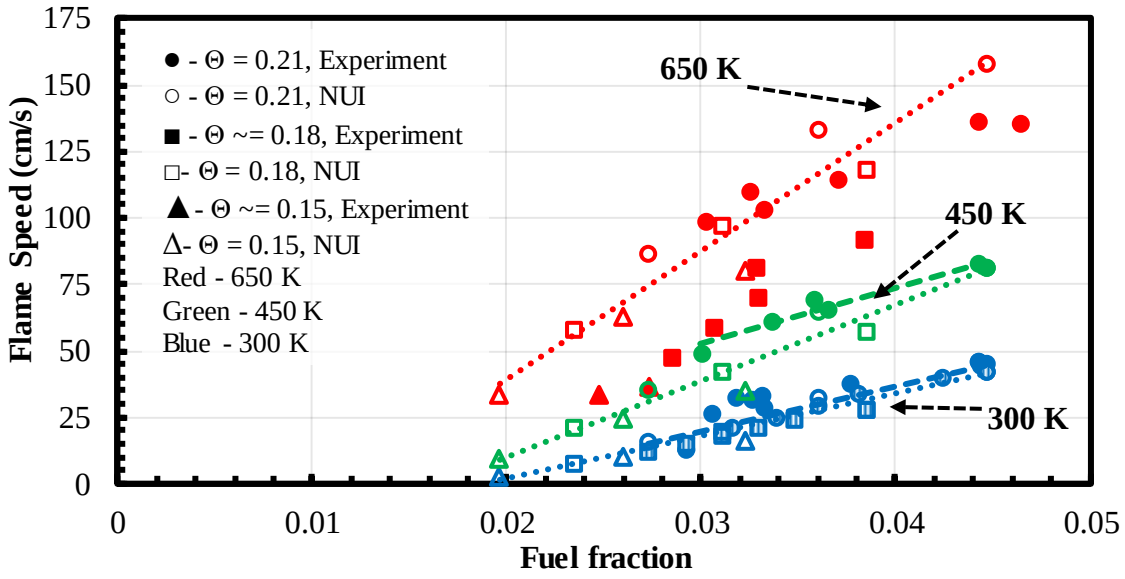

Figure 6.5: Flame speed variation with fuel fraction for lean C_3H_6-air-N_2 mixtures at three preheat temperatures. The 300 K experimental data is from [62] (flat-flame measurements) and is shown as symbols filled with vertical stripes. Dotted lines show linear best fit to the NUI predictions and the dashed lines show linear best fit to the experimental data.

Moving on to the experimental data, recall that dilution results were obtained only at a 650 K preheat temperature and for one Θ less than 0.21 (0.18) for the reasons described earlier in this chapter. Thus Figure 6.5 includes dilution results for 300 K taken from Burke et al. [62] at Θ=0.18 and 0.21. The 300 K experimental results again have a nearly linear dependence on fuel fraction, with essentially the same slope predicted by the NUI mechanism; though, the current measurements produce flame speeds slightly higher than the flat flame results and model predictions. These observations are consistent with the

450 K results (though this set does not include $\Theta<0.21$). As seen in the previous section, the 650 K measurements differ by large margins from the predicted flame speeds. In addition, the measured flame speeds from the two dilution (Θ) levels do not collapse as well onto a single line. So like the predictions, the experimental results indicate that the chemical impact of lowering the O_2 level is more significant for propylene compared to ethylene at higher preheat temperatures - and that this issue may be poorly predicted with the current chemical mechanisms.

So much like what was seen in the previous chapter on preheat temperature dependence, the N_2 dilution results suggest the differences between the chemical kinetics for propylene combustion compared to ethylene may not be accurately captured in the current mechanisms, especially at higher preheat temperatures. In 0, the differences in kinetic pathways of these two fuels is examined using sensitivity analysis and simulations of the premixed flame structure.

6.2 CO_2 dilution effects

A non – reactive diluent (N_2) has been considered to study what are mostly thermal effects due to vitiation on laminar flame speed. Even though N_2 is considered chemically inert, chemical effects were observed for mixtures with low O_2 concentration. To further study chemical effects due to dilution, flame speeds were measured with CO_2 as the diluent. CO_2 was chosen because it has the largest impact on laminar flame speeds amongst the common vitiation diluents that are chemically active [72]. This study is limited to ethylene as the flame speeds for propylene with CO_2 dilution were too low to be captured using the current experimental setup. Furthermore, they are limited to a preheat temperature 650 K

in order to maintain measureable flame speeds at high CO_2 and low O_2 conditions. Measurements were made with $O_2/N_2/CO_2$ oxidizer mixtures having CO_2 fractions up to 20% and O_2 levels as low as 15%. First, the laminar flame speed data is compared to predictions from the chemical kinetic models to check the accuracy of these predictions. Subsequently, areas of disagreement are identified and reasons for these differences are explored.

6.2.1 Experiments vs chemical kinetic models

Laminar flame speeds are measured for various levels of CO_2 concentration in the oxidizer. The CO_2 level in the oxidizer is characterized by a parameter C, defined as:

$$C = \frac{[CO_2]}{[\text{Total Oxidizer}]} \tag{24}$$

Combined with Θ, the fraction of O_2 in the oxidizer, the composition of the oxidizer is completely defined.

Figure 6.6 shows the variation of flame speed with equivalence ratio for both experimental measurements and kinetic model predictions at $\Theta = 0.18$ and C = 0, 0.05 and 0.1. The results at C= 0 (dilution solely by N_2) are the same as presented in the previous section, with the kinetic model predictions within ± 10% of the experimental measurements except at extremely lean conditions ($\phi = 0.6$). As expected, replacing more of the N_2 with CO_2 in the oxidizer leads to decreases in flame speeds for both measurements and predictions. This decrease in flame speed is due to both thermal and chemical effects as CO_2 is a chemically active species for hydrocarbon chemistry. More notably, increasing C also leads to larger differences between the predictions and the measurements for lean

mixtures; whereas at rich and stoichiometric conditions, the differences remains within the 10% margin.

By increasing the CO_2 fraction further and decreasing the O_2 levels, these differences become more pronounced, as illustrated in Figure 6.7. Here, Θ is reduced to 0.15 and C is 0, 0.1 and 0.2. The C=0 results are the same N_2 dilution data reported above, where it was observed that decreasing the O_2 content to 15% results in even more over prediction of the flame speeds compared to the 18% O_2 case. Replacing a portion of the N_2 diluent with CO_2 (C = 0.1) leads to differences between flame speed and measurements becoming higher on the lean side and to a lesser extent at stoichiometric and rich measurements. A further increase in CO_2 (C = 0.2) concentration widens this gap further at all equivalence ratios.

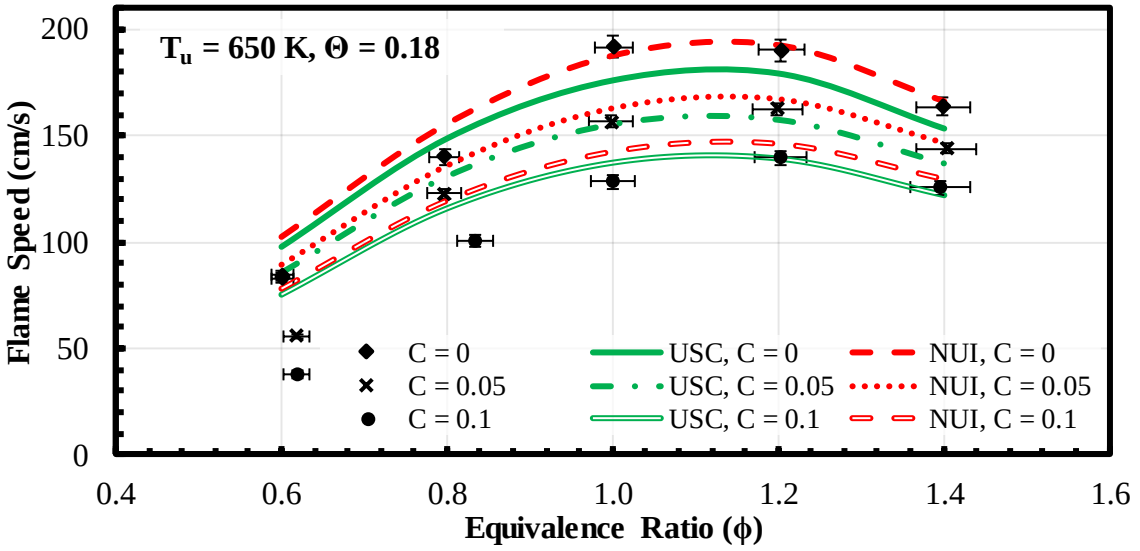

Figure 6.6: Flame speed variation with equivalence ratio for ethylene mixtures at different levels of CO_2 concentration in the oxidizer with Θ = 0.18, at a preheat temperature of 650 K and atmospheric pressure.

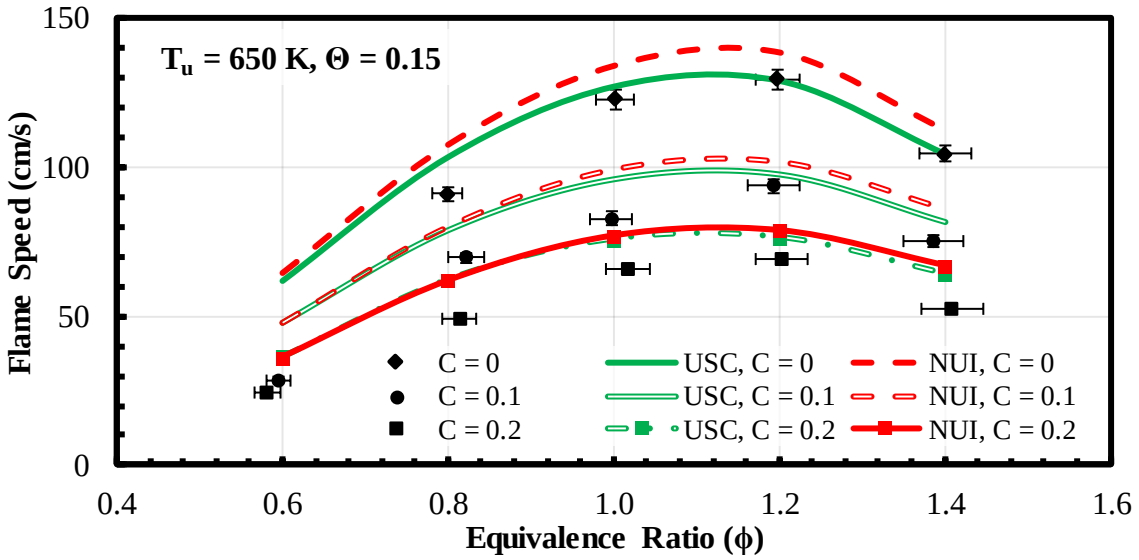

Figure 6.7: Flame speed variation with equivalence ratio for ethylene mixtures at different levels of CO_2 concentration in the oxidizer with Θ = 0.15, at a preheat temperature of 650 K and atmospheric pressure.

A point to note for all the CO_2 diluted mixtures is that at extremely lean conditions (ϕ ~= 0.6) the differences between the models and measurements are large (> 20%) irrespective of the amount of CO_2 in the oxidizer. This could be due to a changes in the lean flammability limit of ethylene mixtures, as addition of CO_2 leads to an increase in the equivalence ratio at the flammability limit compared to N_2 dilution. The specific heat capacity (c_p) of CO_2 is higher than that of N_2 and O_2 leading to lower flame temperatures by just considering thermal effects of CO_2 as a diluent. These differences between models and experiments could be due to experimental issues or systematic errors in the kinetic models which become prominent for high CO_2 dilution cases.

6.2.2 Effects of radiation on flame speed

A fair question to raise at this point is whether dilution with CO_2 leads to some additional systematic errors in the measurements. To this end, the percentage difference between the NUI model predictions and the measurements are displayed in Figure 6.8 as a function of the mole fraction of CO_2 in the combustion products[13]. Irrespective of the CO_2 concentration in the products, the differences are always greater than 10% for extremely lean ($\phi \sim 0.6$) mixtures. Furthermore for high concentrations of CO_2 in the products (due to CO_2 dilution of the oxidizer) and irrespective of equivalence ratio, the percentage difference is also high and increases with CO_2 concentration. As CO_2 concentration is key to these observations, it is prudent to note that the experiment could be suffering from systematic errors due to the presence of excess CO_2.

There are a few possible reasons why the experimental flame speeds with CO_2 dilution cases might be systematically lower than the predicted flame speeds: stretch-induced effects, since the models assume 1-d flames; and radiation, as the models assume adiabatic flames. The analysis in Chapter 4 showed that stretch-induced error are small if tall flames ($H/D > 2$) are considered. Also at high preheat temperature and thus high flame speeds and reduced flame thicknesses, the flame speeds determined with the current Bunsen flame approach are less stretch sensitive. Since these criteria are met for CO_2 diluted flames shown here (as the preheat temperature is 650 K and the flames generated are tall) stretch induced effects can be ruled out as the reason for these differences.

[13] Product mole fraction of CO_2 is chosen here as radiation losses occur from the high temperature products.

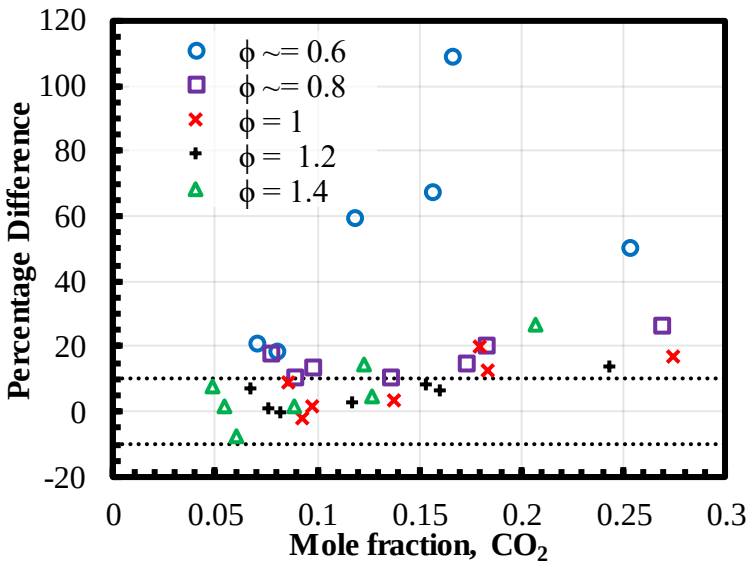

Figure 6.8: Percentage difference between NUI model predictions and current measurements for product mole fraction of CO_2 of ethylene flames (for vitiated and non-vitiated cases) at 650 K and atmospheric pressure.

Considering radiation, it would tend to cause heat loss from the flame and thus reduce the measured flame speeds, which is qualitatively what is observed. Also, CO_2 is a much better infrared radiative emitter than the homonuclear N_2. So it is plausible that the CO_2 diluted flame data could suffer from radiation effects. To study radiation effects, the CHEMKIN-PRO [64] PREMIX model [78] is used to estimate the flame speeds including radiation losses, assuming an optically thin flame, i.e., where emitted energy is not reabsorbed elsewhere in the flame. This should produce the maximum reduction in flame speed. CO, CO_2, H_2O and CH_4 are considered the radiators; these species are chosen as the other radiative species either exist only in cooler regions of the flame or are present in very low concentrations. The Planck mean absorption coefficients (a_i) are provided as a part of the thermodynamic properties of a species, in the form given by:

$$a_i(T) = \sum_j c_j T^j \quad with\, j = 0,1, \ldots, 6 \; (m^{-1}atm^{-1}) \tag{25}$$

where c_j are the polynomial curve-fit parameters for absorption coefficient with temperature. The coefficients are adapted from Barlow et al. [112], who estimated the absorption coefficients using the RADCAL [113] narrow-band radiation model. The heat loss due to radiation is estimated using the formula:

$$\dot{Q}_{radiation} = 4\sigma\left(T^4 - T_b^4\right)\sum_i p_i a_i \tag{26}$$

where σ = 5.669×10^{-8} W/m^{2}K^4, T is the local gas temperature, T_b is the background (environment/surroundings) temperature, p_i is the partial pressure of species i in atmospheres, and a_i is the Planck mean absorption coefficient for species i. For the experiments, T_b is estimated to be 300K, since the walls of the burner enclosure are relatively cold to the touch; this is also a conservative assumption, since hotter walls would reduce the net radiative heat loss from the flame. This heat loss when incorporated into the PREMIX model provides a convergent solution for flame speed, thus giving an insight into the radiation effects on the measured flame speeds. The base chemical kinetic model used for this analysis is the NUI mechanism. If the radiation effects are prominent, then the predicted flame speed should decrease and move much closer to the experimental measurements.

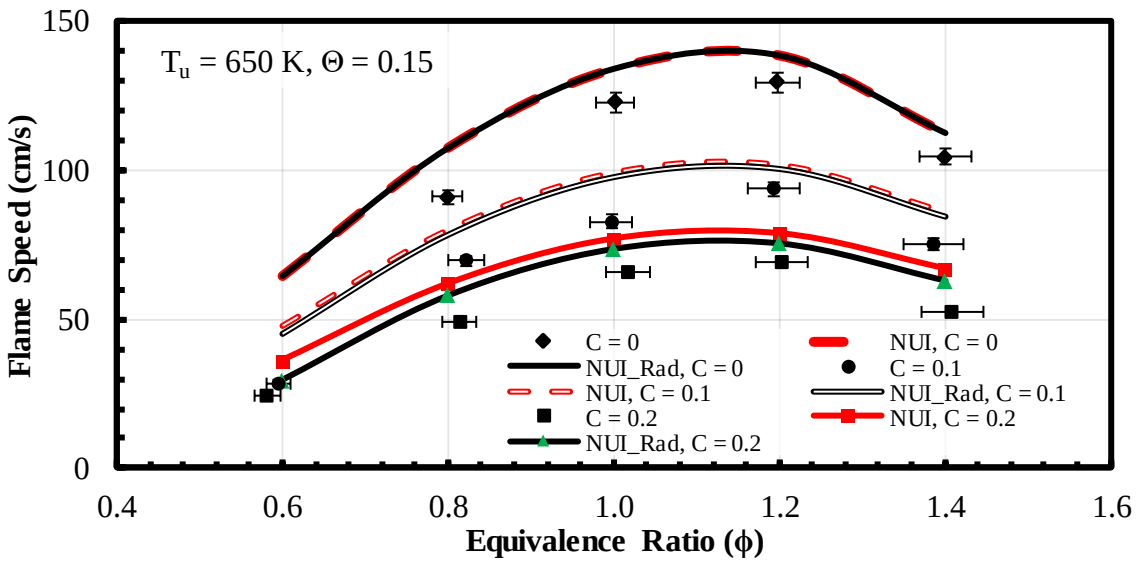

Figure 6.9: Effect of radiation on laminar flame speed at different equivalence ratios and CO_2 dilution levels (C = 0, 0.1 and 0.2). The preheat temperature is 650 K, oxygen level in the oxidizer is Θ = 0.15 and pressure is atmospheric.

Since the largest differences between the predictions and measurements are observed for conditions with low oxygen concentration (Θ = 0.15) and high CO_2 content (C = 0.2), the maximum radiation impact on flame speed should occur at these conditions. Figure 6.9 shows impact of radiation heat losses on the predicted flame speeds for Θ = 0.15 and the three CO_2 dilutions. In general, the radiation effect is minor when compared to the differences between the experiment and predictions. As expected, the greatest radiation impact is observed for cases with the highest CO_2 dilution (C = 0.2), but even at this condition the effects of radiation do not reduce flame speeds by more than 8%. Furthermore, the effect of radiation is nearly independent of equivalence ratio, whereas the measurements and model differences do vary with equivalence ratio. Thus, with confidence it can be concluded that flame radiation is not cause of the lower dependence of the predicted flame speeds on CO_2 dilution levels.

6.2.3 Thermal vs chemical effects

Since systematic experimental errors do not appear to cause the differences between measured and predicted flame speeds, inaccuracies in the chemical mechanisms may be the source of the discrepancy. Furthermore, the chemical effects of CO_2 become more important with higher CO_2 dilution. This can be illustrated by separating the thermal and chemical effects of CO_2. To achieve this, the reaction mechanism is modified by replacing the diluent CO_2 with a new species, FCO_2, which has the same thermodynamic properties as CO_2 but does not participate in the hydrocarbon reaction chemistry. This provides an opportunity to separate the thermal effects of CO_2 from the chemical effects [114, 115].

The thermal effects of the diluent CO_2 are shown in Figure 6.10 using the FCO_2 species for cases with $\Theta = 0.15$ at 650 K preheat and atmospheric pressure. It can be seen that as N_2 in the oxidizer is replaced by FCO_2 the flame speed reduces due to just the heat absorption by the diluent. As the amount of FCO_2 in the oxidizer increases, this leads to higher thermal effects and a larger reduction of flame speeds when compared to N_2 dilution ($C = 0$). When FCO_2 is replaced by chemically active CO_2, the chemical effects of CO_2 can be observed; the result is lower flame speeds.

To characterize the fractional reduction in flame speed due solely to direct chemical effects associated with CO_2 dilution, the following metric can be used:

$$\mathbf{CTR} = \frac{Chemical\ effect}{Thermal\ effect} = \left(\frac{S_{L,\,FCO_2}^{C} - S_{L,\,CO_2}^{C}}{S_{L}^{C_0} - S_{L,\,FCO_2}^{C}} \right) \tag{27}$$

where $S_L^{C_0}$, $S_{L,\,FCO_2}^{C}$ and $S_{L,\,CO_2}^{C}$ are the flame speeds for no CO_2 dilution, FCO_2 dilution and real CO_2 dilution, respectively, at a given equivalence ratio and Θ.

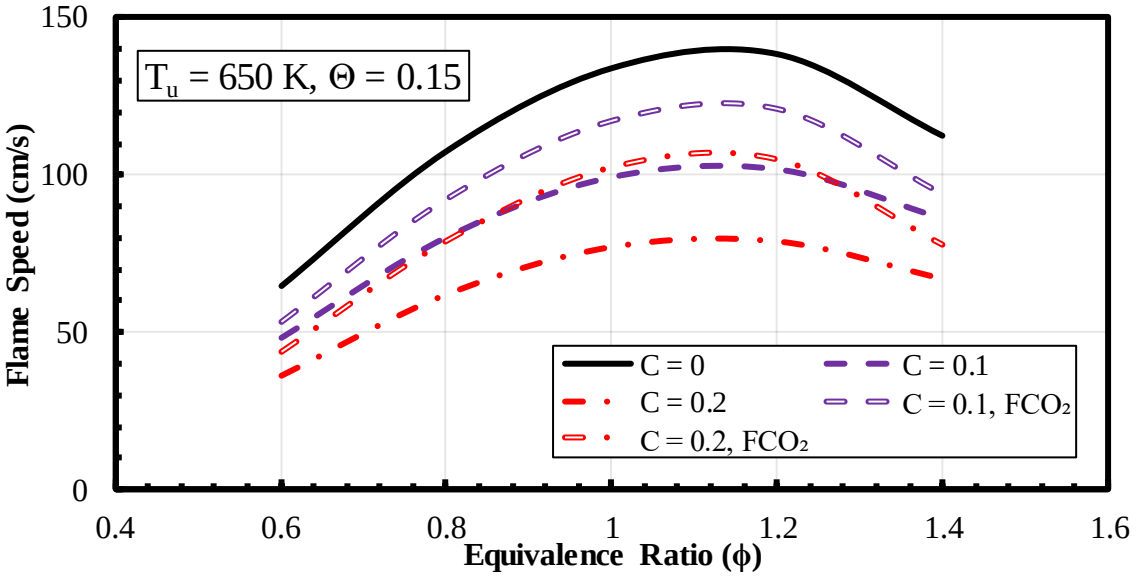

Figure 6.10: Simulation of CO_2 thermal effects on flame speed using FCO_2 species in NUI chemical mechanism at 650 K, Θ = 0.15 and atmospheric pressure conditions.

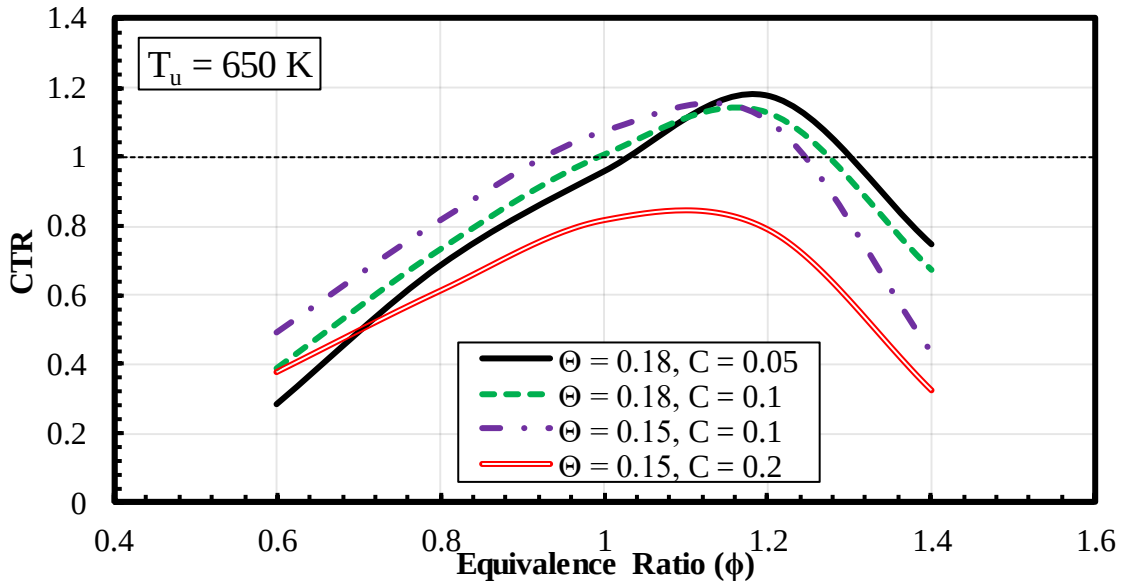

Figure 6.11: Relative importance of chemical effect of CO_2 on laminar flame speed at 650 K, Θ = 0.18 and 0.15, atmospheric pressure conditions, and different levels of CO_2 dilution.

Figure 6.11 compares the chemical effect of CO_2 dilution against the thermal effect using the NUI mechanism for different levels of CO_2 dilution at $\Theta = 0.18$ and 0.15. There are a few interesting observations to be made. For instance, the highest chemical effect is always observed for mixtures with ϕ between 1 and 1.2, irrespective of the amount of CO_2 in the initial reactants. For mixtures with the highest level of dilution, the thermal effects dominate over the chemical effect; this could be due to the large amounts of CO_2 present in the reactants acting as a heat sink and lowering the final flame temperature. For lean mixtures where there is excess oxidizer, it is likely that the mole fraction of CO_2 is also very high, and hence the higher thermal effect again dominates. For rich mixtures, thermal effects are again higher. It is important to note that thermal effect and chemical effect are interlinked, the higher the thermal effect lower the final temperature leading to a reduced impact of the chemical effect. Also, even though at some conditions the thermal effect is dominant, the chemical effect is still comparable over a wide range of equivalence ratios.[14]

Considering that the largest differences between experimental measurements and kinetic model predictions are observed for lean mixtures, it can be inferred that reaction kinetics for lean mixtures are not well captured even though their influence is limited for these mixtures. This points towards the hypothesis that reactions which are important for lean mixtures become less important for stoichiometric and rich conditions. The rate coefficients for these reactions might not have the accurate temperature dependence which can lead to over prediction of flame speeds. This hypothesis is examined in the next chapter.

[14] For example, a CTR of 0.8 implies the chemical effect is 80% as effective as the thermal effect in reducing the flame speed.

6.3 Summary

In this chapter, the effect of adding diluents to oxidizer on flame speed has been studied. Two diluents were used for this purpose: N_2 (chemically inactive) and CO_2 (chemically active). As expected, dilution leads to reductions in flame speed as the oxygen content in the mixture is replaced by the excess diluent. The amount of effect N_2 dilution has on flame speeds varied based on the fuel used; it was higher for propylene mixtures when compared to ethylene mixtures. Further, the chemical mechanisms were able to accurately predict the flame speeds of ethylene mixtures, within ± 10% from the measurements, while for propylene mixtures these differences are greater than 10% and up to 100% for some cases.

It was noted that the normalized flame speed variation with oxygen content in the mixture was independent of the preheat temperature for ethylene mixtures; this is observed in both the experimental and model results. For propylene mixtures, the normalized experimental flame speed was independent of preheat temperature, whereas there was a preheat dependence for the model predictions. Presumably, an important difference in chemistry between ethylene and propylene oxidation leads to these differences. This was further bolstered by examining flame speeds of lean mixtures for both fuels, as flame speeds of lean N_2-diluted mixtures should primarily dependent on the amount of fuel since N_2 and O_2 have similar thermal properties. For ethylene mixtures, this was largely found to be true with some evidence of chemical effects due to the substitution of N_2 for O_2 becoming important for flames at near-stoichiometric conditions and for mixtures with lower O_2 content. For propylene, this was found to be not true, as the trends predicted by the kinetic models and current measurements deviated largely as the amount of O_2 content

in the mixture was lowered. The unique aspects of propylene chemistry are explored in the next chapter.

Addition of a chemically active diluent (CO_2) led to further reduction in flame speed as CO_2 has a higher c_p than N_2 and suppresses the CO+OH heat release reaction. There were systematic differences between experimental measurements and chemical mechanism predictions observed as the amount of CO_2 dilution was increased. The largest differences were observed for $\Theta = 0.15$ cases, possible systematic experimental issues including effects of radiation from the flames were explored and shown not to be the cause. Thermal effects of CO_2 were isolated by simulating a non-reactive CO_2 (FCO_2) molecule and estimating flame speed. The chemical effect of CO_2 was shown to be a significant contributor for reduction in flame, and if models under estimate this contribution it could lead to over estimation of flame speeds.

CHAPTER 7. Reaction mechanism analysis

In this chapter, the chemical reactions of laminar, ethylene and propylene flames are examined using sensitivity analysis, and profiles of species concentrations and rates of production. These tools are used to identify important reactions for flame propagation and their differences in ethylene and propylene flame propagation. Rate coefficients of these key reactions are examined in detail, including possible modifications to improve the predictive capability of the NUI reaction mechanism based on the experimental results presented in the previous two chapters. First, based on unresolved questions raised in Chapter 5, reactions important to propylene chemistry that might cause the differences between the model predictions and experimental findings. Secondly, based on experimental data presented in the vitiation effects chapter (Chapter 6), the kinetic effects of lower O_2 content and the addition of CO_2 diluent are discussed. Reactions which have higher relevance due to the addition of CO_2 to the oxidizer are examined, and modifications to their rate coefficients are tested to assess their impact on the errors in flame speed predictions.

7.1 High temperature effects

The experimental results shown in Chapter 5 (e.g., Figure 5.2) clearly demonstrate that the effect of preheat temperature on S_L is captured well by the mechanisms for ethylene, whereas for propylene the mechanisms do not accurately predict this effect. This suggests important differences in the reaction chemistry for these fuels. This can be observed by comparing the adiabatic flame temperatures (T_{ad}) of ethylene and propylene mixtures. S_L is highly dependent on the mixture's T_{ad}, higher values generally produce

higher flame speeds. The adiabatic flame temperatures of ethylene and propylene mixtures at different preheat temperatures are shown in Figure 7.1.

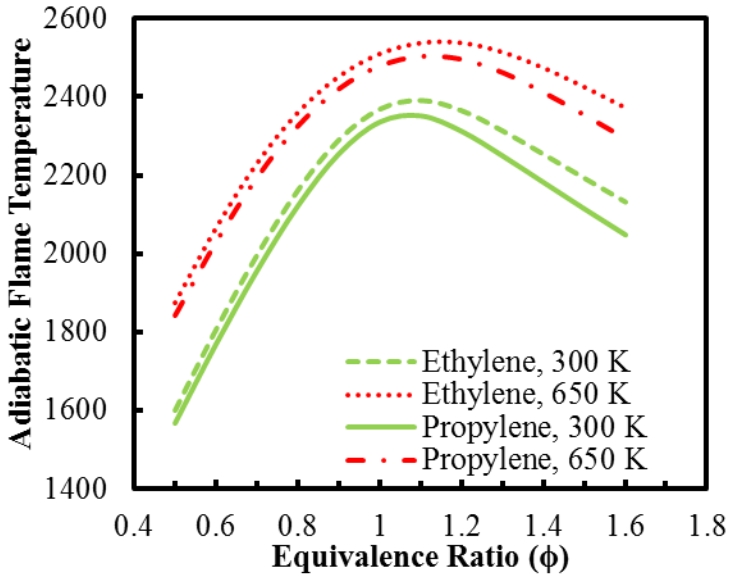

Figure 7.1: Adiabatic flame temperature variation with equivalence ratio for ethylene-air and propylene-air mixtures at different preheat temperatures and atmospheric pressure.

It can be noted that T_{ad} for ethylene is higher, but the temperatures for the two fuels are close for lean and stoichiometric flames. Under fuel rich conditions, however, ethylene flames become noticeably hotter. But as observed in Chapter 5, the flame speeds of propylene are almost 50% lower than those of ethylene at all equivalence ratios, irrespective of preheat temperatures. This indicates that the specific reaction chemistry of the fuels are different leading to propylene flames having lower flame speeds at the same mixture conditions.

In Chapter 5, it was noted that the chemical kinetic models predict S_L with higher accuracy for ethylene-air mixtures when compared to propylene-air mixtures. The NUI

mechanism is used here to understand the differences in reaction chemistry as it is the most updated model for alkenes and has a higher total number of reactions included. It is also more accurate compared to the current experimental results at preheat temperatures other than T_u = 650 K. At this high preheat temperature, the NUI predictions are higher than the experimental values for propylene air mixtures; this could be due to errors in the rate constant expressions in a few reactions or due to errors in thermal and transport properties for various species. It is likely that the discrepancies are caused by errors in rate expressions rather than thermal and transport properties as their temperature dependence is known to a higher accuracy [116].

To identify the reactions which are key for propylene flame propagation a common methodology is to perform sensitivity analysis. Sensitivity analysis provides a first-order sensitivity of flame speed predictions with respect to changes in the pre-exponential factor of the Arrhenius type rate coefficients (i.e., the *A*-factor values). The normalized sensitivity coefficient (s_i) is calculated using the following formula:

$$s_i = \frac{A_i}{S_L} \frac{\partial S_L}{\partial A_i} \tag{28}$$

Here, A_i is the pre-exponential factor of the i^{th} reaction. This analysis is performed using Chemkin-PRO [64], and the sensitivities of the top ten reactions for ethylene-air and propylene-air mixtures are identified. A positive s_i indicates that an increase in A_i enhances S_L, whereas a negative value indicates reduction in S_L with increasing *A*.

Figure 7.2 shows the normalized sensitivities for ethylene-air and propylene-air mixtures at three equivalence ratios and two preheat temperatures. For lean and stoichiometric flames for both fuels, the reactions with highest sensitivity are the oxidation

of CO to CO_2 (which is one of the most important heat release reactions) and the chain branching reaction $H+O_2 \Leftrightarrow O+OH$. There are several chain-terminating reactions which are common between the two fuels; these are more dominant in the fuel lean cases. For rich mixtures, reactions involving species such C_2H_2 and C_2H_3 have larger impact on flame speed due to the presence of excess fuel.

Though the reactions involving H_2/CO have the highest sensitivity, their temperature dependence is known to a high degree of accuracy as they have been subject of numerous studies[117, 118]. The main difference between the two fuels arises from the attack on fuel molecules by radicals; interestingly the flame speed sensitivity for these reactions is positive for ethylene and negative for propylene. The dominant ethylene fuel attack is carried out by O and OH radicals leading to formation of highly reactive CH_2CHO, O and H radicals.

$$C_2H_4 + OH \Leftrightarrow C_2H_3 + H_2O$$

$$C_2H_3 + O_2 \Leftrightarrow CH_2CHO + O$$

$$C_2H_4 + O \Leftrightarrow CH_2CHO + H$$

There are two main pathways for this: the attack by OH results in CH_2CHO and O through the formation of C_2H_3 (vinyl) radical, while the reaction with the O radical directly results in formation of CH_2CHO and H. These reactions result in highly reactive compounds and radicals that enhance the propagation of flames and hence have a positive sensitivity. In contrast, propylene fuel attack through both OH and H radicals results in the formation of a resonantly stable C_3H_5-A (allyl) radical.

$$C_3H_6 + OH \Leftrightarrow C_3H_5\text{-}A + H_2O$$

$$C_3H_6 + H \Leftrightarrow C_3H_5\text{-}A + H_2$$

$$C_3H_5\text{-}A + H(+M) \Leftrightarrow C_3H_6(+M)$$

The allyl radical recombines with an H radical to form C_3H_6; this pathway results in the formation of fuel (a chain terminating pathway) thus reducing flame speed. The other pathway (a chain branching step) for this reaction is to produce vinyl (C_2H_3) and methyl (CH_3) radicals but this reaction is less favored and has a lower sensitivity. Thus, the fuel attack for ethylene-air mixtures has a positive effect on S_L, whereas for propylene-air mixtures it has a negative effect. Since there are significant differences between the experiments and kinetic model results only for propylene-air mixtures (and at high preheat temperatures), the fuel attack of propylene reactions need to be examined further. Burke et al. [61] identified that of the three reactions, the fuel reactions with OH and H radicals have an effect on other experimental targets apart from flame speed, such as autoignition delay. While the allyl-H recombination reaction only effects laminar flame speed values, a closer look at the reaction rate of this reaction is discussed in the next subsection.

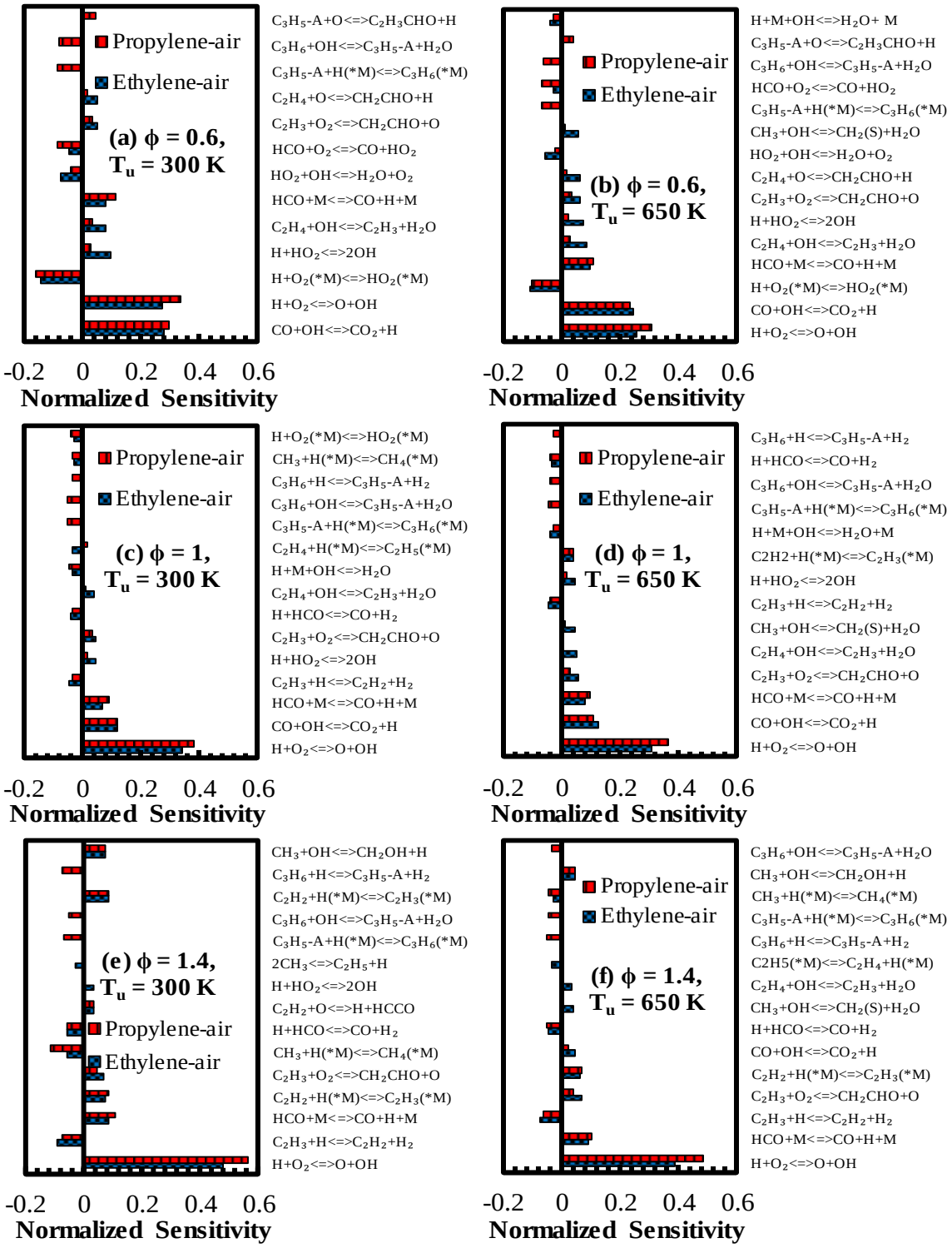

Figure 7.2: Normalized *A*-factor sensitivity of S_L for NUI mechanism. Comparison between propylene-air and ethylene-air mixtures at lean, stoichiometric and rich equivalence ratios at low (300 K) and high (650 K) preheat temperatures.

7.1.1 Rate coefficient of C_3H_5-A + H (+ M) ⇔ C_3H_6 (+ M)

Reaction rate coefficients (k) can be defined by the modified Arrhenius formulation as shown in equation (29). Here, b is the temperature exponent, R is the universal gas constant, T is the temperature and E_a is the activation energy. Typically rate constants are measured using shock-tube reactors or estimated analytically by calculating potential surfaces of species involved in the reaction. The validity of these rate constants is checked by estimating global parameters such as flame speeds and comparing them with experimental data. Minor adjustments to these rate coefficients can also be done based on the disagreements between computationally predicted and experimentally estimated global physical properties.

$$k = AT^b e^{\left(-\frac{E_a}{RT}\right)} \tag{29}$$

The rate coefficient for the C_3H_5-A + H recombination reaction in the NUI mechanism was adopted from the study by Tsang [119]; this is widely adopted by several reaction mechanisms either in its true form or with a modified value. Tsang assigned a large value for the rate constant (2×10^{14} cm^3 $mole^{-1}$ s^{-1}) with an uncertainty factor of 3, as there were no experimental data for this reaction.

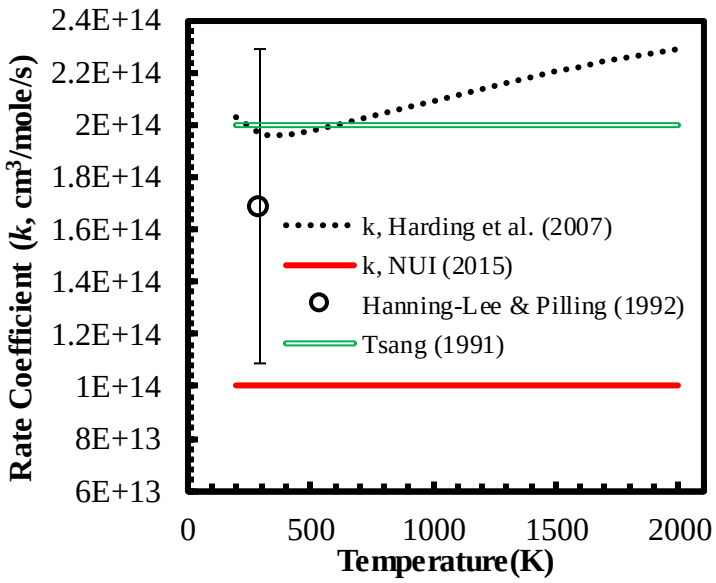

Figure 7.3: Rate coefficient dependence with temperature for allyl-H recombination reaction as predicted by different studies.

Figure 7.3 shows the allyl-H recombination reaction's rate coefficient dependence with temperature. Hanning-Lee et al. [120] measured the rate coefficient at four pressures and found the mean rate coefficient to be 1.7×10^{14} cm^3 $mole^{-1}$ s^{-1} and the uncertainty in this value falls within the value predicted by Tsang. Harding et al. [121] theoretically predicted the rate coefficients dependence with temperature; they indicated a minimal temperature dependence which lies within the error range predicted by Tsang. In the NUI mechanism, to improve agreement with flame speed measurements, the rate constant was reduced by a factor of 2 to increase the flame speed value by 5% [61] for measurements at a preheat temperature of 300 K. This increase can be predicted from the sensitivity analysis shown in Figure 7.2.

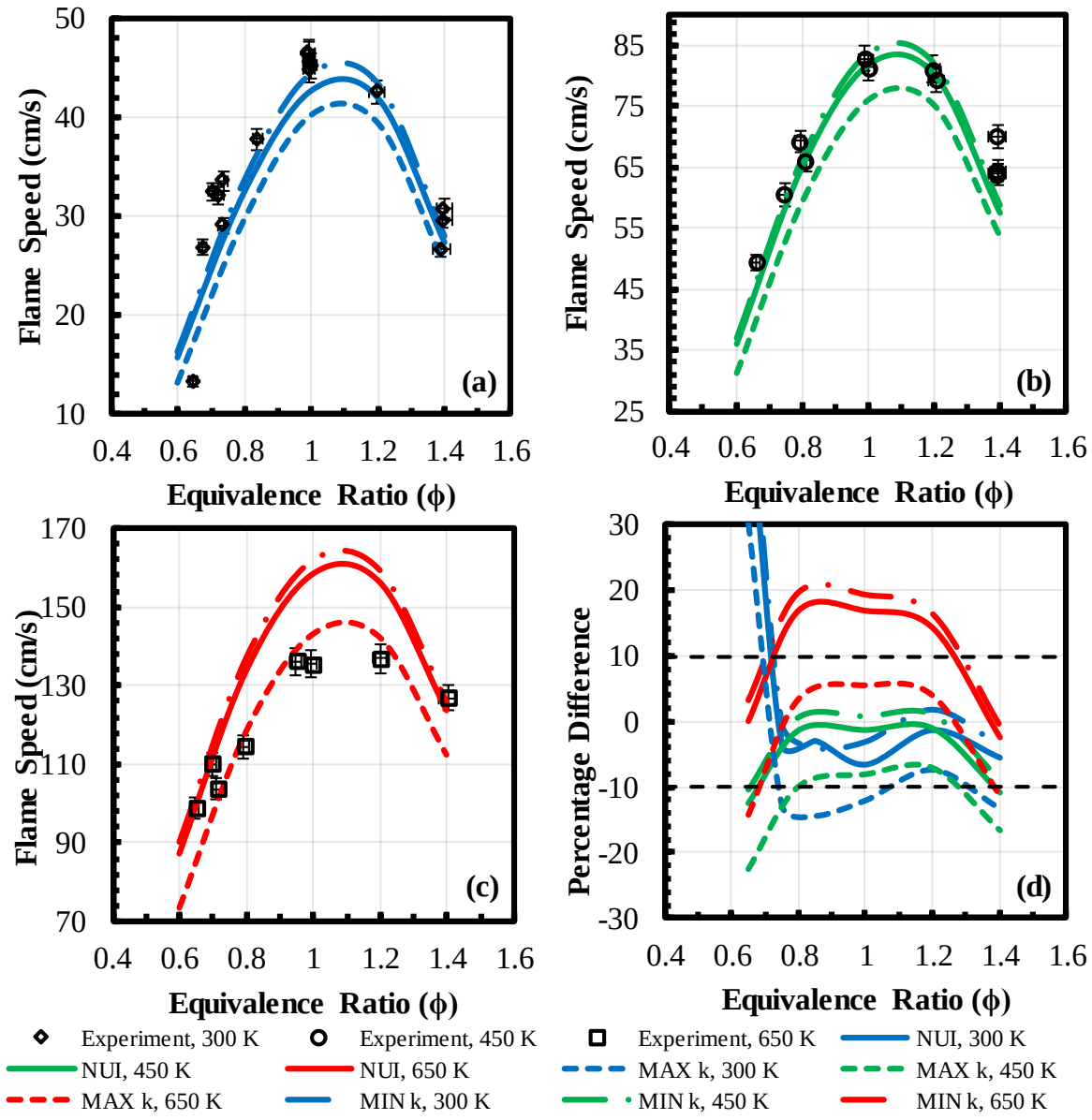

Figure 7.4: Effect of changing rate constant of C_3H_5-A + H(+ M) ⇔ C_3H_6(+ M) on laminar flame speed of propylene-air mixtures at atmospheric pressure conditions, within bounds of uncertainties (minimum (MIN *k*) and maximum (MAX *k*)) as described by at different preheat temperatures (a) T_u = 300 K (blue), (b) T_u = 450 K (green), (c) T_u = 650 K (red) and (d) percentage difference from the experiment.

To study the effects of uncertainty in this value, the reaction rate is changed to the suggested minimum (0.667×10^{14} cm^3 $mole^{-1}$ s^{-1}) and maximum values (6×10^{14} cm^3 $mole^{-1}$ s^{-1}). The flame speed is then calculated at three preheat temperatures and compared with the experimental measurements. Figure 7.4 shows the variation in S_L with change in rate coefficient, in general the increase in rate coefficient of the allyl-H recombination reaction results in a decrease in flame speed at all preheat temperatures as predicted in the sensitivity analysis. At lower preheat temperatures, the experimental values are closer to the NUI mechanism with the minimum reaction rate. At high preheat temperature (650 K), the measurements are closer to the flame speeds predicted using the maximum reaction rate. The percentage differences are shown in Figure 7.4 (d). At the lower temperatures (300 and 450 K), they are within the general ±10% accuracy limit of the technique (from Chapter 4) when the minimum reaction rate value is used in the NUI mechanism. At 650 K, the maximum reaction rate produces prediction within the ±10% limits at all equivalence ratios. Thus one possible conclusion is the allyl-H recombination reaction should have a larger temperature dependence.

Considering that the temperature dependence provided by Harding et al. [121] is within the bound of rate coefficients examined here, attributing this temperature dependence to the rate coefficient did not change the predicted flame speed at all preheat temperatures. From Figure 7.4, it can be inferred that the modification to the rate coefficient should be such that the flame speed gets lowered at the conditions corresponding to higher preheat temperatures. In particular, the rate coefficient modifications should lower the flame speeds for near-stoichiometric mixtures at the highest preheat temperature by ~20% while effecting the flame speed at rich and lean conditions by less than 10%.

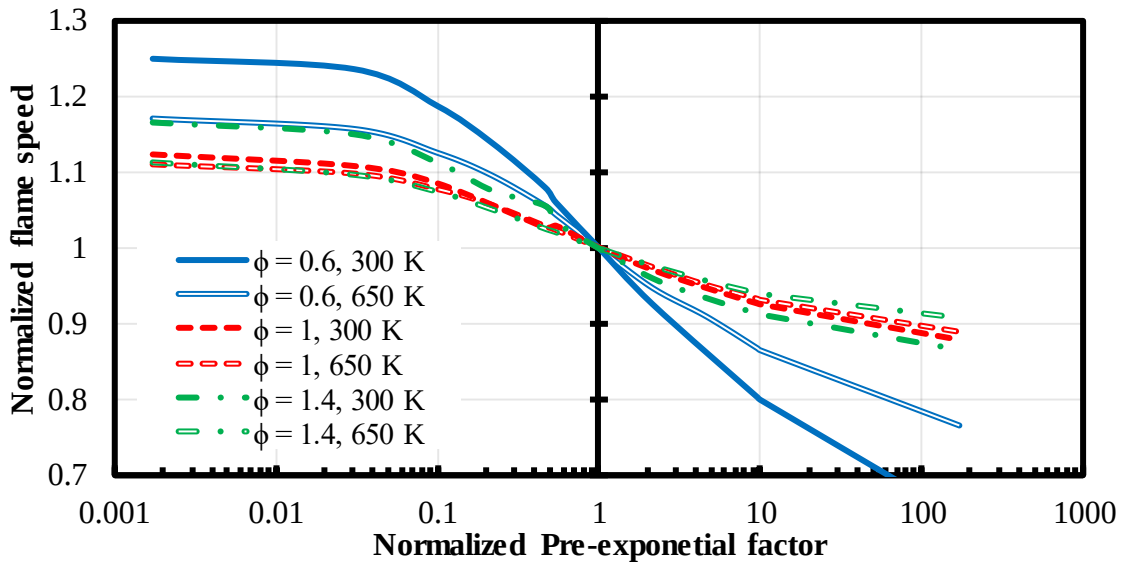

Figure 7.5: Impact on flame speed due to the variation in pre-exponential factor of the allyl-H recombination reaction at two preheat temperatures and three equivalence ratios.

To check whether this is feasible, the pre-exponential factor for the allyl-H recombination reaction (adopted from Harding et al. [121]) is both increased and decreased by larger factor. Figure 7.5 shows normalized flame speed variation with normalized pre-exponential factor; flame speed is normalized with the flame speed predicted from the rate coefficient provided by Harding et al. Similarly, the pre-exponential factor is normalized to the value provided by Harding et al. It is clear from this figure that the largest impact on flame speed occurs for lean mixtures, whereas at stoichiometric and rich equivalence ratios the flames speed is not impacted by more than ~10%. Also, the dependence on the *A*-factor is the same for both preheat temperatures for stoichiometric flames. On the other hand for rich and lean flames, differences can be observed; for lean cases these differences are up to 10%. Considering that the experiments suggest changes are needed in the allyl-H rate constant only for near stoichiometric flames at high preheat temperatures, and to achieve

this the *A*-factor needs to be changed by a factor of 1000, it is safe to conclude that variations in the *A*-factor alone cannot account for these differences.

As variation in *A*-factor for the allyl-H recombination reaction cannot account for the differences in flame speed predictions and experimental measurements for near stoichiometric flames at high preheat temperatures, the temperature dependence of the rate coefficient might be inaccurate. Attributing activation energy (E_a) for rate coefficient of a reaction is generally carried out using theoretical calculations and experimental measurements. As seen in Figure 7.3 there is lack of experimental data and theoretical predictions in literature, to estimate the activation energy of this particular reaction is beyond the scope of this thesis.

7.1.2 Constant flame temperature analysis

Apart from the allyl-H recombination reaction, other reactions can also contribute to the higher flame speed predictions at high preheat temperatures. In general, the competition between chain branching reactions and chain termination/propagation reactions plays a key role. If a calculation over predicts the relative importance of chain branching reactions at lower temperatures within the flame (e.g., in the so-called preheat zone), the result can be over prediction of flame propagation speeds and vice versa. For example for flames with higher preheat temperatures, the temperature at which reactions become active can be achieved in a shorter distance within the flame. If the temperature dependence of rate constants for competing reactions is inaccurate, this could lead to over or under prediction of flame speeds. Similarly if the temperature dependence at the higher temperatures (in the heat release zone) is inaccurate, it could lead to over or under

prediction of flame speeds. To ascertain which reactions in propylene chemistry could possibly lead to these differences, we first examine flames at two preheat temperatures and equivalence ratios chosen to maintain the same adiabatic flame temperature (T_{ad} ≅ 2210 K).

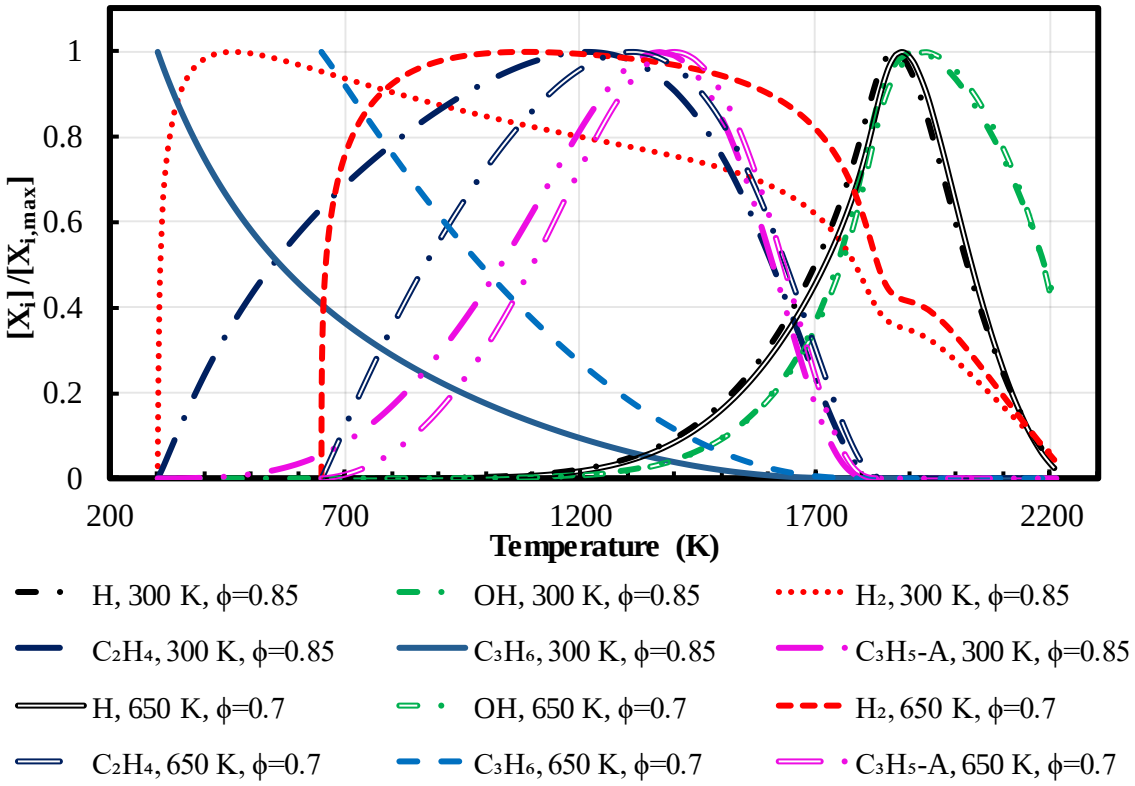

Figure 7.6: Selected species profiles within the adiabatic flame simulated using NUI mechanism. Two flames under consideration are for C_3H_6-air mixtures at 300 and 650 K preheat temperatures with T_{ad} ≅ 2210 K.

Figure 7.6 shows the species profiles as a function of local temperature in the flame; only selected species are shown. These species include the two main radicals that help in flame propagation: H and OH, the top three fuel species within the flame: C_3H_6, C_2H_4 and

H_2, and the allyl radical (C_3H_5-A), which was identified as a key intermediate species in the previous section. Product species such as CO_2 and H_2O are not considered as the formation chemistry of these species is well understood. To keep track of these species within the flame, the normalized species concentration ($[X_i]/[X_{i,max}]$) is examined, where $[X_{i,max}]$ is the maximum concentration of *i* in the flame.

The H and OH radicals for both flames peak at the same temperature and these radicals exist at relatively high concentrations only at high temperatures (e.g., > 1200 K). The allyl radical appears early in the preheat zone (so at intermediate temperatures) and its concentration peaks at nearly the same temperature for both flames. The allyl radical concentration within the flame is low when compared to the other species shown here indicating that this radical disappears as quickly as it is formed within the intermediate temperature zone. The importance of this radical and how it negatively affects flame speed for propylene-air mixtures was discussed in the previous section.

As hypothesized in the previous section, the differences between measured and predicted flame speeds at high preheat temperatures for propylene-air flames may be due to differences in chemistry at lower temperatures. Diatomic hydrogen and ethylene are the two major species at lower temperatures that are converted to products further in the flame[15]. The normalized concentration profiles of C_2H_4 are the same for both flames, whereas the H_2 variation differs.

The presence of these two species in the lower temperature zone is mainly due to diffusion of these species from the intermediate temperature region, where they are

[15] It can be noted that C_3H_6 in the flame goes to zero concentration at the same temperature (~1700 K) for both flames

produced from the destruction of propylene. While diffusion occurs in both directions, i.e., towards lower temperatures as well as higher temperatures, these species are converted to final products in the reaction zone. The H_2 concentration peaks at low temperatures (early) within the flame indicating that this accumulation is due to a diffusional process rather than due to reaction chemistry. Also for the flame with a preheat temperature of 300 K, the concentration of H_2 drops steadily as the temperature increases, while in the 650 K preheat temperature flame there is a zone of constant H_2 concentration in the intermediate temperature zone. These differences can be attributed to the fact that the flame thickness of the 650 K flame is smaller than that of the 300 K flame. As the thickness is lower the diffusion gradient is higher and hence the plateau of H_2 concentration in the middle of the flame.

This can be clearly observed in Figure 7.7; the temperature variation shows that the final temperature is reached within a much shorter distance in the 650 K flame when compared to the 300 K flame. The flame thickness at 300 K is almost twice that of the 650 K flame, and this is mostly due to the long preheat zone for the 300 K flame. From analysis in the previous section, the allyl radical was identified as a key contributor for propylene flame propagation, and C_2H_4, H_2 were identified as key species in the low temperature which could cause differences between model prediction and experimental measurements. To understand which reactions are important in the low temperature regime, differences in how these species are being formed in both flames needs to be examined first. The rates of production of C_3H_5-A, C_2H_4 and H_2 throughout the flame are shown in Figure 7.7. The rate of production of C_3H_5-A is shown as ten times its actual value as the original rate of production is small to be seen on the scale shown here.

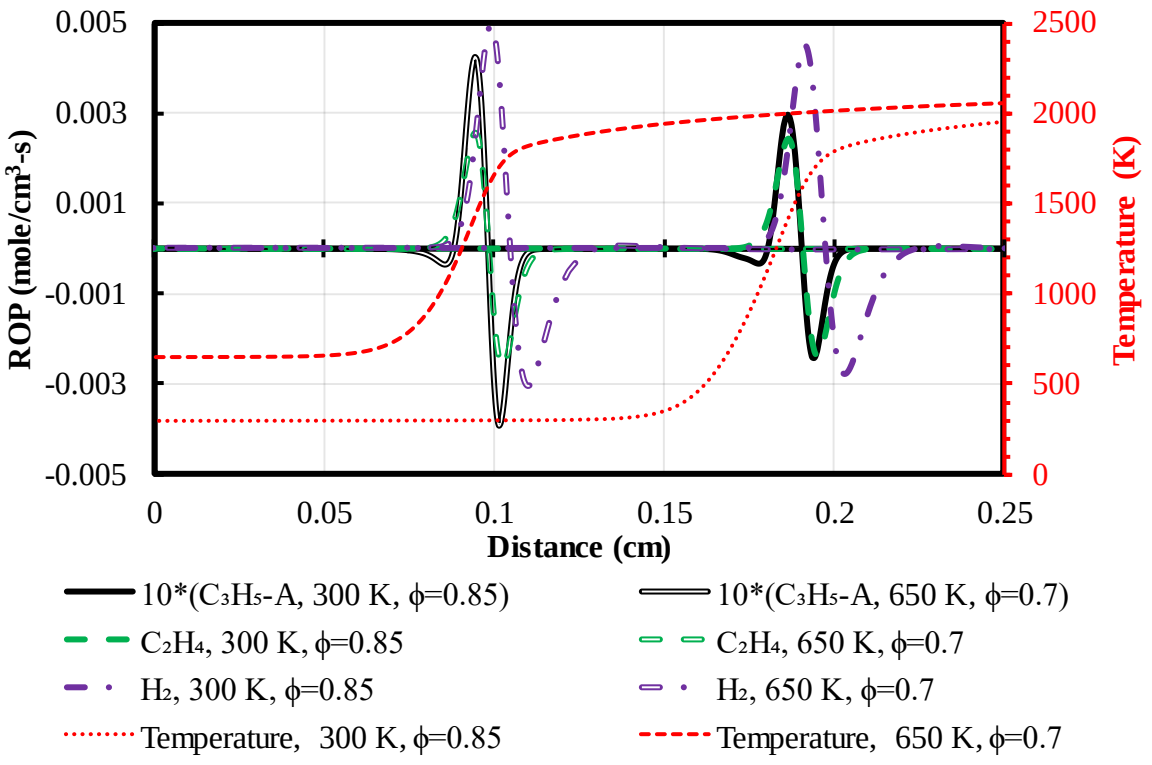

Figure 7.7: Rate of production and temperature variation in the flame for flames with two preheat temperatures (300 and 650 K) and a $T_{ad} \cong 2210$ K.

As noted previously, the 650 K flame is thinner than the 300 K flame; thus the species production happens within a shorter distance. But the key point to note here is all three species are produced at the same location within the flame. Also, the temperatures at which these species are produced is the same for both the flames. C_2H_4 and C_3H_5-A are produced and destroyed within a short distance into the flame whereas H_2 survives into the high temperature zone. The allyl radical has a negative ROP at lower temperatures indicating that as it diffuses in to the lower temperature zones it reacts and gets converted to other species. These species include C_3H_6 and 1-butene (C_4H_8-1), which are fuel species that get converted into products further into the flame. This is further evidence that production of allyl radical negatively contributes to flame propagation. C_2H_4 and H_2 do not

react at lower temperatures and thus diffuse unimpeded into the preheat zone, hence their accumulation.

While the production of C_3H_5-A is detrimental to flame propagation, the production of C_2H_4 and H_2 enhances flame propagation as they readily convert to final products (though through different mechanisms). If there is a reaction in this temperature range which would offer two different pathways one producing the allyl radical while the other producing either ethylene or hydrogen, the pathway chosen could lead to over prediction of flame speeds under certain conditions. If the ethylene or H_2 production pathway is highly preferred over the allyl production pathway then flame speed over prediction could occur just for higher preheat temperature flames.

7.1.3 C_3H_6 + H reaction

The competition for the H radical between chain branching and chain propagating reactions is a key for the propagation of flames. In the initial parts of the reaction zone, attack pathways on the fuel molecule are vital for continued production of radicals. Considering the general importance of the H radical, its reaction with C_3H_6 is examined. There are generally two competing pathways for C_3H_6 reacting with H; the first pathway generates the allyl radical and hydrogen, whereas the second pathway forms ethylene and the methyl radical.

$$C_3H_6 + H \Leftrightarrow C_3H_5\text{-A} + H_2$$

$$C_3H_6 + H \Leftrightarrow C_2H_4 + CH_3$$

This can be seen when reaction pathway analysis (RPA) is carried out (using Chemkin-Pro) for both the flames under consideration. Figure 7.8 and Figure 7.9 show the

reaction pathway for the conversion of propylene to intermediate species in the early reaction zone of the flame (at T ≅ 1000 K) for flames with preheat temperatures of 300 and 650 K. In this analysis, the primary focus is on H radical attack on propylene molecule and its conversion to intermediate species; only the top ten species produced in these pathways are considered here. Reactions involving the H radical are shown as blue lines whereas reactions involving other species are shown as black lines. The number in brackets denote the relative (to the total) rate of production of the species under consideration and the arrow direction denotes the progress of the reaction. For example for the flame with T_u = 300 K and ϕ = 0.85 (Figure 7.8), the ROP of C_2H_4 due to $C_3H_6 + H \Leftrightarrow C_2H_4 + CH_3$ is 29.1% of the total ROP, while the ROP of C_3H_5-A due to $C_3H_6 + H \Leftrightarrow C_3H_5\text{-A} + H_2$ is 5.3%. This provides an indication of the preferred pathway of reaction between C_3H_6 and H in this early reaction zone regime.

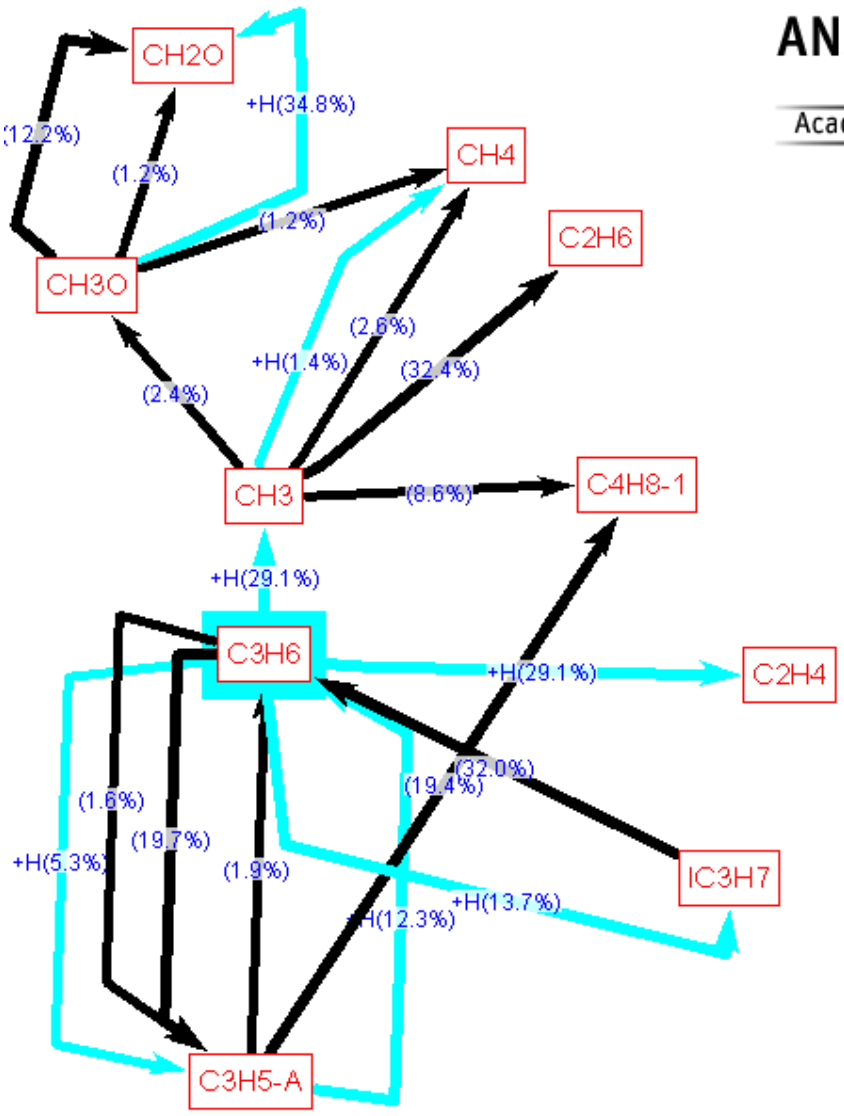

Figure 7.8: Reaction path diagram for the conversion of C_3H_6 to intermediate species in the early reaction zone of the flame (T ≅ 1000 K), propylene air flame at ϕ = 0.85 and T_u = 300 K.

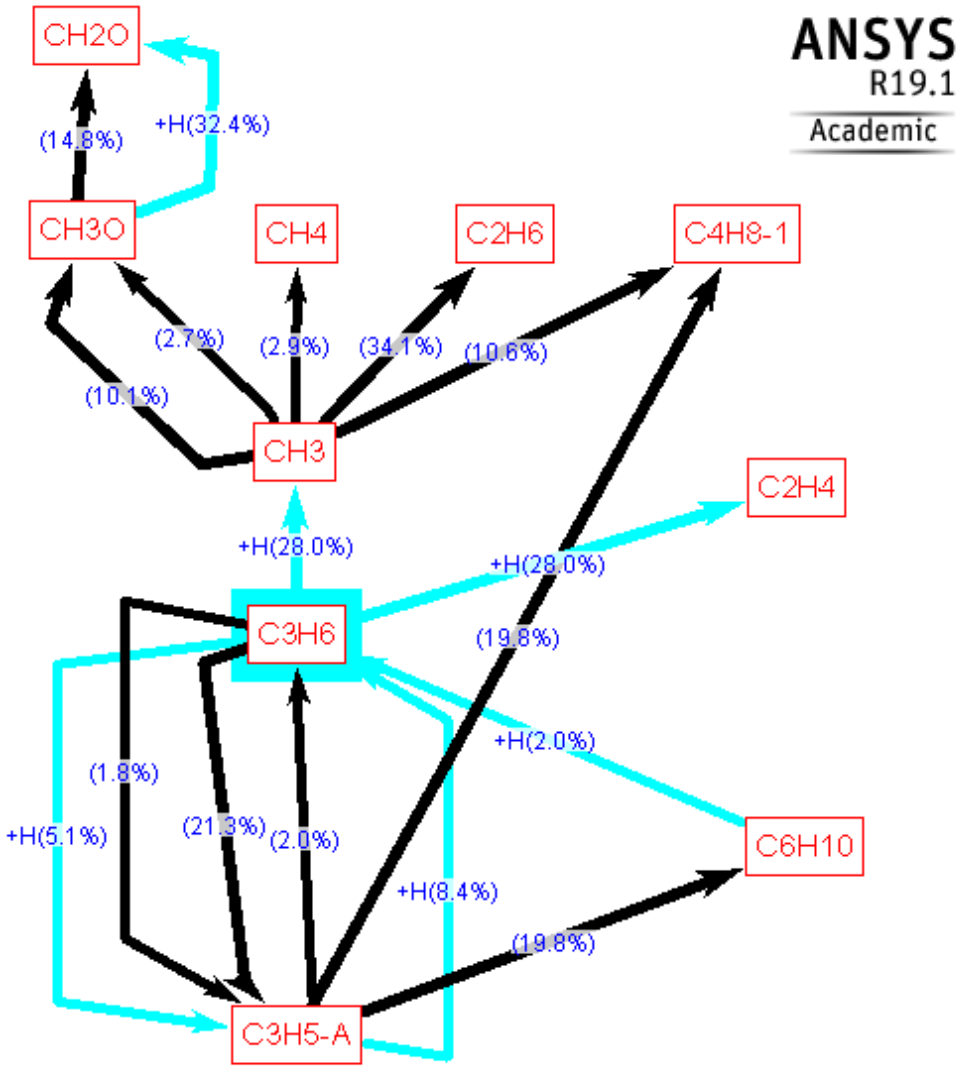

Figure 7.9: Reaction path diagram for the conversion of C_3H_6 to intermediate species in the early reaction zone of the flame (T ≅ 1000 K), propylene air flame at ϕ = 0.85 and T_u = 650 K.

For both the flames under consideration, the C_2H_4 and CH_3 pathway is clearly dominant when compared to the allyl production pathway. It is also evident that production of CH_3 is advantageous for flame propagation is it leads to further intermediate species formation, while most of the allyl radical generated converts back to propylene or 1-

butadiene, which counters the propagation of the flame as these are stable species. One key difference that can be observed is the formation of the IC_3H_7 species (through $C_3H_6 + H \Leftrightarrow IC_3H_7$) for the lower preheat temperature when compared to the higher preheat temperature flame. The production of this species can be observed for the higher preheat temperature if a higher number of species in RPA is considered indicating that this reaction pathway is preferred for the lower preheat temperature. This could be a manifestation of higher equivalence ratio for the lower preheat temperature flame and hence the presence of more fuel, leading to different kinds of C_3H_6 and H reactions becoming more prominent. Primarily the competition for H radical between the two pathways forms the key as they are within the top five reactions for both the flames under consideration.

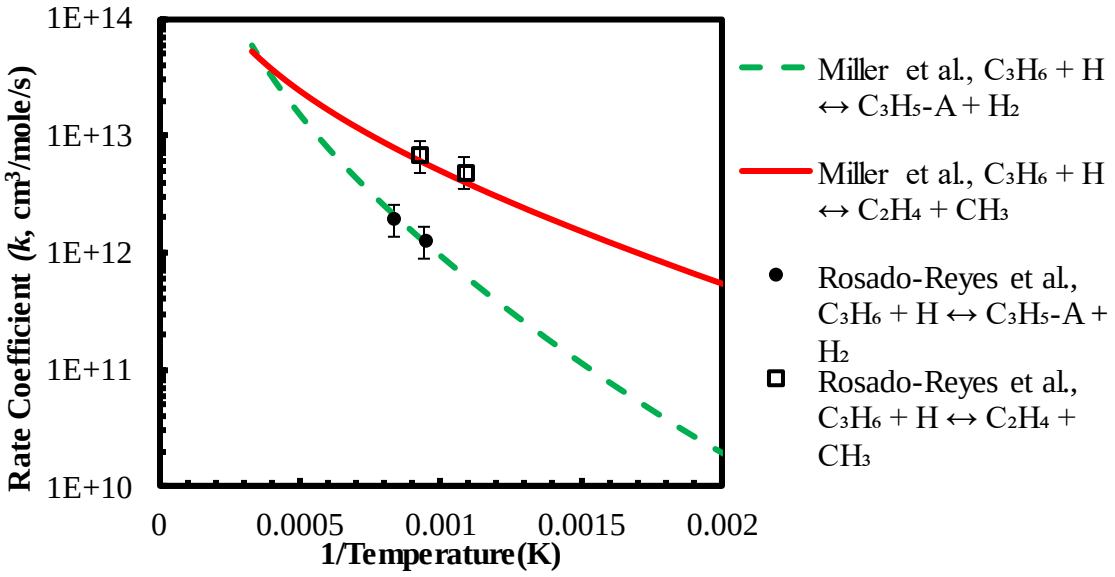

Figure 7.10: Arrhenius plot for both pathways of C_3H_6 + H reaction for temperatures between 500 K and 3000 K.

The allyl pathway negatively contributes to flame speed while the alkene producing pathway positively contributes to flame speed. If the rate constant of the allyl producing

pathway is increased then the flame speed can be reduced. The rate constant of these reactions have been studied by a few research groups. Figure 7.10 shows the variation of the rate constant with temperature (Arrhenius plot) for both the pathways under consideration. The latest theoretical prediction from Miller et al. [122] (used in the NUI mechanism) and experimental measurements from Rosado-Reyes et al. [123] are shown here. The experimental measurements shown here match reasonably well with the theoretical predictions for both reactions, though the measurements exist only for a narrow range of temperatures.

The ethylene forming pathway has a higher rate constant for most temperatures found in typical flames, but the difference narrows at higher temperature. If the relative difference between these two rates is reduced, which is possible given the narrow range of experimental measurements available to test the predicted rates, the relative increase in the allyl production pathway would result in lower flame speeds. To appropriately modify the rate constants, especially the activation energies, for these reactions, further experimental measurements need to be conducted for temperatures at which these reactions are relevant (e.g., 800 -1700 K). Similar to the reactions discussed above, several other reactions exclusive to propylene reaction chemistry have been sparsely studied; revisiting these reactions could improve the predictive capability of chemical kinetic mechanism of large hydrocarbons (such as liquid jet fuels) as these reactions are also a key part of heavy hydrocarbon flame chemistry.

7.2 Vitiation effects

In Chapter 6, experimental measurements were compared to simulation results for atmospheric-pressure, laminar flame speeds under reduced oxygen content conditions, for both ethylene and propylene. While N_2 diluted flame speeds were measured for both fuels, CO_2 dilution measurements were performed only for ethylene. While results were obtained at multiple preheat conditions, the following discussion focuses on the highest temperature (650 K) cases, which are more representative of vitiation conditions. For mixtures with excess N_2 in the oxidizer, ethylene flame speed predictions were within ±10% of experimental measurements, while for propylene these differences were between 10 and 100% depending on the oxygen content in the oxidizer. For CO_2 dilution, large differences between model predictions and experiments were observed for low O_2 content flames (Θ = 0.15). As the amount of CO_2 content in the oxidizer increased the differences between measurements and predictions also increased, and these differences were more pronounced for lean mixtures when compared to near-stoichiometric and rich cases.

In this section, the insights gained about propylene reaction chemistry (discussed in the previous section) are applied to predictions for vitiated flow conditions. Then the reaction chemistry of ethylene mixtures with CO_2 dilution is examined in detail and important reactions relevant to these conditions are identified.

7.2.1 N_2 dilution effects on propylene flame speeds

The allyl radical is a key intermediate for propylene flame propagation. The allyl and H recombination reaction has a significant effect on flame speed of propylene flames.

In the previous section, the rate coefficient of this reaction was examined in detail. For propylene-air flames at preheat temperature of 650 K, a rate coefficient of 6×10^{14} cm^3 $mole^{-1}$ s^{-1} (the maximum in the range suggested in the literature) was shown to provide flame speed predictions that are in good agreement with current measurements. For the vitiated propylene flames, the flame speed predictions are significantly higher than the current measurements. As in the case of the undiluted flames, applying the higher rate constant for the allyl-H recombination would lower the N_2-diluted flame speed predictions.

Figure 7.11 demonstrates the effect of the allyl-H recombination rate constant for vitiated flames. The predicted flame speed decreases in absolute value for all levels of O_2 content in the oxidizer. Figure 7.11 (b) shows that the percentage drop in flame speed is higher for the 15% oxygen content flames when compared to the 21% oxygen content flame (~10% higher). This suggests that the significance of the allyl-H recombination reaction increases with lowering of O_2 content in the flame. As the oxygen content is lowered, the reaction rate for O_2+H drops compared to the higher oxygen content flames. Although this reaction remains the largest consumer of H radicals, the lower rate would increase the relative importance of the allyl-H reaction. Thus errors in this reaction rate would have an increased influence on the laminar flame speed for vitiated propylene flames.

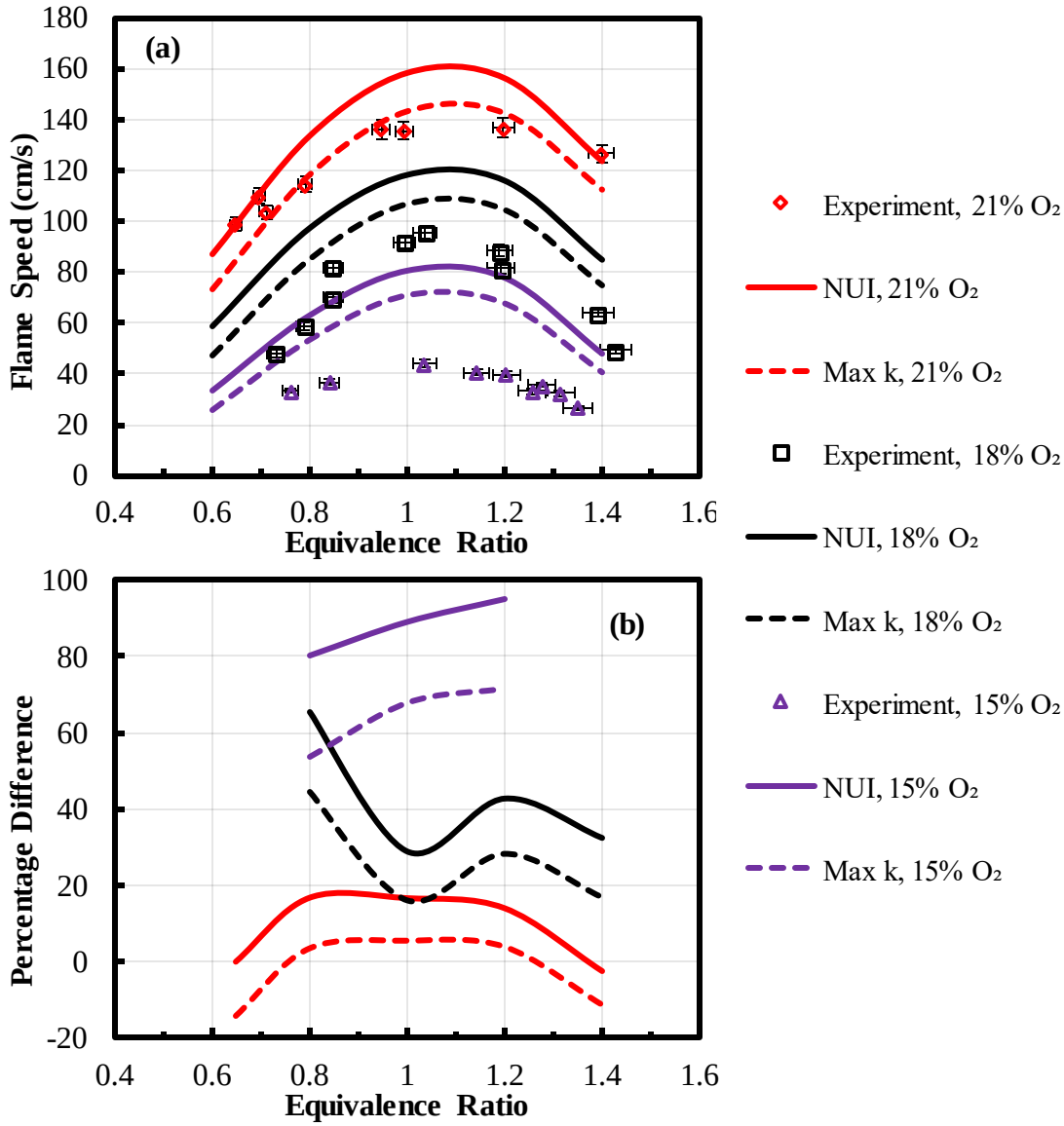

Figure 7.11: Effect of maximum rate coefficient for the allyl recombination reaction on laminar flame speed for propylene mixtures at T_u = 650 K, atmospheric pressure and different dilution levels (a) laminar flame speed and (b) percentage difference between measurements and NUI predictions.

In Chapter 6, the effect of N_2 dilution on flame speed was predominantly attributed to the thermal effect of N_2, but from kinetic analysis of propylene flames there is a certain amount of chemical effect present which cannot be ignored. This could be caused due to

altering of reaction pathways for low oxygen content flames. This might be true only for propylene flames and not for ethylene flames as the kinetic pathways for these fuels are different. It is evident from Figure 7.11 that by adjusting the rate coefficient of one reaction the large differences between flame speed measurements and kinetic model predictions cannot be accounted for. Similar observations were made when examining preheat effects on propylene flames in the previous section, and several key reactions which could lead to over prediction of flame speeds were identified. It is prudent to note that the effect of any modification to the rate coefficient of a reaction involving propylene will be higher for vitiated flames as is demonstrated by the modification of the allyl and H recombination reaction. Thus if the accuracy of key propylene reactions are improved by performing experiments to capture the rate coefficients of these reactions at a wider temperature range, the over prediction of laminar flame speeds for vitiated propylene flames may also be overcome.

7.2.2 CO_2 dilution effects

Flame speed measurements for ethylene mixtures with different levels of CO_2 dilution were presented in Chapter 6. These measurements were made at several equivalence ratios and at a preheat temperature of 650 K. It was observed that as the amount of CO_2 was increased in the oxidizer the differences between flame speed measurements and kinetic model predictions increased. The effects for fixed CO_2 fraction were also more prominent for cases with the lowest amount of O_2 content ($\Theta = 0.15$). Furthermore, the differences for lean mixtures were shown to be higher when compared to the near-stoichiometric and rich flames. Since the impact was largest for $\Theta = 0.15$, the reaction kinetics of these flames were the only ones studied.

To examine which chemical reactions are crucial for propagation of lean flames with CO_2 dilution, we start with a sensitivity analysis for flames with different levels of dilution. Normalized flame speed sensitivity to the *A*-factor of the top ten reactions is shown Figure 7.12; the equivalence ratio under consideration is 0.6 and dilution levels are C = 0,0.1 and 0.2.

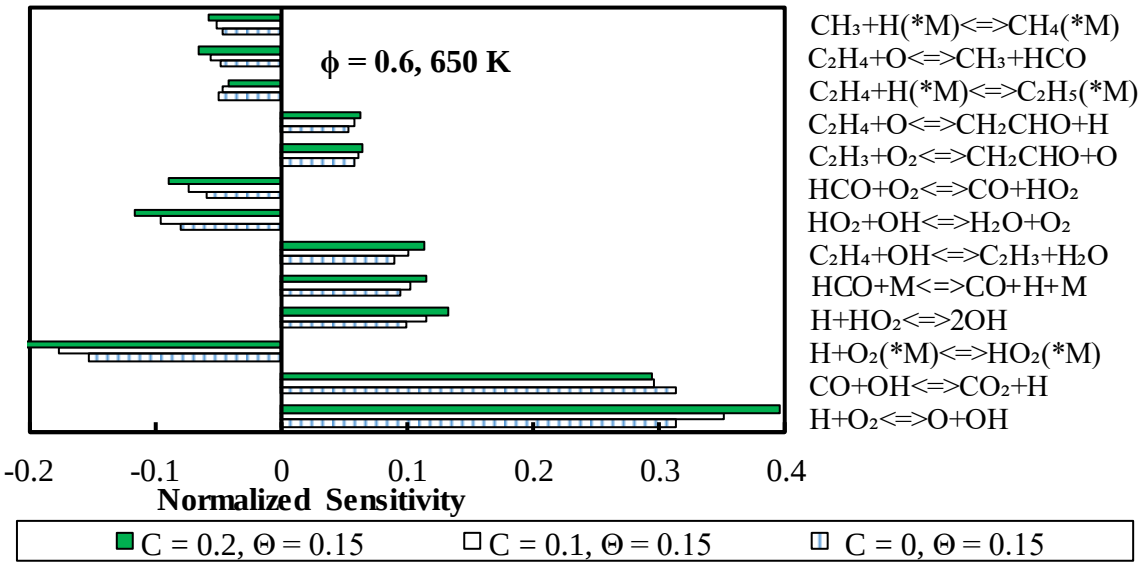

Figure 7.12: Normalized flame speed sensitivity to *A*-factor of rate coefficients of different reactions (using NUI mechanism) for ethylene mixtures with different levels of CO_2 dilution at Θ = 0.15, ϕ = 0.6, T_u = 650 K and atmospheric pressure.

As expected, the H_2/CO reaction chemistry plays a key role in propagation of these flames. Although ethylene reactions are important, their sensitivities are two to three times lower than that of the top three reactions H_2/CO reactions. Also, based on the good agreement between the ethylene-air flame speed measurements and the kinetic mechanism predictions, the reactions that involve ethylene can be considered well established. Due to the addition of a reactive diluent such as CO_2, it is possible that well studied reactions could

be pushed into temperature regimes where uncertainties in rate coefficient could be higher[16]. The top two reactions whose reaction rates could be affected by the presence of excess CO_2 are examined in the next subsections; these reactions are:

$$CO+OH \Leftrightarrow CO_2+H$$

$$H+O_2 (+ M) \Leftrightarrow HO_2 (+ M)$$

The CO+OH reaction is key for the propagation of any hydrocarbon flame as it is in this step most of the heat release occurs in a flame [12]. The presence of excess CO_2 is known to lower heat release from the forward reaction by increasing the rate of the backward reaction. It can also compete for H radicals with the chain branching $H+O_2 \Leftrightarrow O + OH$ reaction, and the three-body $H+O_2+M$ association reaction. The presence of CO_2 in the reactants can also impact the rate of the latter reaction through the third-body efficiency of CO_2. If the CO_2 efficiency is too low, it would lead to over prediction of flame speeds as evidenced by the negative flame speed sensitivity for this reaction. Both of these reactions are examined independently; the rate coefficients are modified and their effect on flame speeds are examined.

7.2.2.1 $CO+OH \Leftrightarrow CO_2+H$ reaction

The rate coefficient of the CO+OH reaction was measured by several research groups at a wide range of temperatures and pressures [124-130].[17] Based on these measurements a curve-fit is established in the modified Arrhenius rate formulation and several groups have published different rate coefficient formulations based on the experimental measurements and theoretical formulations. Experimental measurements by

[16] This is due to the presence of CO_2 in the reactants, for flames with no CO_2 dilution CO_2 is only present in the products so the reaction chemistry in the early parts of the flame is not influenced by CO_2.
[17] A specific discussion of the accuracy of these measurements is beyond the scope of this thesis.

several different research groups and the curve-fits for the rate coefficient developed by Joshi et al. [118] and Davis et al. [131] are shown in Figure 7.13.

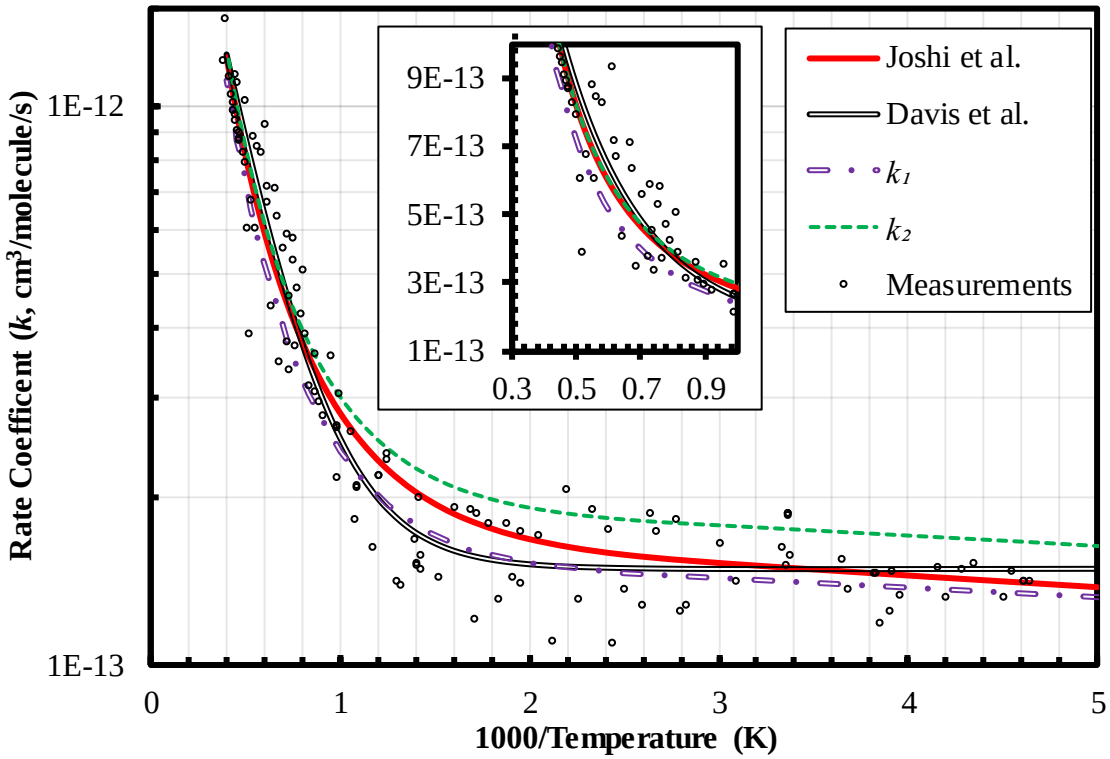

Figure 7.13: Experimental measurements and curve fits from literature for the rate coefficient of CO+OH ⇔ CO_2+H reaction. Also shown are the current curve fits to the experimental data denoted as k_1 and k_2.

The rate coefficient for this reaction does not follow a standard Arrhenius form; it is generally modelled as a summation of two rates with one rate valid at higher temperatures (k_a) and the other rate capturing the variations in rate coefficient at low temperatures (k_b). The NUI mechanism uses the curve-fit developed by Joshi et al., while the curve fit of Davis et al. attributes lower rate coefficients for temperatures between 400 and 1000 K. Two new curve fits: k_1 and k_2, are examined based on the experimental

measurements. While k_1 lowers the rate coefficient at all temperatures when compared to Joshi et al. prediction, k_2 increases the rate coefficient at lower temperatures (300-1000 K) without changing the rate coefficient at higher temperatures. The rate coefficients used are shown in Table 7.1; k_1 is achieved by changing the *A*-factor of k_a, whereas k_2 is achieved by changing the *A*-factor of k_b.

Table 7.1: Various rate coefficient curve-fits for CO+OH reaction.

	k_a (cm^3 $molec^{-1}$ s^{-1})	k_b (cm^3 $molec^{-1}$ s^{-1})
Joshi et al. [118]	$1.16\times10^{-19}(T^{2.053})e^{179.01/T}$	$9.56\times10^{-12}(T^{-0.664})e^{-166.985/T}$
Davis et al. [131]	$1.59\times10^{-12}(T^{0.14})e^{-3700/T}$	$1.22\times10^{-13}(T^{0.03})e^{8.052/T}$
k_1	$3.33\times10^{-20}(T^{2.2})e^{179.01/T}$	$9.56\times10^{-12}(T^{-0.664})e^{-166.985/T}$
k_2	$1.16\times10^{-19}(T^{2.053})e^{179.01/T}$	$1.15\times10^{-11}(T^{-0.664})e^{-166.985/T}$

The effect on flame speed due to the change in rate coefficient of this reaction can be observed in Figure 7.14; the change in flame speed is represented by normalizing flame speed with predictions from the NUI mechanism. Two different effects on flame speed can be observed for k_1 and k_2. By decreasing the rate coefficient at all temperatures (k_1), laminar flame speed drops irrespective of the amount of CO_2 dilution in the mixture. In fact, the largest changes are observed for mixtures with no CO_2 dilution and for extremely lean mixtures. This is opposite to the effect desired, where there should be minimal changes to flame speed for mixtures with C = 0.

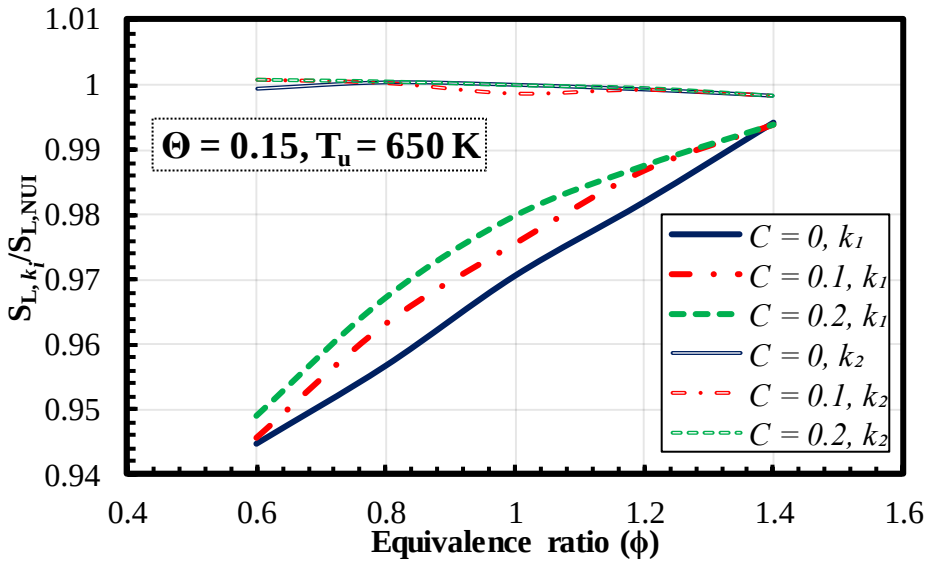

Figure 7.14: Change in laminar flame speed when compared to the NUI predictions for the two rate coefficient curve fits of CO+OH ⇔ CO_2+H under consideration.

Furthermore, increasing the rate coefficient of the CO+OH reaction at lower temperatures had almost no impact on flame speed predictions for every mixture under consideration. This indicates that the CO+OH reaction is not relevant in the early parts of the flame where we expect to see the most impact of CO_2 as a chemically active diluent due to its presence in the reactants.

7.2.2.2 $H+O_2$ (+ M) ⇔HO_2 (+ M) reaction

The recombination reaction of H and O_2 is a chain propagation step that competes with the dominant chain branching reaction ($H+O_2$⇔H+OH) for H radicals. The recombination reaction requires a third body (M) to remove the excess energy from the excited intermediate state to form the final product species. The third body can be any species, but the reaction rate is dependent on the structure of the third body and its collisional efficiency. In most mechanisms, including NUI, the default rate coefficient provided assumes M to be N_2, and the factor by which other species increase or decrease

the rate coefficient is called the *third-body efficiency* of the species for the particular reaction.

Accurately estimating the rate coefficient of this reaction is imperative to correctly predicting the flame speed, especially for lean flames. The significance of this reaction increases with the increase in the CO_2 dilution as observed in the sensitivity analysis shown in Figure 7.12. The rate coefficient of this reaction in the modified Arrhenius format used in the NUI mechanism is adopted from Fernandes et al. [132]; they determined the rate coefficient using laser flash photolysis over a temperature range of 300 – 900 K. Theoretical rate coefficient predictions were also estimated for several bath gases (M = He, Ar, N_2 and H_2O). Third body efficiencies were attributed to these species based on the measurements; for other species, the third body efficiency is estimated and adjusted based on measured fundamental properties of mixtures (e.g., flame speed measurements).

Table 7.2: Third-body efficiencies of several species with respect to $H+O_2$ (+ M) ⇔ HO_2 (+ M) reaction as provided in the NUI and USC mechanisms.

	H_2	O_2	CO	CO_2	H_2O	CH_4	C_2H_6	k (cm^3 $molec^{-1}$ s^{-1})
NUI	1.3	0	1.9	3.8	10	2	3	$7.72\times10^{-12}(T)^{0.44}$
USC	0	0.85	1.09	2.18	11.89	0	0	$8.49\times10^{-12}(T)^{0.44}$

Table 7.2 provides third-body efficiencies of several species for this reaction as provided in the NUI and USC mechanisms. Clearly the efficiencies are different in these mechanisms, and in fact the base rate coefficient in the USC mechanism was increased by a factor of 1.1 in order to match measured fundamental properties. Similarly, it is not far-

fetched that the third-body efficiencies are adjusted, as it is evident that by having different combinations of third-body efficiencies similar flame speed predictions can be achieved. The third-body efficiency of CO_2 is of particular interest for flames with CO_2 dilution, as the presence of excess CO_2 in the reactants could lead to overall rate coefficient of this reaction being affected by this efficiency.

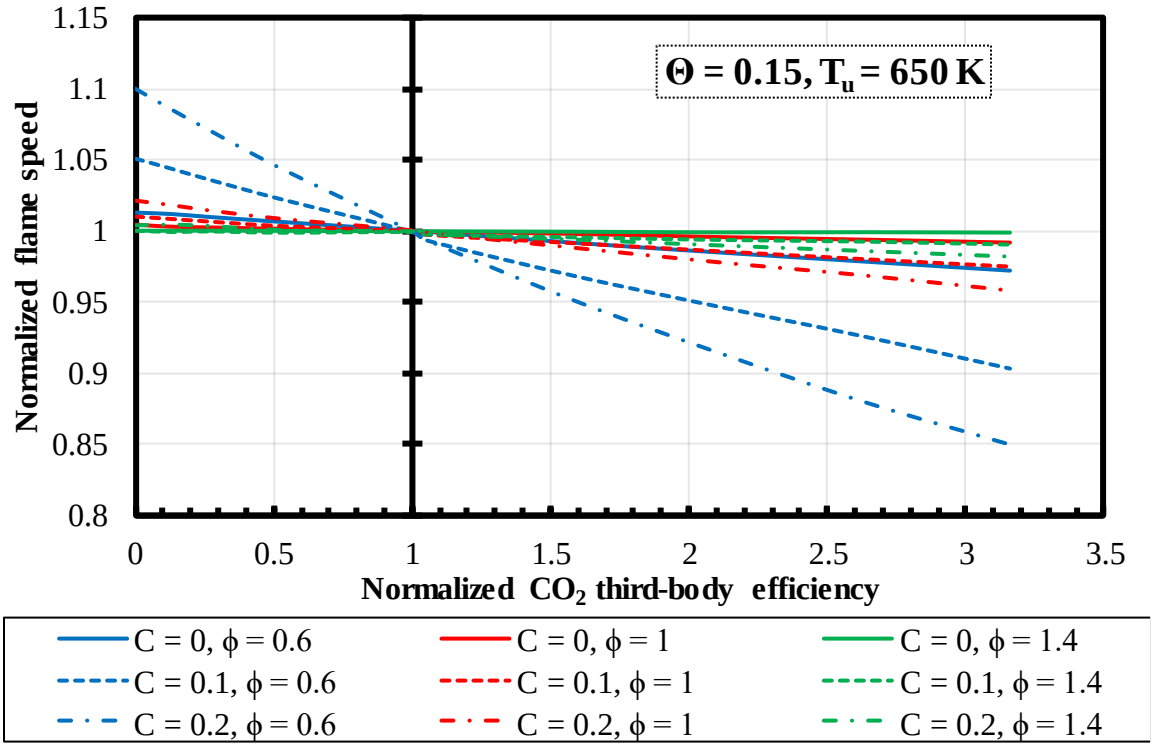

Figure 7.15: Effect of varying the third-body efficiency of CO_2 for $H+O_2$ (+ M) ⇔ HO_2 (+ M) reaction on laminar flame speed predictions.

To study the effect of varying CO_2 third-body efficiency on laminar flame speed, mixtures at three CO_2 dilution levels (C = 0, 0.1 and 0.2) and three equivalence ratios are examined. The oxygen level in the oxidizer of these mixtures is kept constant (Θ = 0.15), as is the preheat temperature (650 K). The third-body efficiency was both increased and decreased (changed between 0 and 12) from the base value (3.8) provided in the NUI

mechanism. To visualize the effect on flame speed, the flame speeds predicted by the new third-body efficiency are normalized by the flame speed predictions of NUI mechanism, and the results are presented in Figure 7.15.

The effect of varying the third-body efficiency of CO_2 on laminar flame speeds is evident from Figure 7.15. The change in this efficiency has a large effect on flame speeds of lean mixtures with CO_2 dilution. For lean mixtures with no CO_2 dilution and for near-stoichiometric and rich cases at all levels of dilution, the effect on flame speed is minimal (less than 5%) even when the third-body efficiency is increased by a factor of three. By increasing the third-body efficiency by a factor of three, the laminar flame speed for lean mixtures ($\phi = 0.6$) at the highest level of CO_2 dilution ($C = 0.2$) can be decreased 15%. This decreases the difference between the measured and predicted by almost 50% while minimally affecting the flame speeds for near-stoichiometric and rich mixtures. Thus by varying third body efficiency of this recombination reaction (forming HO_2) a certain level of improvement can be achieved for flame speed predictions for mixtures with CO_2 dilutions. This indicates that formation of the HO_2 radical may play a key role in flame propagation for CO_2 diluted flames.

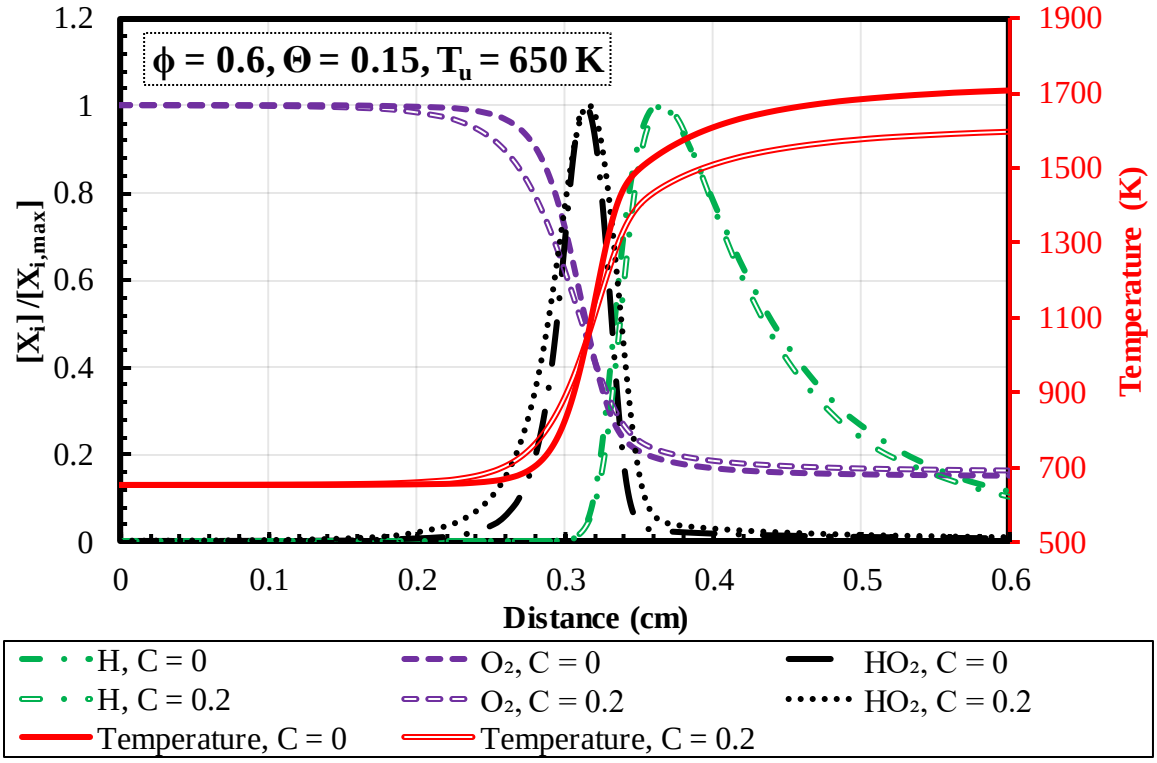

Figure 7.16: Normalized species concentration and temperature variation along the flame axis for two mixtures with no CO_2 dilution (C = 0) and maximum CO_2 dilution (C = 0.2), at $\phi = 0.6$, $\Theta = 0.15$, $T_u = 650$ K and atmospheric pressure.

The variation of species concentrations and temperature within the flame is compared for two flames with the lowest and highest CO_2 dilution in Figure 7.16. The three species under consideration are H, O_2 and HO_2, which are the participating species in the reaction under consideration. The H radical is mostly present in the high temperature regime as expected, whereas the HO_2 radical[18] is present in the earlier parts of the flame. This indicates that a significant portion of the HO_2 radical is produced and destroyed in the early parts of the flame. It is also important to note that for the high dilution case, the

[18] The maximum HO_2 concentration within the flame is orders of magnitude lower than O_2 or H radical concentration, thus to qualitatively describe species variation normalized species profiles are used.

temperature rises much faster within the flame when compared to the flame with no dilution although the final temperature reached is lower. This is surprising because the excess amount of CO_2 in the oxidizer should increase the heat capacity of the mixture thus making the rise in temperature slower, but the opposite seems to occur here. This indicates that low temperature reaction chemistry is active for CO_2 dilution cases which is absent in non-CO_2 diluted flames. Another sign that low temperature chemistry occurs is the drop in oxygen concentration as well as the rise in HO_2 concentration at an earlier location in the flame when compared to the case with no CO_2 dilution.

Modification of the $H+O_2$ three-body recombination reaction could lead to improvements in laminar flame speed predictions for flames with CO_2 dilution in the oxidizer. However, this reaction alone cannot account for the large differences between flame speed predictions and experimental measurements. Other reactions especially in the low temperature regimes where they seem to become important for CO_2 diluted flames should be examined. Modifications to these reactions should be based on measured fundamental properties such as flame speed, ignition delay times etc. at different mixture conditions (different kinds of diluents and at higher preheat temperatures).

CHAPTER 8. Conclusion

This thesis investigated laminar flame speeds of alkenes (ethylene and propylene) over a wide range of mixture conditions relevant to gas turbine combustors and augmenters. Flame speed measurements were acquired using a modified Bunsen flame approach. First measurements were validated for room temperature reactants by comparison to results from other standard flame speed measurement approaches, and the potential systematic errors of the modified Bunsen approach were examined. Then effects of preheat temperature and vitiation/dilution on laminar flame speed were examined. Furthermore, the measured flame speeds were used to test the accuracy of leading chemical kinetic mechanisms. Finally, possible areas of improvement in the mechanisms are suggested. In this chapter, key findings from this thesis are summarized and then suggestions for further study are provided.

8.1 Summary of Results

The key accomplishments of this work can be broadly divided into three topics:

1. Accuracy of current Bunsen flame speed approach
    a. The stretch effects on Bunsen flames were examined using computational tools and the effects of height of a flame on measurements were studied. An estimation of the systematic error in the measured flame speed was discussed.
    b. The Bunsen approach based on measuring the reaction zone area was validated against measurements made using stretch corrected techniques.

2. Laminar flame speed database for alkenes
    a. Bunsen flame approach based on reaction zone was extended to measure alkene flame speed measurements.
    b. Developed a laminar flame speed database for alkenes (ethylene and propylene) at several preheat temperatures and vitiated conditions.
    c. Examined the effect of preheat and vitiation (including both reactive (CO_2) and non-reactive (N_2) diluents) on laminar flame speed.
3. Chemical kinetic model performance
    a. Investigated the performance of chemical kinetic mechanisms for predicting laminar flame speeds at conditions under investigation.
    b. Reaction kinetics of alkenes were examined to identify possible reactions where uncertainty in rate coefficient could cause differences between flame speed predictions and experimental measurements.

8.1.1 Validation of Bunsen flame approach

The reaction-zone area based Bunsen flame approach was first developed by Natarajan et al. [31] to measure flame speeds of syngas fuels. Later this approach was used to measure flame speeds of alkanes over a range of conditions [32, 73]. In this thesis, the technique has been validated for measurements of alkenes over a range of equivalence ratios at room conditions and at high preheat temperatures (at 470 K for ethylene). Furthermore, literature flame speeds measurements at room temperature for syngas and alkane fuels made using this modified Bunsen flame approach were compared to measurements made using stretch corrected methods such as spherical and stagnation flames. The differences between these measurements were generally small (within 10%

from the average) for most fuels, though some uncertainties were observed for mixtures with large deviations from unity Lewis number.

To further examine possible effects due to stretch, various calculations were performed. They showed that the Bunsen flame stretch is maximum near the flame tip. Also, the effect on stretch on both the unburned and burned flame speed was calculated using stagnation flame simulations. The estimates of Bunsen flame stretch were combined with the stretch sensitivity of the unburned and burned flame speeds to determine systematic uncertainties in flame speeds determined from Bunsen flame areas. Measurements at atmospheric-pressure using the modified (burned area) Bunsen approach can produce accurate values for the unstretched, unburned laminar flame speed, though significant systematic errors may occur for low preheat conditions with mixtures having Lewis number greater than unity (highly lean or rich mixtures of heavy and light fuels). When compared with the traditional BFT approach (using unburned flame area), the systematic errors are lower by at least 5-10% in the modified BFT approach for most mixture conditions.[19] The estimated systematic errors due to stretch are much smaller at high preheat condition, in part due to the reduced flame thickness. Previous experimental results showed that a significant decrease in flame height relative to the burner diameter ($H/D < 1.3$) introduced a systematic error and produced a higher than actual flame speed [20, 21]. A set of experiments using propylene indicated that $H/D > 2$ provides sufficiently accurate flame speed measurements.

[19] These systematic errors are first-order conservative estimates and in reality the effect of stretch on the burned flame surface would be lower than predicted in this thesis.

Thus we can conclude that the accuracy of the modified Bunsen approach based on validation at room temperature conditions will be a conservative estimate for the accuracy of flame speed measurements of preheated reactants. Given the shorter preheat residence time of this approach relative to spherical flame methods and the simplicity of the setup, this makes the modified Bunsen approach a sensible choice to measure laminar flame speeds for high preheat temperatures. Overall, it was ascertained that the reaction-zone area based Bunsen flame approach can be used to measure flame speeds of mixture over a wide range of conditions.

8.1.2 Laminar flame speed measurements

Laminar flame speed measurements of alkenes were made at a wide range of mixture conditions using the Bunsen flame technique. Table 8.1 provides an overview of the mixture conditions at which flame speed measurements were made for ethylene and propylene. Apart from the flame speed validation studies, which were mostly carried out at room conditions, most of the flame speed measurements were made at conditions not reported previously in the literature. These conditions include a combination of mixtures at high preheat temperatures, oxidizer composition (based on diluent level) and equivalence ratio for both ethylene and propylene. These measurements were made at conditions relevant to jet-engine combustors and can be used to assess the performance of chemical kinetic mechanisms.

Table 8.1: Range of conditions where flame speed measurements were made. Each symbol corresponds to a preheat temperature (● – 300 K, ■ – 450 K, ✓ – 650 K) and an equivalence ratio sweep was carried out at every condition.

Oxidizer Composition →	O_2/ N_2/ CO_2						
Fuel ↓	21/ 79/ 0	18/ 82/ 0	15/ 85/ 0	18/ 72/ 5	18/ 62/ 10	15/ 75/ 10	15/ 65/ 20
C_2H_4	● ■ ✓	● ■ ✓	■ ✓	■ ✓	✓	✓	✓
C_3H_6	● ■ ✓	✓	✓				

8.1.2.1 Ethylene mixtures

Ethylene-air flame speeds of mixtures at several equivalence ratios were measured first at three different preheat temperatures. The NUI chemical kinetic model results agree well with the measurements, while the USC mechanism tends to under predict flame speed for near stoichiometric and rich mixtures. Laminar flame speed increased with preheat temperatures as expected and the chemical kinetic mechanisms produce similar sensitivity as the experimental data.

For vitiation measurements with N_2 dilution, predictions from the chemical mechanisms were within 10% at all conditions. The NUI mechanism predictions match the measurements at $\Theta = 0.21$ and move closer to the USC mechanism results at $\Theta = 0.15$. In general, the effect of N_2 dilution can be considered as a thermal effect as it is a non-reactive diluent. Some chemical effect can be observed at $\Theta = 0.15$, where the oxygen concentration is low which could lead to differences in chemical paths. Also, the flame speed variation with oxygen content in the mixture (relative to the results for air with other conditions held

constant) is independent of preheat temperature; this was found in both the measurements and model predictions.

Addition of a chemically active diluent (CO_2) decreased the flame speed further; this is expected even without considering chemical effects of CO_2 as the heat capacity of CO_2 is greater than that of N_2. Differences between measurements and kinetic model predictions increases as the amount of CO_2 fraction in the oxidizer increased. These differences were largest for the lowest oxygen case tested ($\Theta = 0.15$). Radiation effects (due to the presence of excess CO_2) on flame speed were ruled out as a reason for these differences as the maximum effect they produced was smaller than the differences between measurements and model predictions. Further, these differences were higher for lean mixtures when compared to stoichiometric and rich flames indicating that reaction chemistry under CO_2 might not be accurately captured by the chemical mechanisms. Another interesting to point to note is that the NUI and USC mechanisms predict the same flame speeds for lean mixtures but differ at stoichiometric and rich conditions. These differences decreased as the preheat temperature increased to 650 K, but remained the same for vitiation cases irrespective of the diluent used at the same preheat temperature.

8.1.2.2 Propylene mixtures

For propylene-air mixtures, chemical kinetic models do not accurately predict flame speed when compared with experimental measurements. The NUI mechanism performed better at lower preheat temperatures, while the USC mechanism was closest to the experimental measurements at the highest preheat temperature (650 K). The flame speed dependence predicted by kinetic models is higher than that of the experiments for near-stoichiometric mixtures. When compared with ethylene mixtures, the temperature

dependence for rich mixture is enhanced for propylene flames. Although both fuels are alkenes, propylene mixtures consistently produce lower flame speeds when compared to ethylene mixtures at similar conditions.

Dilution has a larger effect on flame speed for propylene flames when compared to ethylene mixtures. Chemical kinetic mechanisms were unable to accurately predict flame speeds of propylene mixture with N_2 as additional diluent in the oxidizer, the differences between measurements and model predictions are greater than 10% and are up to a 100% for some cases ($\Theta = 0.15$). Also, as the preheat temperature increased the effect of diluent was underestimated by the models, whereas flame speed measurements showed similar effect of diluent irrespective of the preheat temperature. For propylene mixtures, the decrease in flame speed due to the addition of N_2 to the oxidizer is not just a thermal effect, but also due to chemical effects. These chemical effects are due to the change in O_2 concentration in the mixture which leads to an increase in prominence for reactions that contribute negatively towards flame speed.

8.1.3 Chemical kinetic model performance

In general, the NUI mechanism provided a better estimate of flame speeds for ethylene-air mixtures at all preheat temperatures, while the USC mechanism was closer to flame speed measurements of propylene-air at the highest preheat temperature (650 K). For vitiated ethylene mixtures the USC mechanism was better at predicting flame speeds as the oxygen content in the oxidizer decreased. For vitiated propylene mixtures both the mechanisms over predict flame speed by a large margin. As a reactive diluent (CO_2) was introduced to ethylene mixtures the USC mechanism is closer to measurements but the

differences are much higher when compared to mixtures with only N_2 dilution for the same oxygen level. To understand the reaction kinetics NUI mechanism was considered as the standard and sensitivity and reaction pathway analyses were performed to identify the important reactions for propagation of alkene flames.

8.1.3.1 Propylene chemistry

The allyl (C_3H_5-A) radical plays a key role in propylene combustion. The formation of this radical negatively affects flame speed as further destruction of this radical happens via the allyl-H recombination reaction (C_3H_5-A + H (*M) ⇔ C_3H_6 (*M)) to form fuel species making it harder for the destruction of propylene to occur. This reaction is not well studied in the literature, and varying the pre-exponential factor (*A*) of the reaction rate constant within the uncertainty reported in the literature resulted in a 5-10% change in flame speed depending on the equivalence ratio. As the kinetic modelling over predicts the flame speed dependence on preheat temperature for near stoichiometric mixtures of propylene, it was postulated that the production of the allyl radical was not sufficient at these conditions. The reaction pathways of C_3H_6+H reaction were also examined, and the allyl producing pathway was shown to have lower preference for the temperatures under consideration. Increasing the allyl production at these conditions could lead to lower flame speeds and improve the accuracy of the kinetic models at these conditions. For vitiated propylene flames (N_2 dilution), the allyl-H recombination reaction was shown to have a higher influence on flame speed when compared to the non-diluted mixtures. Given that the predicted flame speeds for N_2-diluted cases showed greater errors compared to the experiments, this further supports the conclusion that allyl chemistry may be the source of the mechanism's deficiency.

8.1.3.2 CO_2 dilution

For ethylene mixtures with CO_2 dilution, the chemical mechanisms over predicted flame speeds. The largest differences between the model predictions and experimental measurements were observed for the highest amount of CO_2 dilution (C = 0.2) and lowest fraction of O_2 content ($\Theta = 0.15$) in the oxidizer. Lean mixtures were observed to have higher differences when compared to stoichiometric and rich mixtures. Two reactions whose reaction rate might be directly affected due to the presence of CO_2 in the reactants were examined in detail: $CO+OH \Leftrightarrow CO_2+H$ and $H+O_2 (+M) \Leftrightarrow HO_2 (+M)$. Changing the rate coefficient of the CO+OH reaction (within the range allowed by experimental data) did not produce changes that could match the experimental flame speeds. Changing the third-body efficiency of CO_2 for the $H+O_2$ (+M) recombination reaction, however, produced changes in the flame speeds for lean mixtures only while minimally affecting the flame speeds of stoichiometric and rich mixtures. This change does not affect the flame speed prediction of mixtures with no CO_2 dilution providing a potential pathway to improve the accuracy of chemical kinetic models. It is also important to note that there are several three body reactions whose influence on flame speed is not well understood. Rate coefficients of such reactions can be validated by using the flame speed data for mixtures with these diluents.

Overall, the chemical kinetic models under consideration predict laminar flame speeds accurately at room conditions and for moderately preheated flames. As the preheat temperature is increased and diluent species are introduced in to the oxidizer the models over predict flame speeds by large margins. These differences could be caused by uncertainties in the rate coefficients of key reactions. The reactions discussed in this thesis

such as the allyl-H recombination and the H-O_2 recombination reaction are also key for propagation of jet fuel flames. Accurate estimation of the rate coefficient of these important reactions is key to precisely modelling reaction chemistry of jet fuels and not just alkenes which were under consideration in this thesis.

8.2 Future work

The current work has shown that laminar flame speed can be accurately measured using reaction zone area measurements of Bunsen flames. To further validate this approach, a more detailed analysis of stretch effects on Bunsen flames should be carried out using computational (full-scale simulation of a Bunsen flame) and experimental (measuring velocity gradients in a Bunsen flame) methods. These effects should be calculated for various inlet velocities and flame heights to develop a more accurate understanding of the limitations of this methodology to measure flame speeds.

The method does have limitations for measuring flame speeds of highly preheated, heavy hydrocarbons (including liquid jet fuel). The long residence times (seconds) typically required to preheat the reactants leads to partial oxidation reactions that consume the parent fuel. To work with these fuels, it would be helpful to develop a preheating approach with much shorter residence times (order of ms) while keeping the flow laminar. Such methodologies are hard develop and are unavailable in literature, however, in their recent work, Ferris et al. [133] demonstrated that laminar flame speed measurements could be made for preheat temperatures up to 832 K using spherical flames in a shock tube. This methodology has shown promise in achieving high preheat temperatures (in a short residence time) for laminar flames, but it is novel and needs to be vigorously tested. Since

preheating effects generally impact flame chemistry at intermediate temperatures and where species diffusing from the high temperature reaction zone are present, other approaches to address chemistry at similar temperatures and compositions should be explored. This might include measuring extinction strain rates for non-premixed flames, e.g., in an opposed jet flame configuration.

The rate coefficients for the reactions under consideration are highly dependent on temperature. In this thesis, the temperature dependence of the rate coefficients was not varied in most cases due to the lack of experimental data for these reactions. The rate coefficients for these reactions need to be measured at several temperatures in the intermediate temperature regime of a flame (~800-1600 K). These measurements can then be used to accurately fit the rate coefficient with temperature while also taking the theoretical calculations into consideration. The third-body efficiency of species also need to be examined in detail to accurately predict laminar flame sped. To achieve this, rate coefficient measurements need to be carried out with different kinds of bath gases to accurately capture the third – body efficiency of relevant species.

Ethylene and propylene are two key intermediate species for jet fuel combustion; based on approaches such as the HyChem model, other species such as 1-butene, *iso*-butene, and benzene are also expected to contribute towards flame propagation for jet fuels. Although chemical kinetic mechanisms were able to predict laminar flame speeds accurately at room conditions, they were unable to accurately capture the effect of preheat for propylene flames and the effect of dilution for both ethylene and propylene flames. By measuring the flame speeds of the other intermediate species at vitiated mixture conditions, the accuracy of jet fuel chemical kinetic mechanisms can be improved. Flame speed

measurements also have to be carried out at higher pressure conditions as this would cover a different regime of operating conditions and can help in improving the mechanisms. Further, higher pressures can lead to greater importance of three-body reactions and thus provide more sensitive data for adjusting the third-body efficiency of relevant species. One key obstacle to measuring diluted propylene mixture flame speeds in the current work was the low fuel flow rate required at certain conditions. Measuring flame speeds for mixtures which require higher fuel flow rate such as mixtures with helium dilution and high oxygen content can expand the range of dilution levels and equivalence ratios at which flame speeds can be measured especially for heavy fuels such as propylene.

Appendix – A

Liquid fuel vaporizer design and reactant delivery system

This section details the development of a liquid fuel vaporizer at Georgia Institute of technology. Also, the modifications performed to the existing reactant delivery system to study liquid fuel vitiated combustion are detailed. These modifications were carried out as a part of Master's degree work of Mr. Daniel Bloomer.

Additions to the reactant delivery system were necessary to be able to perform experiments on premixed liquid fuel combustion with steam dilution. The system needed to incorporate a means of vaporizing the liquid fuel and vaporizing water for dilution. The reactant delivery system is shown schematically in Figure A.1. The reactant gas flows are metered individually with a bank of rotameters and introduced sufficiently far upstream to mix thoroughly before passing through the nozzle. The reactant delivery system is shown in Figure A.2; it incorporates separate subsystems for vaporizing both liquids: fuel and water. The desired mixture of O_2, N_2 and CO_2 is used as a carrier gas for the water vaporizer, a commercial, (Bronkhorst W-303B) system. This vaporizer comes with a pre-calibrated flow rate with an accuracy of 2%. The mildly preheated (~ 400 K) output of the first vaporizer is then sent through the fuel vaporizer, which was developed for these experiments.

Liquid fuel is delivered to the vaporizer using a pressure feed system. Nitrogen is used to pressurize the fuel tank. The oxidizer flow into the fuel vaporizer is pre-heated due to the upstream Bronkhorst vaporizer, and the fuel vaporizer itself is heated with electrical

resistance tape. Liquid fuel on the upstream side of the orifice injector is exposed to elevated temperatures due to heat conduction through the vaporizer walls. Fuel coking is prevented by limiting the fuel vaporizer temperature. The thermal coking breakpoint for Jet-A type fuels has been reported to be at or above 200 °C [134, 135]. Thus, the vaporizer wall temperatures are maintained below 200 °C, and no evidence of fuel coking was observed.

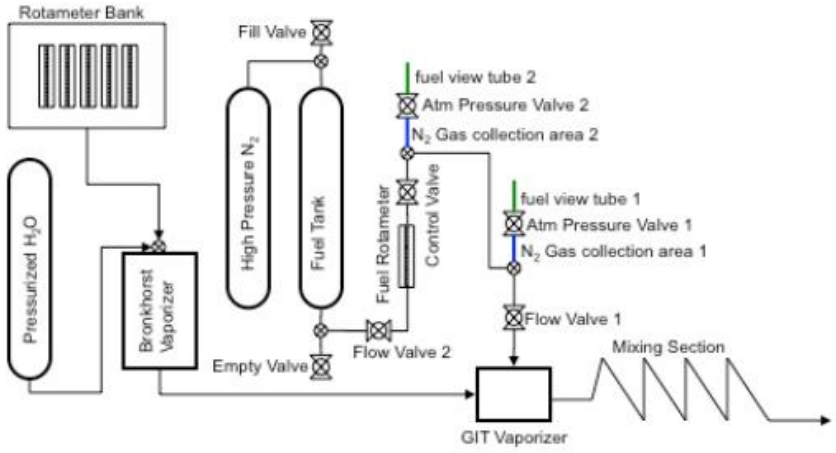

Figure A.1: Reactant delivery system schematic.

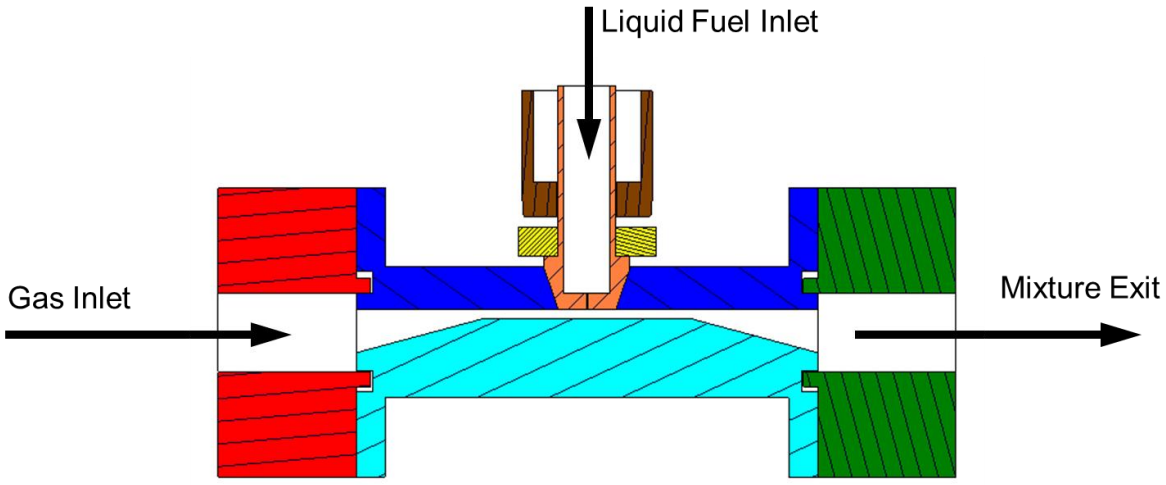

Figure A.2: A schematic showing the working of an in-house liquid fuel vaporizer

The vaporizer system for the liquid fuel was developed in-house to handle the low fuel flow rates. Liquid fuel is injected into the oxidizer mixture through a 0.008" (200 μm) diameter orifice. The vaporizer was designed to accelerate the oxidizer mixture to high velocity to shear off small droplets of the liquid fuel at the orifice interface. Figure A.2 provides a schematic which demonstrates the working concept of the fuel vaporizer. The liquid fuel is stored in a chamber at higher pressure than the operating pressure of the vaporizer. To achieve this N_2 gas is used to apply overhead pressure on the liquid, the chamber is first filled with n-decane and then N_2 is introduced to raise the pressure to ~ 50 psig. Due to the high pressure in the liquid chamber it is certain that the fuel will flow into the oncoming oxidizer mixture rather than the oxidizer traveling up the fuel and forming bubbles.

Table A.1: Fuel flow Weber Number through injector orifice

Fuel (mL/min)	Weber Number
0.2	0.173
0.3	0.389
0.4	0.692
0.5	1.08
0.6	1.56
0.7	2.12

In order to achieve a pre-mixed laminar flame with liquid hydrocarbon fuels in the current facility, the flow rate of the liquid fuel must be low. Weber numbers for liquid *n*-decane flow through the orifice over the expected flow range are shown in Table A.1. The critical Weber number for a liquid jet to atomize is 13. Based on this, the fuel jet does not have enough inertia to overcome its surface tension and atomize. For this reason, the

vaporizer was designed to accelerate the oxidizer mixture to high velocity in order to shear off small droplets of the liquid fuel at the orifice interface.

The vaporizer was designed to operate at sub-atmospheric and elevated pressure. A simplified finite element model (Pro/Engineer) of the vaporizer was created. The FEM elements were created with an aspect ratio less than 7 and a turning angle less than 10°. The mesh was successfully created with less than 2% of elements violating each of these constraints. A pressure load of 5 atm was applied to the internal flow channel in Pro/E. The mesh, loads, and constraints were imported into Ansys 12.0, which was utilized to complete FEA on the model. The analysis found a maximum von Mises stress of 4.7 MPa, two orders of magnitude lower than the yield stress for stainless steel (~603 MPa).

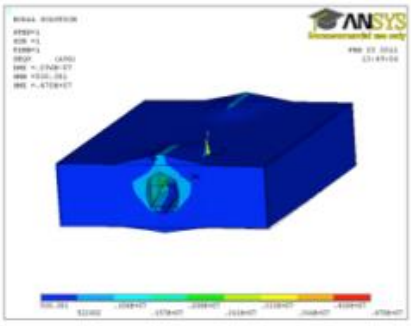

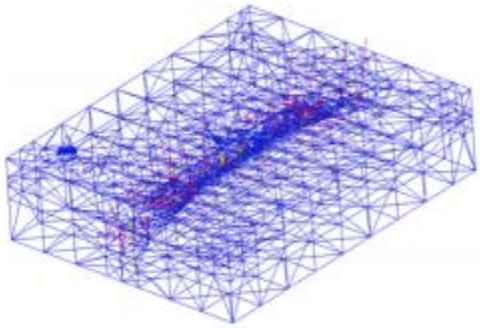

Figure A.3: Stress results from Ansys. **Figure A.4: Mesh of the simplified vaporizer.**

The gas rotameters are calibrated at the same operating supply pressure with a bubble flow meter. The liquid fuel rotameter is calibrated by operating the system for a fixed time and measuring the collected mass with a precision scale. The combined uncertainty (accuracy) in total mass flow rate is better than 3%.

Appendix – B

Uncertainty analysis

This appendix discusses various sources of uncertainty in laminar flame speed measurements using the reaction zone area based Bunsen flame technique. The error analysis approach shown here is adapted from [20]. The primary sources of error in flame speed are due to uncertainties in flow rate measurement and uncertainty in the area of the flame measured. Error in the equivalence ratio is primarily due to the uncertainty in the flow rate.

Flow rate uncertainty

Flow rate of each individual gas was monitored using a high accuracy rotameter with a ±1% full scale accuracy. Oscillations in flow can cause the rotameter float to fluctuate by ± 2 divisions, this can lead to an error of ±1.3% (±2/150). This is a conservative estimate as the oscillation in the float were observed to be lower than this value. Each individual gas flow meter is independent as the supply lines are choked, the combined total uncertainty in the flow rate can be determined as the root sum of squares. Assuming each individual flow meter has the same uncertainty, the total uncertainty in flow rate is given by:

$$u(\dot{Q}) = \sqrt{\sum_{i=1}^{n} u(\dot{Q}_i)^2} \approx \sqrt{n}\, u(\dot{Q}_i)$$

where the subscript i represents the i^{th} component in a mixture of n gases. Typically there are 2-4 gases used to create a required mixture, thus the combined uncertainty is ± 1.9-

2.7%. Further, fluctuations in room temperature and pressure introduce an error in the total calibrated flowrate. The flow rate at room conditions and the calibrated flow rate are related by the following equation:

$$\dot{Q}_r = \dot{Q}_{calibrated} \sqrt{\frac{P_{calibrated}}{P_r} \text{ x } \frac{T_r}{T_{calibrated}}}$$

where subscript *r* represents room conditions. The total uncertainty in flow rate while accounting for uncertainty in room temperature and pressure is given by:

$$\frac{u(\dot{Q}_r)}{\dot{Q}_r} = \sqrt{\left(\frac{u(\dot{Q})}{\dot{Q}}\right)^2 + \frac{1}{2}\left(\frac{u(T_r)}{T_r}\right)^2 + \frac{1}{2}\left(\frac{u(P_r)}{P_r}\right)^2}$$

A systematic uncertainty of 3 K and 0.02 atm is assumed for room temperature and pressure respectively. Based on this formulation the total uncertainty in the measured flow rate is ±2.5-3.1% depending on the number of gases used.

Uncertainty in flame surface area

Unsteadiness in the flame surface results in fluctuation of the measured reaction zone area. As mentioned in the thesis if this fluctuation is too high the data set is rejected, but it is still prudent to calculate the random error in the flame area. This is quantified by the standard deviation of the mean surface area of the reaction zone. The average reaction zone area is typically determined from over 50-100 flame images (100-200 flame area values when both halves of the flame are considered). The uncertainty in the mean area at a 95% confidence level is given by the expression, $\pm 1.96 \times \sigma/\sqrt{n}$, where σ is the standard deviation and n is the total number of flame images used to calculate the mean area. The

standard deviation was typically lower 5% for a total of 100 flames. Thus the total random uncertainty in the flame surface area is ± 1% at a 95% confidence level.

Total error

The total uncertainty in flame speed can be calculated from the uncertainty in flow rate and the uncertainty in the flame surface area using the following equation:

$$\frac{u(S_L)}{S_L} = \sqrt{\left(\frac{u(\dot{Q}_r)}{\dot{Q}_r}\right)^2 + \left(\frac{u(A_b)}{A_b}\right)^2}$$

where A_b is the burned flame area. The total uncertainty in flame speed calculated via this method is less than 4% depending on the mixture conditions and the unsteadiness in the flame area. This error is very small and depending on the scale of the graph the error bar might be smaller than the symbol used to represent flame speed.

The total error in the equivalence ratio is ±1.9%-2.7% based on the uncertainty in the flow rate measurement of the fuel and oxidizer, this does not include the uncertainties in room temperature and pressure. The flow rate error is the major source of error when compared to the burned surface area error, it is important to remember these are conservative estimates and the actual error might be lower than these values.

REFERENCES

[1]. Wulff, A. and J. Hourmouziadis, "Technology review of aeroengine pollutant emissions," *Aerospace science and technology*, 1997. **1**(8): p. 557-572.

[2]. Lefebvre, A.H., "Gas turbine combustion." 2010: *CRC Press*.

[3]. Lovett, J.A., T.P. Brogan, D.S. Philippona, B.V. Keil, and T.V. Thompson, "Development needs for advanced afterburner designs," in *Proceedings of 40th Joint Propulsion Conference and Exhibit*. 2004.

[4]. Daggett, D., R. Hendricks, and R. Walther, "Alternative fuels and their potential impact on aviation," 2006.

[5]. Gicquel, L.Y., G. Staffelbach, and T. Poinsot, "Large eddy simulations of gaseous flames in gas turbine combustion chambers," *Progress in energy and combustion science*, 2012. **38**(6): p. 782-817.

[6]. Kim, W.-W., S. Menon, and H.C. Mongia, "Large-eddy simulation of a gas turbine combustor flow," *Combustion Science and Technology*, 1999. **143**(1-6): p. 25-62.

[7]. Boudier, G., L. Gicquel, T. Poinsot, D. Bissieres, and C. Bérat, "Comparison of LES, RANS and experiments in an aeronautical gas turbine combustion chamber," *Proceedings of the Combustion Institute*, 2007. **31**(2): p. 3075-3082.

[8]. Lindstedt, R. and L. Maurice, "Detailed chemical-kinetic model for aviation fuels," *Journal of Propulsion and Power*, 2000. **16**(2): p. 187-195.

[9]. Naik, C.V., K.V. Puduppakkam, A. Modak, E. Meeks, Y.L. Wang, Q. Feng, and T.T. Tsotsis, "Detailed chemical kinetic mechanism for surrogates of alternative jet fuels," *Combustion and Flame*, 2011. **158**(3): p. 434-445.

[10]. Turns, S.R., "An introduction to combustion." Vol. 287. 1996: *McGraw-hill New York*.

[11]. Law, C.K., "Combustion physics." 2006: *Cambridge university press*.

[12]. Glassman, I., R.A. Yetter, and N.G. Glumac, "Combustion." 2014: *Academic press*.

[13]. Powling, J., "A new burner method for the determination of low burning velocities and limits of inflammability," *Fuel*, 1949. **28**(2): p. 25-28.

[14]. Botha, J. and D.B. Spalding, "The laminar flame speed of propane/air mixtures with heat extraction from the flame," *Proc. R. Soc. Lond. A*, 1954. **225**(1160): p. 71-96.

[15]. Bosschaart, K.J. and L.P.H. de Goey, "Detailed analysis of the heat flux method for measuring burning velocities," *Combustion and Flame*, 2003. **132**(1): p. 170-180.

[16]. Konnov, A.A., A. Mohammad, V.R. Kishore, N.I. Kim, C. Prathap, and S. Kumar, "A comprehensive review of measurements and data analysis of laminar burning velocities for various fuel+air mixtures," *Progress in Energy and Combustion Science*, 2018. **68**: p. 197-267.

[17]. Wu, F., W. Liang, Z. Chen, Y. Ju, and C.K. Law, "Uncertainty in stretch extrapolation of laminar flame speed from expanding spherical flames," *Proceedings of the Combustion Institute*, 2015. **35**(1): p. 663-670.

[18]. Egolfopoulos, F.N., N. Hansen, Y. Ju, K. Kohse-Höinghaus, C.K. Law, and F. Qi, "Advances and challenges in laminar flame experiments and implications for combustion chemistry," *Progress in Energy and Combustion Science*, 2014. **43**: p. 36-67.

[19]. Faghih, M. and Z. Chen, "The constant-volume propagating spherical flame method for laminar flame speed measurement," *Science Bulletin*, 2016. **61**(16): p. 1296-1310.

[20]. Kochar, Y.N., "Laminar flame speed and stretch sensitivity of hydrocarbon fuels at high preheat, pressure and vitiation." 2014, Georgia Institute of Technology.

[21]. Natarajan, J., "Experimental and Numerical Investigation of Laminar flame speeds of H2/CO/CO2/N2 Mixtures." 2008, Georgia Institute of Technology.

[22]. Davis, S., C. Law, and H. Wang, "Propene pyrolysis and oxidation kinetics in a flow reactor and laminar flames," *Combustion and Flame*, 1999. **119**(4): p. 375-399.

[23]. Hirasawa, T., C. Sung, A. Joshi, Z. Yang, H. Wang, and C. Law, "Determination of laminar flame speeds using digital particle image velocimetry: binary fuel blends of ethylene, n-butane, and toluene," *Proceedings of the Combustion Institute*, 2002. **29**(2): p. 1427-1434.

[24]. Lewis, B. and G. Von Elbe, "Combustion, flames and explosions of gases." 2012: *Elsevier*.

[25]. Law, C.K. and C.J. Sung, "Structure, aerodynamics, and geometry of premixed flamelets," *Progress in Energy and Combustion Science*, 2000. **26**(4): p. 459-505.

[26]. Linnett, J., "Methods of measuring burning velocities," in *Symposium (International) on Combustion*. 1953. Elsevier.

[27]. Andrews, G.E. and D. Bradley, "Determination of burning velocities: A critical review," *Combustion and Flame*, 1972. **18**(1): p. 133-153.

[28]. Rallis, C.J. and A.M. Garforth, "The determination of laminar burning velocity," *Progress in Energy and Combustion Science*, 1980. **6**(4): p. 303-329.

[29]. Natarajan, J., Y. Kochar, T. Lieuwen, and J. Seitzman, "Laminar Flame Speed Measurements of H2/CO/CO2 Mixtures Up to 15 atm and 600 K Preheat Temperature," in *ASME Turbo Expo 2008: Power for Land, Sea, and Air*. 2008. American Society of Mechanical Engineers.

[30]. Natarajan, J., Y. Kochar, T. Lieuwen, and J. Seitzman, "Pressure and preheat dependence of laminar flame speeds of H 2/CO/CO 2/O 2/He mixtures," *Proceedings of the Combustion Institute*, 2009. **32**(1): p. 1261-1268.

[31]. Natarajan, J., T. Lieuwen, and J. Seitzman, "Laminar flame speeds of H2/CO mixtures: Effect of CO2 dilution, preheat temperature, and pressure," *Combustion and Flame*, 2007. **151**(1–2): p. 104-119.

[32]. Kochar, Y., J. Seitzman, T. Lieuwen, W. Metcalfe, S. Burke, H. Curran, M. Krejci, W. Lowry, E. Petersen, and G. Bourque, "Laminar flame speed measurements and modeling of alkane blends at elevated pressures with various diluents," in *ASME 2011 Turbo Expo: Turbine Technical Conference and Exposition*. 2011. American Society of Mechanical Engineers.

[33]. Gokulakrishnan, P., C.C. Fuller, M.S. Klassen, R.G. Joklik, Y.N. Kochar, S.N. Vaden, T.C. Lieuwen, and J.M. Seitzman, "Experiments and modeling of propane combustion with vitiation," *Combustion and Flame*, 2014. **161**(8): p. 2038-2053.

[34]. Bouvet, N., C. Chauveau, I. Gökalp, S.-Y. Lee, and R.J. Santoro, "Characterization of syngas laminar flames using the Bunsen burner configuration," *International Journal of Hydrogen Energy*, 2011. **36**(1): p. 992-1005.

[35]. Mazas, A., B. Fiorina, D. Lacoste, and T. Schuller, "Effects of water vapor addition on the laminar burning velocity of oxygen-enriched methane flames," *Combustion and Flame*, 2011. **158**(12): p. 2428-2440.

[36]. Boushaki, T., Y. Dhué, L. Selle, B. Ferret, and T. Poinsot, "Effects of hydrogen and steam addition on laminar burning velocity of methane–air premixed flame: experimental and numerical analysis," *international journal of hydrogen energy*, 2012. **37**(11): p. 9412-9422.

[37]. Edwards, T., "Liquid Fuels and Propellants for Aerospace Propulsion: 1903-2003," *Journal of Propulsion and Power*, 2003. **19**(6): p. 1089-1107.

[38]. Edwards, T. and L.Q. Maurice, "Surrogate mixtures to represent complex aviation and rocket fuels," *Journal of Propulsion and Power*, 2001. **17**(2): p. 461-466.

[39]. Honnet, S., K. Seshadri, U. Niemann, and N. Peters, "A surrogate fuel for kerosene," *Proceedings of the Combustion Institute*, 2009. **32**(1): p. 485-492.

[40]. Gokulakrishnan, P., M. Klassen, and R. Roby, "Ignition characteristics of a Fischer-Tropsch synthetic jet fuel," in *ASME Turbo Expo 2008: Power for Land, Sea, and Air*. 2008. American Society of Mechanical Engineers.

[41]. Edwards, T., D. Minus, W. Harrison, E. Corporan, M. DeWitt, S. Zabarnick, and L. Balster, "Fischer-Tropsch Jet Fuels–Characterization for Advanced Aerospace Applications," in *Proceedings of the 40th AIAA/ASME/SAD/ASEE Joint Propulsion Conference and Exhibit*. 2004.

[42]. Skjøth-Rasmussen, M., M. Braun-Unkhoff, C. Naumann, P. Frank, C. Chauveau, and C. Vovelle, "Experimental and numerical study of n-decane chemistry," in *Proceedings of the European Combustion Meeting*. 2003. France.

[43]. Kumar, K. and C.-J. Sung, "Laminar flame speeds and extinction limits of preheated n-decane/O 2/N 2 and n-dodecane/O 2/N 2 mixtures," *Combustion and Flame*, 2007. **151**(1): p. 209-224.

[44]. Zhao, Z., J. Li, A. Kazakov, F.L. Dryer, and S.P. Zeppieri, "Burning velocities and a high-temperature skeletal kinetic model for n-decane," *Combust. Sci. and Tech.*, 2004. **177**(1): p. 89-106.

[45]. Ji, C., E. Dames, Y.L. Wang, H. Wang, and F.N. Egolfopoulos, "Propagation and extinction of premixed C 5–C 12 n-alkane flames," *Combustion and Flame*, 2010. **157**(2): p. 277-287.

[46]. Nishiie, T., D. Singh, and L. Qiao, "Laminar Burning Velocity and Markstein Length of n-Decane-Air, Jet-A-Air and S-8-Air Flames," in *Proceedings of the 6th US National Combustion Meeting, Ann Arbor, MI, May*. 2009.

[47]. Lefebvre, A., "Influence of fuel properties on gas turbine combustion performance." 1985, *DTIC Document*.

[48]. Colket, M., T. Edwards, S. Williams, N.P. Cernansky, D.L. Miller, F. Egolfopoulos, P. Lindstedt, K. Seshadri, F.L. Dryer, and C.K. Law, "Development of an experimental database and kinetic models for surrogate jet fuels," in *45th AIAA Aerospace Sciences Meeting and Exhibit*. 2007.

[49]. Douté, C., J.-L. Delfau, R. Akrich, and C. Vovelle, "Experimental Study of the Chemical Structure of Low-Pressure Premixed n> Heptane-02-Ar and lso-Octane-02-Ar Flames," *Combustion science and technology*, 1997. **124**(1-6): p. 249-276.

[50]. Zeppieri, S.P., S.D. Klotz, and F.L. Dryer, "Modeling concepts for larger carbon number alkanes: a partially reduced skeletal mechanism for n-decane oxidation and pyrolysis," *Proceedings of the Combustion Institute*, 2000. **28**(2): p. 1587-1595.

[51]. Kumar, K., G. Mittal, C.-J. Sung, and C.K. Law, "An experimental investigation of ethylene/O 2/diluent mixtures: Laminar flame speeds with preheat and ignition delays at high pressures," *Combustion and Flame*, 2008. **153**(3): p. 343-354.

[52]. Kay, I.W., W.T. Peschke, and R.N. Guile, "Hydrocarbon-fueled scramjet combustor investigation," *Journal of Propulsion and Power*, 1992. **8**(2): p. 507-512.

[53]. Wang, H., R. Xu, K. Wang, C.T. Bowman, R.K. Hanson, D.F. Davidson, K. Brezinsky, and F.N. Egolfopoulos, "A physics-based approach to modeling real-fuel combustion chemistry - I. Evidence from experiments, and thermodynamic, chemical kinetic and statistical considerations," *Combustion and Flame*, 2018. **193**: p. 502-519.

[54]. Xu, R., K. Wang, S. Banerjee, J. Shao, T. Parise, Y. Zhu, S. Wang, A. Movaghar, D.J. Lee, R. Zhao, X. Han, Y. Gao, T. Lu, K. Brezinsky, F.N. Egolfopoulos, D.F. Davidson, R.K. Hanson, C.T. Bowman, and H. Wang, "A physics-based approach to modeling real-fuel combustion chemistry – II. Reaction kinetic models of jet and rocket fuels," *Combustion and Flame*, 2018. **193**: p. 520-537.

[55]. Tao, Y., R. Xu, K. Wang, J. Shao, S.E. Johnson, A. Movaghar, X. Han, J.-W. Park, T. Lu, K. Brezinsky, F.N. Egolfopoulos, D.F. Davidson, R.K. Hanson, C.T. Bowman, and H. Wang, "A Physics-based approach to modeling real-fuel combustion chemistry – III. Reaction kinetic model of JP10," *Combustion and Flame*, 2018. **198**: p. 466-476.

[56]. Wang, K., R. Xu, T. Parise, J. Shao, A. Movaghar, D.J. Lee, J.-W. Park, Y. Gao, T. Lu, F.N. Egolfopoulos, D.F. Davidson, R.K. Hanson, C.T. Bowman, and H. Wang, "A physics-based approach to modeling real-fuel combustion chemistry – IV. HyChem modeling of combustion kinetics of a bio-derived jet fuel and its blends with a conventional Jet A," *Combustion and Flame*, 2018. **198**: p. 477-489.

[57]. Raezer, S. and H.L. Olsen, "Measurement of laminar flame speeds of ethylene-air and propane-air mixtures by the double kernel method," *Combustion and Flame*, 1962. **6**: p. 227-232.

[58]. Egolfopoulos, F., D. Zhu, and C. Law, "Experimental and numerical determination of laminar flame speeds: Mixtures of C 2-hydrocarbons with oxygen and nitrogen," in *Symposium (International) on Combustion*. 1991. Elsevier.

[59]. Jomaas, G., X. Zheng, D. Zhu, and C. Law, "Experimental determination of counterflow ignition temperatures and laminar flame speeds of C 2–C 3 hydrocarbons at atmospheric and elevated pressures," *Proceedings of the Combustion Institute*, 2005. **30**(1): p. 193-200.

[60]. Hassan, M.I., K.T. Aung, O.C. Kwon, and G.M. Faeth, "Properties of Laminar Premixed Hydrocarbon/Air Flames at Various Pressures," *Journal of Propulsion and Power*, 1998. **14**(4): p. 479-488.

[61]. Burke, S.M., W. Metcalfe, O. Herbinet, F. Battin-Leclerc, F.M. Haas, J. Santner, F.L. Dryer, and H.J. Curran, "An experimental and modeling study of propene oxidation. Part 1: Speciation measurements in jet-stirred and flow reactors," *Combustion and Flame*, 2014. **161**(11): p. 2765-2784.

[62]. Burke, S.M., U. Burke, R. Mc Donagh, O. Mathieu, I. Osorio, C. Keesee, A. Morones, E.L. Petersen, W. Wang, T.A. DeVerter, M.A. Oehlschlaeger, B. Rhodes, R.K. Hanson, D.F. Davidson, B.W. Weber, C.-J. Sung, J. Santner, Y. Ju, F.M. Haas, F.L. Dryer, E.N. Volkov, E.J.K. Nilsson, A.A. Konnov, M. Alrefae, F. Khaled, A. Farooq, P. Dirrenberger, P.-A. Glaude, F. Battin-Leclerc, and H.J. Curran, "An experimental and modeling study of propene oxidation. Part 2: Ignition delay time and flame speed measurements," *Combustion and Flame*, 2015. **162**(2): p. 296-314.

[63]. Zhao, Z., A. Kazakov, J. Li, and F.L. Dryer, "The initial temperature and N2 dilution effect on the laminar flame speed of propane/air," *Combustion Science and Technology*, 2004. **176**(10): p. 1705-1723.

[64]. Design, R., "CHEMKIN-PRO 15131." 2013: San Diego.

[65]. Wang, H., E. Dames, B. Sirjean, D. Sheen, R. Tangko, A. Violi, J. Lai, F. Egolfopoulos, D. Davidson, and R. Hanson, "A high-temperature chemical kinetic model of n-alkane (up to n-dodecane), cyclohexane, and methyl-, ethyl-, n-propyl and n-butyl-cyclohexane oxidation at high temperatures," *JetSurF version*, 2010. **2**: p. 19.

[66]. Gokulakrishnan, P., G. Gaines, M. Klassen, and R. Roby, "Autoignition of aviation fuels: experimental and modeling study," in *Proceedings of the 43rd AIAA/ASME/SAE/ASEE Joint Propulsion Conference and Exhibit*. 2007.

[67]. Ranzi, E., A. Frassoldati, S. Granata, and T. Faravelli, "Wide-range kinetic modeling study of the pyrolysis, partial oxidation, and combustion of heavy n-alkanes," *Industrial & engineering chemistry research*, 2005. **44**(14): p. 5170-5183.

[68]. Kang, D., V. Kalaskar, D. Kim, J. Martz, A. Violi, and A. Boehman, "Experimental study of autoignition characteristics of Jet-A surrogates and their validation in a motored engine and a constant-volume combustion chamber," *Fuel*, 2016. **184**: p. 565-580.

[69]. De Toni, A.R., M. Werler, R.M. Hartmann, L.R. Cancino, R. Schießl, M. Fikri, C. Schulz, A.A.M. Oliveira, E.J. Oliveira, and M.I. Rocha, "Ignition delay times of Jet

A-1 fuel: Measurements in a high-pressure shock tube and a rapid compression machine," *Proceedings of the Combustion Institute*, 2017. **36**(3): p. 3695-3703.

[70]. Won, S.H., B. Windom, B. Jiang, and Y. Ju, "The role of low temperature fuel chemistry on turbulent flame propagation," *Combustion and Flame*, 2014. **161**(2): p. 475-483.

[71]. Wang, H., X. You, A. Joshi, S. Davis, A. Laskin, F. Egolfopoulos, C. Law, and U.M. Version II, "High-Temperature Combustion Reaction Model of H 2/CO/C 1–C 4 Compounds, May 2007."

[72]. Fuller, C., P. Gokulakrishnan, M. Klassen, S. Adusumilli, Y. Kochar, D. Bloomer, J. Seitzman, H.H. Kim, S.H. Won, and F. Dryer, "Effects of vitiation and pressure on laminar flame speeds of n-decane," in *AIAA 50th Aerospace Science Meeting*. 2012. p. 2012-0167.

[73]. Gao, X., Y. Zhang, S. Adusumilli, J. Seitzman, W. Sun, T. Ombrello, and C. Carter, "The effect of ozone addition on laminar flame speed," *Combustion and Flame*, 2015. **162**(10): p. 3914-3924.

[74]. Gao, X., Y. Zhang, S. Adusumilli, J.M. Seitzman, W. Sun, T. Ombrello, and C.D. Carter, "The Effect of Ozone Addition on Flame Propagation," in *53rd AIAA Aerospace Sciences Meeting*. 2015.

[75]. Gao, X., "The effects of ozone addition on flame propagation and stabilization." 2017, Georgia Institute of Technology.

[76]. Sun, C.J., C.J. Sung, L. He, and C.K. Law, "Dynamics of weakly stretched flames: quantitative description and extraction of global flame parameters," *Combustion and Flame*, 1999. **118**(1): p. 108-128.

[77]. Choi, C.W. and I.K. Puri, "Contribution of curvature to flame-stretch effects on premixed flames," *Combustion and Flame*, 2001. **126**(3): p. 1640-1654.

[78]. Kee, R.J., J.F. Grcar, M.D. Smooke, J.A. Miller, and E. Meeks, "PREMIX: a Fortran program for modeling steady laminar one-dimensional premixed flames," *Sandia National Laboratories Report*, 1985(SAND85-8249).

[79]. Larson, R.S., "PLUG: A FORTRAN program for the analysis of PLUG flow reactors with gas-phase and surface chemistry." 1996, *; Sandia Labs., Livermore, CA (United States)*. p. Medium: ED; Size: 26 p.

[80]. Lutz, A.E., R.J. Kee, J.F. Grcar, and F.M. Rupley, "OPPDIF: A Fortran program for computing opposed-flow diffusion flames." 1997, *Sandia National Labs., Livermore, CA (United States)*.

[81]. Chen, Z., "On the extraction of laminar flame speed and Markstein length from outwardly propagating spherical flames," *Combustion and Flame*, 2011. **158**(2): p. 291-300.

[82]. Kelley, A. and C. Law, "Nonlinear effects in the experimental determination of laminar flame properties from stretched flames," in *Eastern State Fall Technical Meeting Chemical & Physical Processes in Combustion*. 2007.

[83]. Clavin, P., "Dynamic behavior of premixed flame fronts in laminar and turbulent flows," *Progress in Energy and Combustion Science*, 1985. **11**(1): p. 1-59.

[84]. Gu, X.J., M.Z. Haq, M. Lawes, and R. Woolley, "Laminar burning velocity and Markstein lengths of methane–air mixtures," *Combustion and Flame*, 2000. **121**(1): p. 41-58.

[85]. Rozenchan, G., D. Zhu, C. Law, and S. Tse, "Outward propagation, burning velocities, and chemical effects of methane flames up to 60 atm," *Proceedings of the Combustion Institute*, 2002. **29**(2): p. 1461-1470.

[86]. Liao, S., D. Jiang, and Q. Cheng, "Determination of laminar burning velocities for natural gas," *Fuel*, 2004. **83**(9): p. 1247-1250.

[87]. Qin, X. and Y. Ju, "Measurements of burning velocities of dimethyl ether and air premixed flames at elevated pressures," *Proceedings of the Combustion Institute*, 2005. **30**(1): p. 233-240.

[88]. Sun, H., S.I. Yang, G. Jomaas, and C.K. Law, "High-pressure laminar flame speeds and kinetic modeling of carbon monoxide/hydrogen combustion," *Proceedings of the Combustion Institute*, 2007. **31**(1): p. 439-446.

[89]. Chen, Z., X. Qin, B. Xu, Y. Ju, and F. Liu, "Studies of radiation absorption on flame speed and flammability limit of CO2 diluted methane flames at elevated pressures," *Proceedings of the Combustion Institute,* 2007. **31**(2): p. 2693-2700.

[90]. Prathap, C., A. Ray, and M.R. Ravi, "Investigation of nitrogen dilution effects on the laminar burning velocity and flame stability of syngas fuel at atmospheric condition," *Combustion and Flame,* 2008. **155**(1): p. 145-160.

[91]. Tang, C., Z. Huang, C. Jin, J. He, J. Wang, X. Wang, and H. Miao, "Laminar burning velocities and combustion characteristics of propane–hydrogen–air premixed flames," *international journal of hydrogen energy*, 2008. **33**(18): p. 4906-4914.

[92]. Lowry, W., J. de Vries, M. Krejci, E. Petersen, Z. Serinyel, W. Metcalfe, H. Curran, and G. Bourque, "Laminar flame speed measurements and modeling of pure alkanes and alkane blends at elevated pressures," in *ASME Turbo Expo 2010: Power for Land, Sea, and Air*. 2010. American Society of Mechanical Engineers.

[93]. Halter, F., T. Tahtouh, and C. Mounaïm-Rousselle, "Nonlinear effects of stretch on the flame front propagation," *Combustion and Flame*, 2010. **157**(10): p. 1825-1832.

[94]. Krejci, M.C., O. Mathieu, A.J. Vissotski, S. Ravi, T.G. Sikes, E.L. Petersen, A. Kérmonès, W. Metcalfe, and H.J. Curran, "Laminar flame speed and ignition delay time data for the kinetic modeling of hydrogen and syngas fuel blends," *Journal of Engineering for Gas Turbines and Power*, 2013. **135**(2): p. 021503.

[95]. Han, M., Y. Ai, Z. Chen, and W. Kong, "Laminar flame speeds of H2/CO with CO2 dilution at normal and elevated pressures and temperatures," *Fuel*, 2015. **148**: p. 32-38.

[96]. Hu, E., X. Li, X. Meng, Y. Chen, Y. Cheng, Y. Xie, and Z. Huang, "Laminar flame speeds and ignition delay times of methane–air mixtures at elevated temperatures and pressures," *Fuel*, 2015. **158**: p. 1-10.

[97]. Bouvet, N., C. Chauveau, I. Gökalp, and F. Halter, "Experimental studies of the fundamental flame speeds of syngas (H2/CO)/air mixtures," *Proceedings of the Combustion Institute,* 2011. **33**(1): p. 913-920.

[98]. Li, H.-M., G.-X. Li, and Y.-H. Jiang, "Laminar burning velocities and flame instabilities of diluted H2/CO/air mixtures under different hydrogen fractions," *International Journal of Hydrogen Energy*, 2018. **43**(33): p. 16344-16354.

[99]. Dong, Y., C.M. Vagelopoulos, G.R. Spedding, and F.N. Egolfopoulos, "Measurement of laminar flame speeds through digital particle image velocimetry: mixtures of methane and ethane with hydrogen, oxygen, nitrogen, and helium," *Proceedings of the combustion institute*, 2002. **29**(2): p. 1419-1426.

[100]. Davis, S., J. Quinard, and G. Searby, "Markstein numbers in counterflow, methane- and propane-air flames: a computational study," *Combustion and flame*, 2002. **130**(1-2): p. 123-136.

[101]. Law, C. and O. Kwon, "Effects of hydrocarbon substitution on atmospheric hydrogen–air flame propagation," *International Journal of Hydrogen Energy*, 2004. **29**(8): p. 867-879.

[102]. Park, O., P.S. Veloo, N. Liu, and F.N. Egolfopoulos, "Combustion characteristics of alternative gaseous fuels," *Proceedings of the Combustion Institute*, 2011. **33**(1): p. 887-894.

[103]. Park, O., P.S. Veloo, and F.N. Egolfopoulos, "Flame studies of C2 hydrocarbons," *Proceedings of the Combustion Institute*, 2013. **34**(1): p. 711-718.

[104]. Park, O., P.S. Veloo, D.A. Sheen, Y. Tao, F.N. Egolfopoulos, and H. Wang, "Chemical kinetic model uncertainty minimization through laminar flame speed measurements," *Combustion and flame*, 2016. **172**: p. 136-152.

[105]. Kondo, S., K. Takizawa, A. Takahashi, and K. Tokuhashi, "Extended Le Chatelier's formula and nitrogen dilution effect on the flammability limits," *Fire Safety Journal*, 2006. **41**(5): p. 406-417.

[106]. Amirante, R., E. Distaso, P. Tamburrano, and R.D. Reitz, "Laminar flame speed correlations for methane, ethane, propane and their mixtures, and natural gas and gasoline for spark-ignition engine simulations," *International Journal of Engine Research*. **0**(0): p. 1468087417720018.

[107]. Metghalchi, M. and J.C. Keck, "Burning velocities of mixtures of air with methanol, isooctane, and indolene at high pressure and temperature," *Combustion and flame*, 1982. **48**: p. 191-210.

[108]. Stone, R., A. Clarke, and P. Beckwith, "Correlations for the laminar-burning velocity of methane/diluent/air mixtures obtained in free-fall experiments," *Combustion and Flame*, 1998. **114**(3): p. 546-555.

[109]. Liu, X., C. Ji, B. Gao, S. Wang, C. Liang, and J. Yang, "A laminar flame speed correlation of hydrogen–methanol blends valid at engine-like conditions," *International Journal of Hydrogen Energy*, 2013. **38**(35): p. 15500-15509.

[110]. Nguyen, D.-K. and S. Verhelst, "Development of Laminar Burning Velocity Correlation for the Simulation of Methanol Fueled SI Engines Operated with Onboard Fuel Reformer." 2017, *SAE International*.

[111]. Galmiche, B., F. Halter, F. Foucher, and P. Dagaut, "Effects of dilution on laminar burning velocity of premixed methane/air flames," *Energy & Fuels*, 2011. **25**(3): p. 948-954.

[112]. Barlow, R.S., A.N. Karpetis, J.H. Frank, and J.Y. Chen, "Scalar profiles and NO formation in laminar opposed-flow partially premixed methane/air flames," *Combustion and Flame*, 2001. **127**(3): p. 2102-2118.

[113]. Grosshandler, W.L., "RADCAL: A Narrow-Band Model for Radiation," *Calculations in a Combustion Environment, NIST Technical Note*, 1993. **1402**.

[114]. De Persis, S., F. Foucher, L. Pillier, V. Osorio, and I. Gökalp, "Effects of O2 enrichment and CO2 dilution on laminar methane flames," *Energy*, 2013. **55**: p. 1055-1066.

[115]. Hu, X., Q. Yu, and J. Liu, "Chemical effect of CO2 on the laminar flame speeds of oxy-methane mixtures in the condition of various equivalence ratios and oxygen concentrations," *International Journal of Hydrogen Energy*, 2016. **41**(33): p. 15068-15077.

[116]. Brown, N.J., L.A. Bastien, and P.N. Price, "Transport properties for combustion modeling," *Progress in Energy and Combustion Science*, 2011. **37**(5): p. 565-582.

[117]. Hong, Z., D. Davidson, E. Barbour, and R. Hanson, "A new shock tube study of the H+ O2→ OH+ O reaction rate using tunable diode laser absorption of H2O near 2.5 μm," *Proceedings of the Combustion Institute*, 2011. **33**(1): p. 309-316.

[118]. Joshi, A.V. and H. Wang, "Master equation modeling of wide range temperature and pressure dependence of CO + OH → products," *International Journal of Chemical Kinetics,* 2006. **38**(1): p. 57-73.

[119]. Tsang, W., "Chemical Kinetic Data Base for Combustion Chemistry Part V. Propene," *Journal of Physical and Chemical Reference Data,* 1991. **20**(2): p. 221-273.

[120]. Hanning-Lee, M.A. and M.J. Pilling, "Kinetics of the reaction between H atoms and allyl radicals," *International Journal of Chemical Kinetics*, 1992. **24**(3): p. 271-278.

[121]. Harding, L.B., S.J. Klippenstein, and Y. Georgievskii, "On the Combination Reactions of Hydrogen Atoms with Resonance-Stabilized Hydrocarbon Radicals," *The Journal of Physical Chemistry A*, 2007. **111**(19): p. 3789-3801.

[122]. Miller, J.A. and S.J. Klippenstein, "Dissociation of Propyl Radicals and Other Reactions on a C3H7 Potential," *The Journal of Physical Chemistry A*, 2013. **117**(13): p. 2718-2727.

[123]. Rosado-Reyes, C.M., J.A. Manion, and W. Tsang, "H Atom Attack on Propene," *The Journal of Physical Chemistry A*, 2011. **115**(13): p. 2727-2734.

[124]. Smith, I.W. and R. Zellner, "Rate measurements of reactions of OH by resonance absorption. Part 2.—Reactions of OH with CO, C 2 H 4 and C 2 H 2," *Journal of the Chemical Society, Faraday Transactions 2: Molecular and Chemical Physics*, 1973. **69**: p. 1617-1627.

[125]. Westenberg, A. and N. DeHaas, "Rates of CO+ OH and H2+ OH over an extended temperature range," *The Journal of Chemical Physics*, 1973. **58**(10): p. 4061-4065.

[126]. Davis, D., S. Fischer, and R. Schiff, "Flash photolysis-resonance fluorescence kinetics study: Temperature dependence of the reactions OH+ CO→ CO2+ H and OH+ CH4→ H2O+ CH3," *The Journal of Chemical Physics*, 1974. **61**(6): p. 2213-2219.

[127]. Clyne, M.A. and P.M. Holt, "Reaction kinetics involving ground X 2 Π and excited A 2 Σ+ hydroxyl radicals. Part 1.—Quenching kinetics of OH A 2 Σ+ and rate constants for reactions of OH X 2 Π with CH 3 CCl 3 and CO," *Journal of the*

Chemical Society, Faraday Transactions 2: Molecular and Chemical Physics, 1979. **75**: p. 569-581.

[128]. Ravishankara, A. and R. Thompson, "Kinetic study of the reaction of OH with CO from 250 to 1040 K," *Chemical physics letters*, 1983. **99**(5-6): p. 377-381.

[129]. Frost, M.J., P. Sharkey, and I.W. Smith, "Reaction between hydroxyl (deuteroxyl) radicals and carbon monoxide at temperatures down to 80 K: Experiment and theory," *The Journal of Physical Chemistry*, 1993. **97**(47): p. 12254-12259.

[130]. Golden, D., G. Smith, A. McEwen, C.-L. Yu, B. Eiteneer, M. Frenklach, G. Vaghjiani, A. Ravishankara, and F. Tully, "OH (OD)+ CO: Measurements and an optimized RRKM fit," *The Journal of Physical Chemistry A*, 1998. **102**(44): p. 8598-8606.

[131]. Davis, S.G., A.V. Joshi, H. Wang, and F. Egolfopoulos, "An optimized kinetic model of H2/CO combustion," *Proceedings of the combustion Institute*, 2005. **30**(1): p. 1283-1292.

[132]. Fernandes, R.X., K. Luther, J. Troe, and V.G. Ushakov, "Experimental and modelling study of the recombination reaction H + O2 (+M) → HO2 (+M) between 300 and 900 K, 1.5 and 950 bar, and in the bath gases M = He, Ar, and N2," *Physical Chemistry Chemical Physics*, 2008. **10**(29): p. 4313-4321.

[133]. Ferris, A.M., A.J. Susa, D.F. Davidson, and R.K. Hanson, "High-temperature laminar flame speed measurements in a shock tube," *Combustion and Flame*, 2019. **205**: p. 241-252.

[134]. Vranos, A. and P. Marteney, "Experimental Study of the Stability of Aircraft Fuels at Elevated Temperatures," *NASA Lewis Research Center, Cleveland, OH, NASA Contractor Report No. CR-165165*, 1980.

[135]. Marteney, P. and L. Spadaccini, "Thermal decomposition of aircraft fuel," *Journal of Engineering for gas Turbines and Power*, 1986. **108**(4): p. 648-653.